Mapping the Biomechanical Properties of Human Knee Cartilage

by

Jessica M. Deneweth

A dissertation submitted in partial fulfillment
of the requirements for the degree of
Doctor of Philosophy
(Kinesiology and Mechanical Engineering)
in The University of Michigan
2013

Doctoral Committee:

Assistant Professor Scott G. McLean, Co-Chair
Michael J. Bey, Co-Chair, Henry Ford Hospital
Professor Ellen M. Arruda
Assistant Professor Mark L. Palmer
Associate Professor Riann M. Palmieri-Smith
Professor Noel C. Perkins

ACKNOWLEDGEMENTS

I would like to deeply thank my advisors Dr. Scott McLean, Dr. Ellen Arruda, and Dr. Mike Bey for their mentorship, guidance, and encouragement throughout this process. I am tremendously grateful to Scott for being not only a wonderful mentor but also a friend. Thank you for bringing me into this program, for teaching me how to be an independent researcher, for keeping me motivated when things were not working, for teaching me biomechanics, for being a constant advocate for my success, and for pushing me to be the best that I could be. I would like to thank Dr. Arruda for her ideas that sent this dissertation in an entirely different, and I believe much better, direction than how it began, for opening up her lab and resources to me to make these studies possible, for sharing her invaluable knowledge of tissue mechanics and modeling from which I have learned immensely, and for her constant support and enthusiasm for this research. I would like to thank Mike for opening my eyes to the wonderful world of biomechanics research, for seeing my potential when I did not, for welcoming me into the Motion Lab, and for his invaluable support and mentorship over these last six years.

I would like to thank my entire committee for their advice, insight, and support of this work. I am very grateful to their openness to this interdisciplinary research and the Individual Interdepartmental Degree Program.

I would like to thank Dr. Grant Goulet for his advice and support in putting this dissertation together, Sasha Voloshina for her help with coding, and Dr. Andrea Kussman for teaching me how to dissect my first knee.

I would like to thank the members of the Human Performance Innovation Lab, the Materials Testing Lab, and the Motion Analysis Lab for their assistance with this work. I am especially grateful to Kevin Lapprich for building the materials testing device used in this research, for Harish Iyer for help in piloting the device and for patiently teaching me Abaqus, for Jinjin Ma and Keqin Cao for their assistance with digital image correlation, and for Kelly Newman, Shannon Pomeroy, and Stephen Sylvia who processed much of the data in this work. I would like to thank the Horowitz lab, especially Rachael Nelson and Sean Newsom, for helping me prepare the gallons of PBS solution used in these studies and Ken Guire for his crucial help with statistical analysis.

I would like to thank Charlene Ruloff and the Mechanical Engineering Academic Services Office for the extensive administrative support required for this unconventional degree program.

I am grateful to the non-profit agencies (Anatomy Gifts Registry and MedCure) that provided cadaveric knees and to the individuals and their families whose generous donations made this research possible.

This work, as well as many of my academic expenses, was supported with funding from the National Defense Science and Engineering Fellowship Program, the Rackham School of Graduate Studies, the School of Kinesiology, and the Department of Mechanical Engineering.

TABLE OF CONTENTS

LIST OF FIGURES

LIST OF TABLES

LIST OF APPENDICES

LIST OF ABBREVIATIONS

A	anterior
AC	articular cartilage
ANOVA	analysis of variance
AOI	area of interest
BMI	body mass index
C	central
CI	confidence interval
DIC	digital image correlation
DZ	deep zone (of cartilage)
FJC	isotropic eight-chain network model with freely jointed chains
J	Joule
K	Kelvin
K1,…,K8	knee 1,…, knee 8
kPa	kilopascals
L	lateral
LWB	less weightbearing region of femoral cartilage, i.e., primary contact at knee flexion angles > 30°
m	meter
M	medial
MAC	isotropic eight-chain network model with MacKintosh chains
mm	millimeter
MPa	megapascals
MR, MRI	magnetic resonance, magnetic resonance imaging
msec	milliseconds
MZ	middle zone (of cartilage)
N	Newtons
OA	osteoarthritis
PBS	phosphate-buffered saline
SD	standard deviation
sec	seconds
STZ	superficial tangential zone
TI	transversely isotropic eight-chain network model
WB	weightbearing region of femoral cartilage, i.e., primary contact at knee flexion < 30°

LIST OF SYMBOLS

1	material direction oriented with the loading axis
2, 3	material directions perpendicular to the loading axis
a, b, c	orthonormal material axes of the orthotropic eight-chain network model
B	bulk compressibility near $J = 1$
C_R	rubbery modulus
d_{AB}	effect size between region A and region B
d_{rel}	relative distance measure used to determine the number of data points for computing $E_{10\%}$
$E_{10\%}$	elastic tangent modulus at 10% strain
f_{chain}	force in chain
$\mathbf{F}$	deformation gradient
J	ratio of deformed volume to undeformed volume
k	Boltzmann's constant
l	rigid segment length of chain
l_p	persistence length of chain
L	contour length of chain
$\mathcal{L}(x)$	Langevin of x, $\mathcal{L}(x) = \coth(x) - 1/x$
n	unit chain density
n	number of samples, effects, etc.
N	number of rigid links per chain
P	initial normalized chain length
r	current end-to-end chain length
r_0	initial end-to-end chain length
$r_{f=0}$	end-to-end chain length under no applied tension
R^2	goodness of fit parameter
T_1	axial true stress
T_{o1}	axial nominal stress
U	strain energy
U_O	constant related to the nonzero entropy of the undeformed chains
α	constant governing curvature of the hydrostatic pressure versus volume curve for larger volume changes
$\beta_r, \beta_p, \beta_P$	inverse Langevin of r, ρ, P, respectively
λ_i	network stretches in the i^{th} – direction, i = 1, 2, 3
Θ	absolute temperature
ρ	normalized deformed chain length

ABSTRACT

Knee osteoarthritis is one of the most common musculoskeletal pathologies, and results in severe joint pain, loss of mobility, compromised quality of life, and high medical costs. With no cure other than total joint replacement, and the incidence of osteoarthritis rising worldwide, the need to understand how the disease develops has reached a critical level. The mechanism(s) underlying the initiation and progression of knee osteoarthritis remain unknown despite years of extensive research. Alterations in the spatial loading pattern on the joint's articular cartilage, for example, due to knee injury, have been hypothesized to trigger the onset of the disease. The theory presupposes that the mechanical properties of knee cartilage are non-uniform such that the underlying cartilage is unable to sustain the new loading pattern and deteriorates. However, this tenet is challenging to test directly because it requires detailed knowledge of spatial mechanical properties of the cartilage, which is currently unknown.

Therefore, this dissertation sought to address current knowledge gaps by mapping the elastic modulus of healthy human knee articular cartilage across the joint surface. This work represented the first such mapping with fine spatial resolution and employing a physiologically relevant compressive strain rate. Significant variations in modulus were found across the femur and tibial cartilage.

Moreover, these variations conformed to a consistent regional pattern across knees, which has not previously been demonstrated.

These findings subsequently motivated the development of a constitutive relation that could successfully simulate spatially dependent, high strain rate mechanics. A transversely isotropic hyperelastic model was developed and compared with isotropic hyperelastic models to determine which constitutive relation best represented the natural cartilage mechanics. The transversely isotropic model replicated the spatial mechanical dependence of the tissue through variations in a single model parameter. The model is mechanistic, has a structure and parameters that are analogous to human cartilage physiology, is computationally efficient, and is straightforward to implement in commercial finite element packages. The transversely isotropic model represents a novel method for implementing the non-uniform mechanics of knee cartilage that are critical to understanding the initiation and progression of knee osteoarthritis. The characterization of regional mechanical properties of human knee cartilage performed herein has contributed essential baseline knowledge that will fundamentally advance experimental and computational studies of knee osteoarthritis development toward widespread prevention of this devastating disease.

Chapter 1: Introduction and Specific Aims

1.1 Introduction

Osteoarthritis (OA) is a common, debilitating joint disease that is characterized by loss of articular cartilage (AC), bone spurs, significant pain, and loss of joint mobility (Felson 2000). The knee is one of the joints most commonly affected by osteoarthritis (Lawrence 2008; Symmons 2003). Approximately 27 million Americans (12.1% of the adult population) are afflicted with the disease (Lawrence 2008). These numbers are expected to grow 25% by 2030 (Hootman and Helmick 2006). Likewise, the economic costs related to knee OA are high, exceeding $89 billion annually in the US (Leigh 2001), and continuing to mount (Bitton 2009; Hootman and Helmick 2006). Thus elucidating the mechanism(s) by which knee OA develops is critical to maintaining lifelong health and wellness for the vast number of individuals living with or at risk for developing this serious disease.

Knee mechanics have been hypothesized to substantially influence OA development (Andriacchi 2009; Tashman 2004a). In support of this tenet, individuals at high risk for developing the disease exhibit abnormal knee mechanics when executing dynamic tasks (Chouliaras 2009; Deneweth 2010; Tashman 2007). In my own recent work for example, I determined that individuals with a surgically repaired anterior cruciate ligament, who are at

increased risk of developing early-onset knee OA, exhibited significant kinematic differences between their repaired and uninjured contralateral knees during a single-leg landing task (Deneweth 2010). Deneweth et al. 2010 is reprinted with permission in Appendix A. Likewise, the degree of disease severity in patients with arthritic knees has been associated with differences in knee mechanics (Astephen 2008; Sharma 2001b). Recently, increased anterior tibial translation in individuals with repaired anterior cruciate ligaments was associated with early signs of AC degeneration (Haughom 2012), which offers further evidence for a direct link between knee mechanics and OA. While indirect support for the role of knee mechanics in OA appears strong, a clear connection between altered joint motions and detrimental changes in AC loading remains to be established.

Developing a more complete understanding of knee AC mechanical properties is essential to determining the extent to which joint mechanics influences OA development. The mechanical hypothesis of OA development implies that abnormal joint motions induce deviations from the normal joint contact pattern (Andriacchi 2006; Andriacchi 2009; Andriacchi and Mundermann 2006; Carter 2004; Chaudhari 2008). When these deviations produce a mismatch between the loads placed on the AC and its intrinsic ability to support these loads, AC stresses may become excessively high and cause damage to the tissue. This hypothesis implicitly requires that knee AC is mechanically non-uniform, which several studies have indicated (Elliott 2002; Froimson 1997; Jurvelin 2000; Shepherd and Seedhom 1999a; Swann and Seedhom 1993; Thambyah 2006; Young 2007). To date, however, little is known about the extent

of variability of AC mechanical properties across the human knee joint, particularly in response to physiologically relevant dynamic loading.

Successful investigation of knee OA initiation and development also relies on the use of computational models of knee AC (Carter and Wong 2003; Wilson 2005b). These models serve as powerful tools for investigating interactions among joint contact mechanics, AC properties, and AC degeneration (Besier 2005; DiSilvestro and Suh 2002; Haut Donahue 2004; Korhonen 2003; Pena 2007; Pena 2006; Shirazi 2008; Wilson 2004; Wilson 2003). For example, joint kinematics or kinetics that present in individuals at high risk for knee OA can be implemented into the model and the resulting joint contact pattern and local tissue strains and stresses can be compared to the control case. The extent to which hypothesized “risky” mechanics influence the mechanical state of the AC can be examined from these simulations. The effectiveness of these models, however, depends heavily on the validity of the underlying AC material model (Carter and Wong 2003; Taylor and Miller 2006; Wilson 2005b). While much work has been done to develop analytical models to capture the complex mechanics of AC (Ateshian 1994; Boschetti 2006; Keenan 2012; Kwan 1990; Lai 1991; Lai 1993; Mak 1987; Mow 1980; Spilker 1992; Wilson 2005a), few models are suited to the high strain rate loading and large, non-linear deformations that occur during walking and other normal daily activities (Hasler 1999; Li and Gu 2011; Liu 2010; Taylor and Miller 2006). More accurate models tend to employ several material constants (Cohen 1992; DiSilvestro 2001; Lai 1991; Seifzadeh 2012; Suh and Bai 1998; Wilson 2006; Wilson 2005a), which can be challenging

to implement into dynamic computer simulations (Wilson 2005b). Furthermore, none have sought to incorporate the spatial mechanical inhomogeneity that has been suggested as pivotal to OA development (Andriacchi 2004; Carter 2004; Chaudhari 2008). Thus, an analytical model that captures the non-linear, large deformation, and potentially spatially inhomogeneous physiological response of AC via a minimal set of parameters would be advantageous to the study of knee OA initiation and development.

1.2 Specific Aims

Therefore, the Specific Aims of this dissertation research comprised the following:

AIM 1: Determine the extent to which non-arthritic human proximal tibial articular cartilage exhibits regional mechanical properties under physiologically relevant loading.

Hypothesis 1A: The mechanical properties of cartilage covering the proximal tibia are spatially heterogeneous across the tibial plateau.

Hypothesis 1B: The mechanical inhomogeneity of proximal tibial cartilage manifests in a consistent regional pattern across individuals.

AIM 2: Determine the extent to which non-arthritic human distal femoral articular cartilage exhibits regional mechanical properties under physiologically relevant loading.

Hypothesis 2A: The mechanical properties of cartilage covering the distal femur are spatially heterogeneous across the femoral trochlea and condyles.

Hypothesis 2B: The mechanical inhomogeneity of distal femoral cartilage manifests in a consistent regional pattern across individuals.

Significance of Aims 1 and 2: Spatial variations in the mechanics of knee articular cartilage are hypothesized to contribute substantially to knee osteoarthritis

development. However, few data are available on these spatial variations, particularly when the cartilage is subjected to physiologically relevant loading conditions. Therefore, mapping the regional variability of healthy human knee cartilage provides foundational data that is essential for investigating the interaction of joint mechanics, contact patterns, and osteoarthritis.

AIM 3: Develop a transversely isotropic statistical mechanics model to simulate non-arthritic human tibiofemoral joint articular cartilage mechanics under physiologically relevant loading and compare to existing isotropic statistical mechanics models.

Hypothesis 3A: The transversely isotropic statistical mechanics model will accurately simulate the tibiofemoral joint cartilage stress-strain response elicited under physiological loading.

Hypothesis 3B: The transversely isotropic model will perform superiorly to isotropic statistical mechanics models.

Hypothesis 3C: When used to simulate tibial cartilage, parameters of the transversely isotropic model will exhibit regional dependency similar to that determined in AIM 1.

Hypothesis 3D: When used to simulate femoral cartilage, parameters of the transversely isotropic model will exhibit regional dependency similar to that determined in AIM 2.

Significance of Aim 3: Statistical mechanics models, such as the popular eight-chain network model, are well suited to non-linear, high strain rate, and large deformation responses synonymous with *in vivo* articular cartilage loading. Therefore, the eight-chain model could represent an improvement to traditional continuum models for modeling physiological cartilage mechanics. Development of a material model of tibiofemoral joint articular cartilage that accurately models its physiological mechanics, including any regional dependence, will immediately improve the potential to successfully model the complex interactions between joint mechanics and osteoarthritis development.

1.3 Structure of Dissertation

The dissertation was structured such that its main body (**Chapters 4 – 7**) detailed four separate studies conducted over a period of three years (2010-2013) at the University of Michigan. All studies have been accepted or submitted for publication in peer-reviewed journals. Minor changes have been made from the original manuscripts in certain cases to maintain consistency throughout the document, to minimize redundancy, and to provide additional details where word-count constraints prevented their inclusion in the journal manuscripts. Common experimental materials and methods are detailed in **Chapter 3** and referenced in subsequent chapters. Likewise, where similar methods have already been presented, they are referenced to the initial chapter in which they were presented.

Chapter 2 provides a review of the relevant literature underlying the motivation for and formulation of the studies presented in latter chapters. In **Chapter 4**, the elastic tangent modulus of healthy tibial AC was characterized via unconfined compression conducted at a high, physiologically relevant strain rate. A spatial mapping of the modulus at 21 locations on the tibial plateau was constructed. Statistical analyses were used to determine the extent to which variations in spatial moduli conform to a similar pattern across individual specimens. **Chapter 5** represents the completion of the experimental work initiated in Chapter 4. The elastic tangent modulus was mapped across 29 sites on the distal femur. Similar spatial mapping and statistical analyses were conducted to develop a complete mechanical characterization of tibiofemoral joint AC. In **Chapter 6**, three constitutive relations were presented to describe knee AC. Included in these models was a newly developed transversely isotropic eight-chain network. The ability of these models to represent high-rate tibial AC mechanics was examined by simulating each model against the experimental data acquired in Chapter 4. The model determined to best fit the data was subsequently investigated to verify its ability to replicate the spatial dependency of AC mechanical response. **Chapter 7** evaluated the effectiveness of the three models developed in Chapter 6 to simulate the high-rate mechanics of distal femoral AC detailed in Chapter 5. Similarly, the best-fitting model was determined and the extent to which it modeled the regional mechanical variations across the femoral AC surface was examined. Together, Chapters 6 and 7 described a material model for tibiofemoral joint cartilage that successfully

simulated its high strain rate, non-uniform mechanical response and is ready for implementation into finite element models of the knee joint. **Chapter 8** highlights the key outcomes of Chapters 4 – 7, discusses the limitations of the four studies, and proposes directions for future work related to this body of research.

Chapter 2: Background

2.1 Knee Osteoarthritis

2.1.1 Prevalence and Symptoms

Osteoarthritis is the most common form of arthritis (Bitton 2009). The disease afflicts approximately 27 million individuals in the United States and 700 million worldwide, and these numbers are likely rising (Bitton 2009; Hootman and Helmick 2006; Symmons 2003). The knee is the joint most frequently affected by osteoarthritis. Individuals suffering with knee OA report frequent knee pain, crepitus, stiffness and swelling (Symmons 2003). Radiological exam typically reveals thinning or absent joint AC, narrowing of the joint space, bony deformity, and the presence of osteophytes (Murphy and Helmick 2012; Symmons 2003). These symptoms most often lead to compromised joint mobility, reduced quality of life, an increased risk of comorbidity, reduced capacity to work, and increased medical costs (Bitton 2009; Murphy and Helmick 2012). The OA-related economic burden in the United States exceeds $89 billion dollars (Bitton 2009).

Knee OA is irreversible. Pharmacologic, non-pharmacologic, and surgical treatments may provide moderate symptom relief but cannot place the disease in remission (Davis 2012; Hawker 2011; Seed 2009). The most effective treatment to halt disease progression is joint replacement (Seed 2009). Joint replacement,

however, is costly, invasive, and not suited for the growing number of young OA sufferers (Gomoll 2012). Consequently, an urgent need exists to develop preventative measures for knee OA. Effective prevention depends on thorough knowledge of the disease process.

2.1.2 Role of Mechanics in the Disease Process

Numerous genetic, biological, and mechanical factors have been suggested in the initiation and progression of OA (Belo 2007; Bierma-Zeinstra and Koes 2007; Cimmino and Parodi 2005; Dieppe and Lohmander 2005; Felson 2004; Felson 2007; Hunter 2005; Leveille 2005; McKinley 2004b). For example, genes regulating tissue growth and differentiation, production of the cartilage extracellular matrix, and inflammatory responses have been linked with susceptibility to knee OA (Adatia 2012). Genetic susceptibility to the disease may also occur through inherited variations in joint structure that promote a damaging mechanical environment (Sandell 2012). Biological factors also have been suggested to influence disease development, particularly biological changes in the subchondral bone as these have been noted early in the disease process (Baker-LePain and Lane 2012; Suri and Walsh 2012). Two potential pathways have been suggested for OA initiation via bone but both require further investigation: 1) local biological factors produced in the bone may be transmitted to the AC via small channels and disrupt AC homeostasis, or 2) altered subchondral bone turnover changes the bony geometry and/or mechanical properties, which in turn promote a AC biomechanical environment favorable to

OA development (Baker-LePain and Lane 2012; Laufer 2003). These theories are additionally supported by the association of bone marrow lesions with some instances of knee OA (Hunter 2006; Zhang 2011). Inflammation due to systematic (e.g., obesity) or local (e.g., injury) factors has been correlated with knee OA, but it is unclear whether it promotes OA initiation and/or development (van der Kraan 2012). Similarly, body mass, lower limb alignment, activity, and joint geometry are mechanical factors that have been linked with OA but whose explicit roles remain unknown (Felson 1996, 2004).

Given the findings presented in the previous paragraph and the varied ways that knee OA presents, the disease likely occurs through a complex interaction of genetic, biological, and mechanical factors (Cimmino and Parodi 2005). Of these factors, substantial evidence suggests that mechanics exert a strong influence on the disease process and warrant further research (Andriacchi 2009; Andriacchi and Mundermann 2006; Andriacchi 2004; Astephen 2008; Besier 2008; Eckstein 2008; Fleming 2005; Maly 2008; McKinley 2004a; Sharma 2001b). For example individuals with injured anterior cruciate ligaments, which are a population at high risk for knee OA, exhibit abnormal joint kinematics several years before the onset of arthritic symptoms (Ristanis 2005; Stergiou 2007; Tashman 2004b; Tashman 2007). In this same population, individuals whose injured limb displays unusually large anterior tibial translations have biological markers of early AC degeneration under magnetic resonance imaging (MRI) examination (Haughom 2012). These markers do not appear in injured individuals with normal anterior tibial translations.

Mechanical links also appear in the idiopathic OA population. Disease severity, for example, has been associated with differing patterns of kinematics, kinetics, and muscle activation among healthy, moderate OA, and severe OA populations (Astephen 2008; Creaby 2010; Foroughi 2009; Heiden 2009; Hubley-Kozey 2009). Lower limb alignment has also been found to distinguish between rates and locations of knee AC loss (Brouwer 2007; Moisio 2011).

Based on these and similar findings, altered knee mechanics due to injury, malalignment, or other mechanical factors are believed to shift the pattern of joint contact from AC regions well-adapted to specific loading patterns to regions poorly suited for such loads (Andriacchi 2009; Andriacchi 2004; Chaudhari 2008). This sudden change of loading pattern may induce a deleterious AC stress state to which the tissue is unable to adapt (Bevill 2008; Carter 2004; Koo and Andriacchi 2007). Repetition of this loading state may eventually damage the collagen matrix and initiate OA development (Anderst 2005; Anderst and Tashman 2009; Andriacchi and Mundermann 2006; Carter 2004; Setton 1999). Further work is required, however, to establish a clear link between abnormal knee mechanics and OA. In particular, a detailed understanding of regional variations in knee AC mechanics must be developed. This knowledge is critical to determining whether spatial shifts of the AC loading pattern would produce the hypothesized damaging AC stresses.

2.2 Anatomy and Function of the Knee

The knee is an important lower limb joint and its healthy function is essential for maintaining mobility and a high quality of life. The knee is composed of three major bones: the distal portion of the femur, the proximal portion of the tibia (tibial plateau), and the patella (Fig. 2.1). The knee can be decomposed into two separate joints: the tibio-femoral joint based on the articulation of the femoral condyles and the tibial plateau, and the patello-femoral joint formed by the articulation of the patella over the trochlea region of the distal femur (Fig. 2.1) (Flandry and Hommel 2011; Gray 1918).

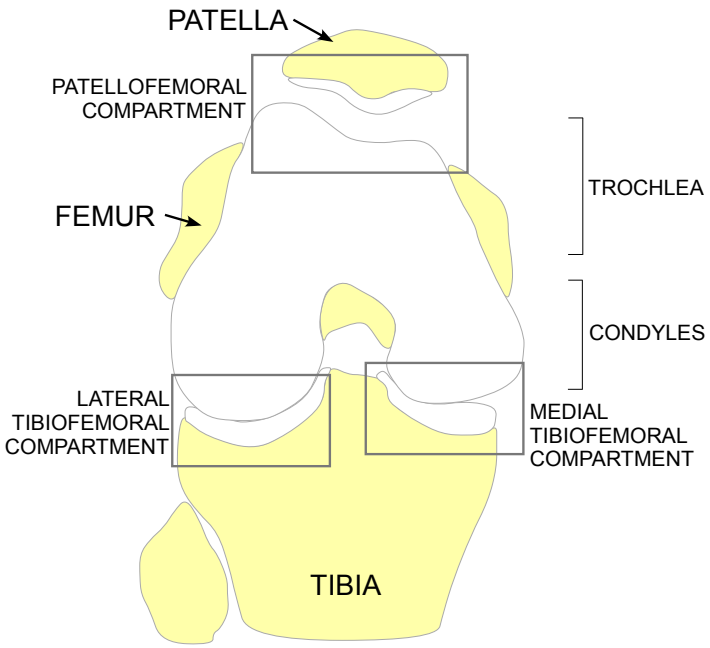

Figure 2.1: Schematic of the anterior view of the flexed knee. The trochlea of the femur articulates with the patella to form the patellofemoral joint. The condyles of the femur articulate with the tibial plateau to form the tibiofemoral joint. The tibiofemoral joint is typically described as having separate medial and lateral compartments. Yellow – bone, white – cartilage. Adapted from www.conformis.com.

Several soft tissue structures provide stability, ease of motion and/or load support to the knee (Giuliani 2009; Goodfellow 1976; Gray 1918; LaPrade 2007a; LaPrade 2007b; Sanchez 2006) (Fig. 2.2). These include, but are not limited to, the anterior cruciate, posterior cruciate, medial collateral, and lateral collateral ligaments that connect the femur and tibia at various locations; the crescent-shaped medial and lateral menisci that rest on the tibial plateau; and the AC covering the medial and lateral compartments of the tibial plateau, the femoral condyles, the femoral trochlea, and the posterior aspect of the patella.

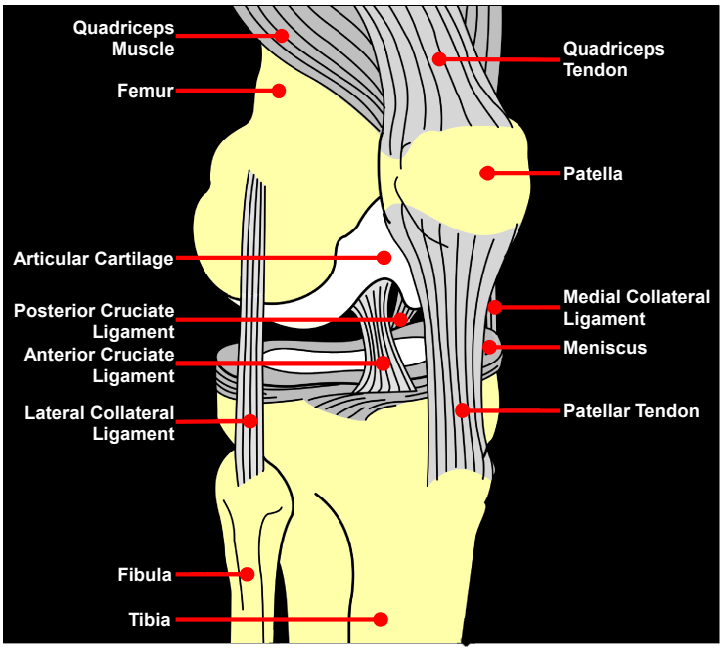

Figure 2.2: Anatomy of the human knee joint. Adapted from commons.wikimedia.org.

2.3 Articular Cartilage of the Knee

Articular cartilage serves an essential role in healthy knee function by establishing a minimal friction environment and helping to dissipate joint loads

(Hendren and Beeson 2009; Mow 1993). Articular cartilage depends on its unique physiology and mechanical properties to maintain painless joint mobility (Buckwalter 2005). Degeneration of AC is the hallmark of OA (Dieppe and Lohmander 2005; Eckstein 2010), but the mechanism by which deterioration occurs remains unknown. Knowledge of AC physiology and mechanics, particularly regional variations in these properties, could lend important insight into the OA disease process.

2.3.1 Physiology of Knee Articular Cartilage

2.3.1.1 General

Articular cartilage is a biphasic material composed of a fluid phase and a solid phase. The fluid phase primarily consists of water and permeable ions and represents 65% - 80% of the total tissue weight (Mow and Guo 2002). The largest component of the solid phase is collagen, which represents 50% - 75% of dry tissue weight (Hasler 1999; Mow and Guo 2002; Mow 1984). Collagen II fibers form a chemically cross-linked meshwork and represent 85 - 95% of the collagen content (Eyre 1991; Hasler 1999). Collagen III, VI, IX, XI, XII, and XIV molecules are also present but in small concentrations (Eyre 2002; Eyre 1991). Negatively-charged proteoglycan macromolecules make up 15-30% of the solid matrix by dry weight (Brandt and Palmoski 1976). Large aggregates of the proteoglycans aggrecan and versican are immobilized within the collagen matrix and produce a net negative charge in the solid matrix (Roughley 2006; Sztrolovics 2002). This negative charge attracts and holds water within the

tissue. Smaller proteoglycans (e.g., decorin, fibromodulin) are also present in much lower concentrations and are more mobile than their larger counterparts (Noyori 1998; Roughley 2006). Chondrocytes form the final major component of the solid matrix and are responsible for maintaining the tissue's extracellular matrix (Poole 1997). Chondrocytes represent approximately 10% of the total tissue volume (Hasler 1999).

2.3.1.2 Depth-wise Properties

Knee AC is highly inhomogeneous along its thickness. The tissue has been traditionally divided into four zones: the superficial tangential zone (STZ) at the articulating surface of the cartilage, the middle (transition) zone (MZ), the deep (radial) zone (DZ), and the calcified cartilage at the interface with the subchondral bone layer (Poole 2001; Setton 1999) (Fig. 2.3). The relative composition of the solid and fluid phases, the shape of the chondrocytes, and the primary orientation of the collagen fibrils are zone-dependent (Mow and Guo 2002). In the superficial zone, the collagen fibers are densely packed, oriented parallel to the AC surface, and display a moderate amount of in-plane anisotropy (Eyre 2006). The chondrocytes are flattened, small, and densely packed (Poole 2001; Youn 2006). Proteoglycan content comprises a low 10% of dry matrix weight (Muir 1970). Water makes up 85% of total tissue weight, the highest proportion present along the zones (Hasler 1999; Treppo 2000).

Continuing along the depth to the relatively thicker MZ, the fibrils begin to change orientation towards the direction perpendicular to the surface and their

overall orientation becomes more random (Eyre 2006). The chondrocytes assume a larger and more spherical shape, while the water content remains high (Hasler 1999; Youn 2006). Proteoglycan content peaks at 25% of the dry matrix weight (Maroudas 1968; Muir 1970; Setton 1998).

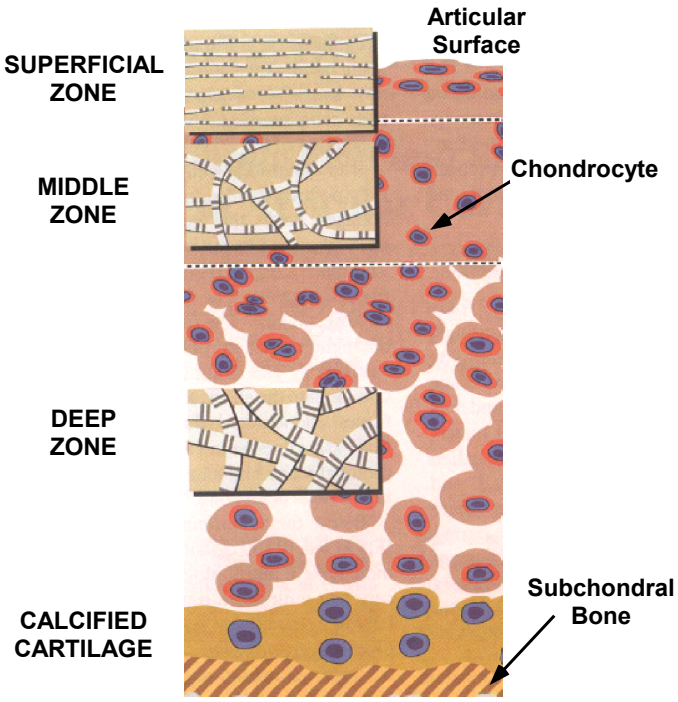

Figure 2.3: Depth-wise physiology of human articular cartilage. Insets highlight how the collagen fibril alignment and diameter changes along the depth of the tissue. Adapted from Poole 2001.

Finally in the DZ the collagen fibrils form large-diameter, radially-oriented bundles that that insert into the calcified zone (Jeffery 1991; Poole 2001). The chondrocytes generally appear in radial columns in parallel to the collagen (Poole 1997). Water content drops to its lowest levels in this zone and proteoglycan content also decreases slightly (Hasler 1999; Muir 1970).

2.3.1.3 Regional Properties

Physiological inhomogeneity also manifests regionally but has been less extensively documented compared to the tissue's depth-dependent properties. Femoral AC displays lower water content and higher proteoglycan content compared to AC of the tibial plateau (Treppo 2000). Within the tibial plateau, collagen fibrils are more densely packed in the periphery (i.e., the AC beneath the menisci) compared to the center (Clark 1991) (Fig. 2.4). The peripheral region also tends to possess a thicker STZ and a thinner DZ (Clark 1991). Comparing mediolaterally, the lateral plateau tends towards higher overall collagen density compared to the medial plateau (Clark 1991).

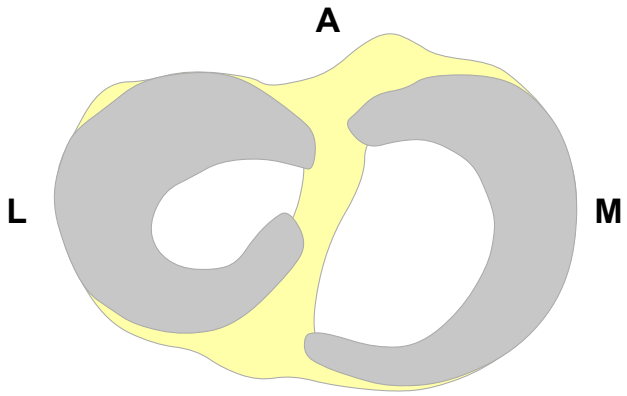

Figure 2.4: Schematic of the menisci on the tibial plateau. Physiological differences have been determined between the cartilage beneath the menisci and exposed cartilage. Gray – meniscus, white – cartilage, yellow – bone, L – lateral, M – medial, A – anterior.

Regional differences within the distal femoral surface have been minimally examined. Water and proteoglycan content have been found to be similar among the trochlea, anterior femoral condyles, and posterior femoral condyles (Treppo

2000). Within the trochlea, however, proteoglycan is lower in the region that contacts the patella at 90° of knee flexion than in the region that makes contact at 30° knee flexion (Froimson 1997).

2.3.2 Mechanics of Knee Articular Cartilage

The mechanical response of AC to applied loading is highly complex (Lu and Mow 2008; Mow and Guo 2002). Several key features characterize the response: time dependence, strain and strain rate dependence, anisotropy, tension-compression non-linearity, and depth and regional inhomogeneity.

2.3.2.1 Time Dependence

Articular cartilage displays characteristic creep and stress relaxation behavior (DiSilvestro and Suh 2001; Mak 1986; Mow 1980). Application of a constant load or deformation produces an instantaneous strain or stress, respectively, followed by a transient period of several seconds to minutes before an equilibrium state is reached. This time dependent behavior arises from two distinct mechanisms within the tissue: the viscoelasticity of the solid matrix (i.e., flow-independent stress) and the frictional drag force produced as the fluid phase flows through the solid matrix (i.e., flow-dependent stress) (Mow 1984; Mow and Wang 1999).

2.3.2.2 Strain and Strain Rate Dependence

Cartilage behaves linearly in the low strain regime (i.e. 5 – 10% strain) and stiffens non-linearly with increasing strains (Fig. 2.5) (Fortin 2000; Langelier and Buschmann 2003; Lotjonen 2009; Wilson 2007). The intrinsic non-linearity of the solid matrix is partially responsible for this behavior (Li and Herzog 2004b; Li 2002). Increasing strain also increases compaction of the solid matrix, the density of proteoglycans, and the fixed charged density, which reduce the permeability of the tissue (Mansour and Mow 1976; Muir 1970). This strain-dependent permeability exerts a considerable influence on the tissue's mechanics (Lai 1981).

Articular cartilage stiffens not only with increasing strain but also with increasing strain rate (Fig. 2.5) (Lai 1981; Langelier and Buschmann 2003; Li and Herzog 2004b; Oloyede 1992). For example, the stiffness of AC compressed at $1x10^5$% strain/sec is an order of magnitude higher than AC compressed at 0.005% strain/sec (Oloyede 1992). The behavior of AC under strain rates elicited by normal human activities, such as walking, is of particular interest for understanding long-term AC disease processes, i.e. OA. Knee AC during these activities deforms at a strain rate of approximately 100-1000% strain/sec (Liu 2010; Mann and Hagy 1980). The strain rate dependence of the tissue saturates in this range (Fig 2.5). At this relatively high strain rate, there is insufficient time for the fluid to move relative to the solid collagen matrix. Therefore, the AC response is driven by the collagen matrix, and in particular the collagen matrix of the STZ (Bader and Kempson 1994; Bader 1992; Mizrahi 1986). Consequently

tissue can be approximated to behave nearly incompressibly under these physiological loading rates, and any time-dependent effects can be effectively ignored (Ateshian 2007; Mow 1980; Wong 2000).

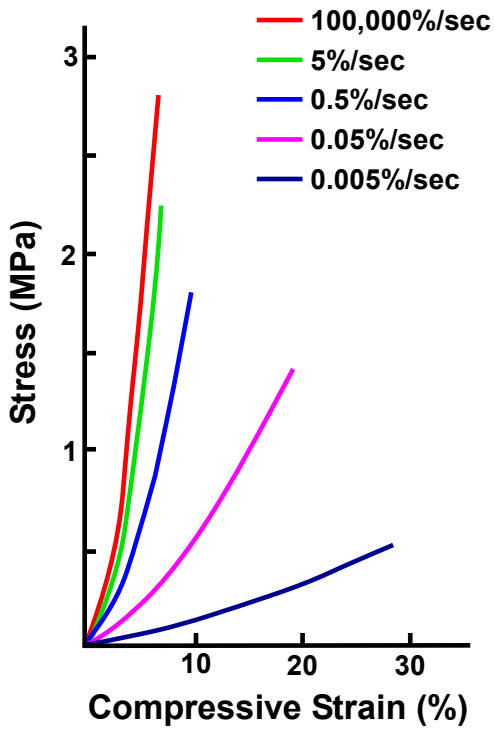

Figure 2.5: Stress-strain data from several bovine cartilage specimens compressed over a range of strain rates. Data obtained from Oloyede 1992.

2.3.2.3 Anisotropy

Articular cartilage is highly anisotropic and this behavior is due largely to the directional mechanics of the collagen fibrils of the solid matrix (Federico and Herzog 2008; Jurvelin 2003; Kempson 1968; Kiviranta 2006). Collagen fibrils supply maximum resistance to stretch along the fibril axis and substantially less resistance to compression in any direction or to stretch along other axes (Korhonen and Herzog 2008; Li and Herzog 2004a; Li 2005b). Therefore, AC

exhibits preferred material direction in line with the predominant collagen fiber alignment (Askew and Mow 1978; Federico and Herzog 2008; Jurvelin 2003; Woo 1976; Woo 1979). The alignment of the collagen fibers also influences the direction of fluid flow through the tissue (Federico and Herzog 2008; Reynaud and Quinn 2006). Since the collagen fiber alignment varies depth-wise and regionally (Clark 1991; Eyre 2006; Jeffery 1991), AC anisotropy may also vary throughout the tissue (Ateshian 2009; Wilson 2006, 2007). In the STZ, AC has been suggested to be at least transversely isotropic due to the tendency of the collagen fibers to align parallel to the surface (Fig. 2.6) (Askew and Mow 1978; Lanir 1987a). Orthotropicity (Chahine 2004; Chegini and Ferguson 2010; Wan 2010) and other more complex anisotropies (Ateshian 2009) also have been suggested to explain various AC behaviors.

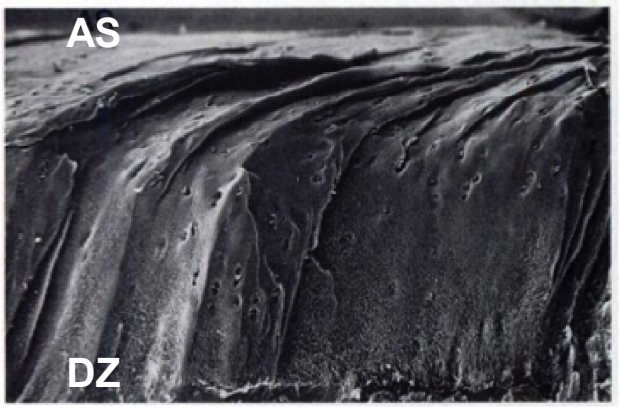

Figure 2.6: Scanning electron microscopy image of bovine cartilage showing the collagen fibers extending upward from the subchondral bone in the deep zone (DZ), changing direction through the intermediate zone, and finally orienting parallel to the articular surface (AS) in the superficial tangential zone. Reprinted with permission and copyright © of the British Editorial Society of Bone and Joint Surgery, Jeffery 1991.

2.3.2.4 Tension-Compression Nonlinearity

Articular cartilage can be as much as two orders of magnitude stiffer in tension than in compression (Laasanen 2003; Li 2005b; Mow and Guo 2002; Soltz and Ateshian 2000). The flow-independent response of the collagen matrix dominates the tensile behavior of the tissue whereas the flow-dependent response dictated by proteoglycan and water content produces compressive behavior (Park and Ateshian 2006). The differences between these mechanisms result in a marked tension-compression non-linearity (Chahine 2004; Huang 2001).

2.3.2.5 Depth and Regional Inhomogeneity

Depth-wise and regional inhomogeneities follow from AC's physiological inhomogeneity (Armstrong 1984; Chan 2009; Edelsten 2010; Oloyede 1992; Swann and Seedhom 1993). Along the depth of the tissue, the tensile modulus tends to be highest in the STZ and declines to its minimum in the DZ, regardless of the relationship between the testing configuration and preferred collagen direction (Mow and Guo 2002; Verteramo and Seedhom 2004). Conversely, the compressive modulus is relatively low for the STZ and increases along the depth (Chen 2001; Schinagl 1997; Wang 2001; Wong and Sah 2010). Hydraulic permeability, i.e., the ease of fluid flow through the AC, also is lowest at the surface, which is believed to be necessary to restrict fluid exudation from the tissue and in turn maintain the high hydrostatic pressure required to support normal joint loading (Federico and Herzog 2008; Gannon 2012; Krishnan 2003;

Setton 1993). Shear modulus follows a different pattern: its lowest value occurs in the MZ and it peaks in the DZ near the calcified AC boundary (Buckley 2010; Buckley 2008). Axial, transverse, and shear strains accordingly display complex non-uniformity along the tissue depth (Chan 2009; Erne 2005).

Mechanical inhomogeneity manifests regionally among the tibial plateau, trochlea, and femoral condyles, as well as within each articulating area. Articular cartilage covering the femoral condyles is stiffer on average than AC on the corresponding tibial surface or the trochlea region (Barker and Seedhom 2001; Jurvelin 2000; Swann and Seedhom 1993; Treppo 2000). Conversely hydraulic permeability is lower in the femoral condyles compared to the tibial plateau (Treppo 2000). Cartilage from the trochlea tends to be more compliant than AC from the femoral condyles (Barker and Seedhom 2001; Shepherd and Seedhom 1999a).

Within the tibial plateau, the peripheral (covered by meniscus) regions of the medial and lateral tibial plateaus tend to be stiffer and thinner than the center (not covered by meniscus) regions of the plateaus (Barker and Seedhom 2001; Shepherd and Seedhom 1999a; Thambyah 2006; Young 2007). High-resolution mappings of tibial plateau stiffness, however, suggests that regional differences are more complex than the peripheral versus central dichotomy (Swann and Seedhom 1993; Young 2007). The extent of this variability, though, is not yet known. Additionally, whether these mechanical variabilities manifest in consistent patterns across the plateau remains unclear.

Similar to the tibial plateau, the trochlear and condylar regions of the distal femur are highly inhomogeneous (Swann and Seedhom 1993). Within the condylar regions, the medial condyle may be more compliant than the lateral femoral condyle (Barker and Seedhom 2001). Mediolateral variations across the trochlea have not been studied but the contact pattern of the patellofemoral joint preferentially loads the lateral aspect, followed by the medial and then grooved central regions (Han 2005; Powers 1998).

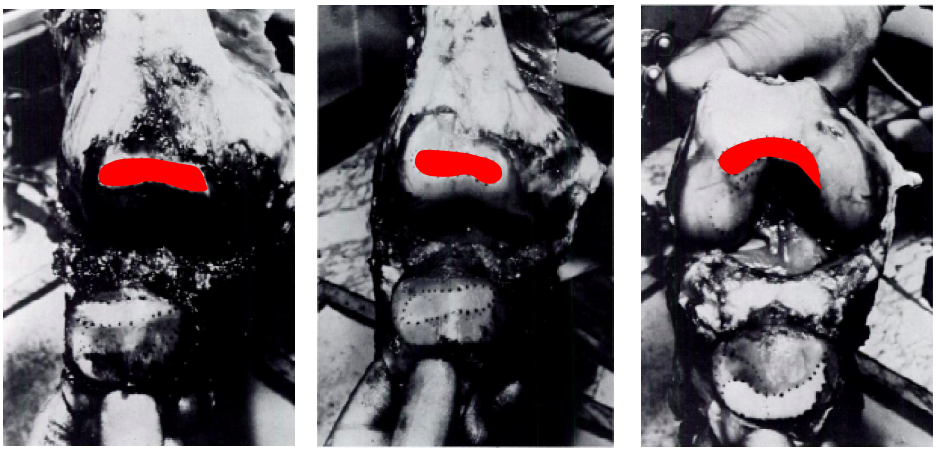

Figure 2.7: Patellar contact areas on the trochlea (highlighted in red) at 20, 45, and 90 degrees of knee flexion. Reproduced with permission and copyright © of the British Editorial Society of Bone and Joint Surgery, Goodfellow 1976.

A “weightbearing” mechanical dependence also has been suggested for the distal femur: areas of the condyles or trochlea that contact their respective opposing joint surfaces between -5° and 30° knee flexion are considered weightbearing regions and areas that tend to make contact only for knee flexion angles greater than 30° may be considered less weightbearing (Fig. 2.7)

(Goodfellow 1976; van Eijden 1986). Across the trochlea, AC of less weightbearing regions was found to be stiffer, thinner, and less permeable than AC of weightbearing regions (Froimson 1997). Although the mechanics have not been examined between the weightbearing classifications of the condyles, the less weightbearing regions tend to be thinner compared to weightbearing regions (Koo 2011) and this may translate to tissue mechanics (Eckstein 2001). The AC thicknesses of the external, central and inner thirds of each condyle also are unequal, and the relative differences depend on position along the length of the condyle (Hellio Le Graverand 2009; Li 2005a). Taken together, these findings suggest the presence of unique region-dependent mechanics for both the femoral and tibial AC surfaces although the details of these mechanics remain unknown.

2.4 Analytical Modeling of Articular Cartilage

Analytical modeling represents an important tool for investigating AC mechanics, injury, and disease processes. Analytical models of AC are numerous and range from simple homogeneous linear elastic to complex multi-phasic anisotropic viscoelastic formulations (Armstrong 1984; Cohen 1992; Gu 1997; Hayes 1972; Korhonen 2003; Kwan 1990; Lai 1991; Mak 1987; Mow 1989; Myers 1984; Parsons and Black 1977; Wilson 2005a; Woo 1980). The following sections provide a brief overview of several AC models.

2.4.1 Single-phase Linear Elastic Model

The simplest AC models treat the tissue as thin isotropic linear elastic layer (Hayes 1972; Sokoloff 1966). These models have been found to reasonably approximate initial ($t \rightarrow 0$) or equilibrium responses ($t \rightarrow \infty$) to small deformations. Single-phase isotropic linear elastic models are most commonly used in conjunction with indentation experiments, joint contact problems, and other scenarios in which time-, rate-, and direction-dependent effects are unimportant (Blankevoort and Huiskes 1996; Donahue 2002; Hori and Mockros 1976).

2.4.2 Single-phase Viscoelastic Models

Single-phase viscoelastic models were subsequently introduced to incorporate the time-dependent properties of AC. These formulations employed either mechanical spring-and-dashpot assemblies (Hayes and Mockros 1971; Parsons and Black 1977) or continuum-based approaches (Woo 1979; Woo 1980) to describe the creep response of the tissue. Recent work has revived this approach for replication of the creep indentation response of patellar AC (Keenan 2012). Like the linear elastic model, the single-phase viscoelastic is best suited for small deformations.

2.4.3 Linear Biphasic Model

The linear biphasic model provides an alternative approach to single-phase viscoelastic models for analyzing time-dependent AC behavior (Armstrong 1984; Mak 1986; Mak 1987; Mow 1977; Mow 1980). The model represents AC

as a porous incompressible linearly elastic solid filled with inviscid incompressible fluid. Tissue stress arises from two-components: elastic strain of the solid matrix and the frictional flow of fluid through the solid matrix. Time-dependent AC mechanics (i.e., creep and stress relaxation) are accounted for by the stress dissipation of these flow-independent and flow-dependent mechanisms. The linear biphasic model is highly utilized for confined compression (Armstrong and Mow 1982; Schinagl 1997), unconfined compression (Armstrong 1984; Brown and Singerman 1986), indentation (Athanasiou 1991; Spilker 1992), and joint contact (Ateshian 1994; Wu 1998) and represents the most popular AC modeling approach. The linear nature of the model, however, prevents it applicability to finite deformations. Likewise, its isotropic configuration neglects the depth- and region-dependent mechanical properties of the tissue. Test configurations in which relative fluid-solid velocity is low (e.g., unconfined compression) or strain rate dependence is important also pose a challenge for the model (Taylor and Miller 2006).

2.4.4 Variants on the Isotropic Linear Biphasic Model

Several approaches have been taken to improve the ability of the isotropic linear biphasic formulation to predict finite deformations, mechanical anisotropy, and rate dependence. To permit finite deformations, the biphasic model has been revised to include a hyperelastic solid phase (Holmes and Mow 1990; Kwan 1990). These finite deformation biphasic models have been successfully employed for several test configurations (Ateshian 1997; Suh and Bai 1998;

Wang 2001). Several biphasic implementations also replace the constant permeability of the linear model with an exponential term dependent on solid matrix strain (Lai 1981).

Poroviscoelastic (DiSilvestro and Suh 2002; DiSilvestro 2001; Huang 2001; Mak 1986; Setton 1993), viscoelastic fibril-reinforced biphasic (Fortin 2000; Li 1999; Soulhat 1999), and viscoelastic finite deformation biphasic (Li and Herzog 2004a; Li 2005b) models have been developed to provide strain rate dependence to the mechanical response. Tension-compression non-linearity can be accounted for through the conewise linear biphasic model, which successfully models different tension and compression responses in a single formulation (Li 2005b; Soltz and Ateshian 2000). Depth-dependent stiffness has been incorporated into linear biphasic and fibril-reinforced biphasic models (Ateshian 2009; Wilson 2007; Wilson 2005a; Wilson 2004). Transversely isotropic (Askew and Mow 1978; Lanir 1987a) and orthotropic (Bachrach 1998; Chegini and Ferguson 2010) linear biphasic models have also been developed to accommodate AC anisotropies.

2.4.5 Multiphasic Models

In recent years, a triphasic model has gained substantial traction (Lai 1991; Lu and Mow 2008; Sun 2004). This model extends the biphasic version with the additional consideration of the moveable ions as a third phase. The model predicts flow-dependent and -independent viscoelasticity, tissue swelling, and other electrokinetic behaviors (Mow and Guo 2002). Other multiphasic

continuum models and have also been proposed (Eisenberg and Grodzinsky 1985, 1987; Kovach 1996; Lanir 1987b).

2.4.6 Statistical Mechanics Models

Statistical mechanics is an alternative approach to continuum-based models presented in the previous sections. In this framework a material is represented as a cross-linked network of flexible molecular chains (Arruda 2011; Arruda and Boyce 1993) (Fig. 2.8). The chains, which can be analogized to "entropy springs," produce significant forces when stretched but have minimal resistance to compression, much like collagen fibrils. As the material is deformed, the chains rotate and stretch to accommodate the deformation, altering the statistical entropy of the chain network and producing network stress. These models have two key components: the mathematical description of the chains and the manner in which the chains are assembled to form a network. Some common chain models include the freely jointed chain model (Kühn and Grun 1942) and the MacKintosh chain model (MacKintosh 1995). These chains have been implemented into several different networks including the isotropic three-chain (Wang and Guth 1952), isotropic four-chain (Treloar 1946), isotropic eight-chain network (Arruda and Boyce 1993; Palmer and Boyce 2008) and orthotropic eight-chain network (Bischoff 2002).

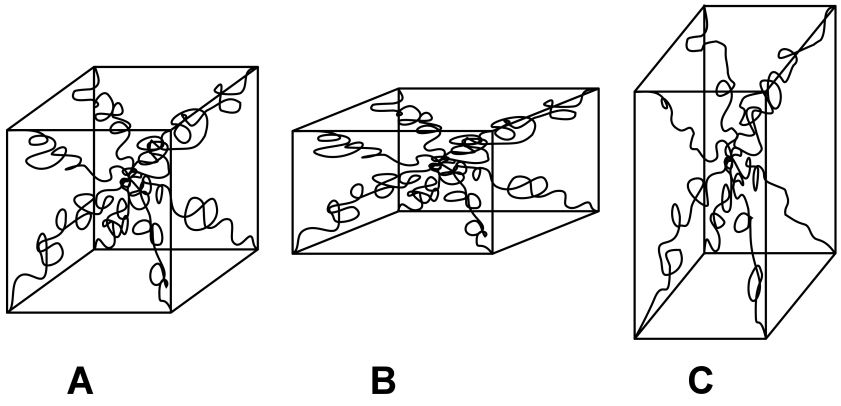

Figure 2.8: Eight-chain isotropic network model (a) undeformed, (b) in unconfined compression, and (c) in uniaxial tension. The chains rotate and stretch to accommodate each deformation state. Adapted from Arruda 2011.

Statistical mechanics models may be useful in the study of physiological AC mechanics because they offer the ability to predict finite deformations; utilize few parameters, each with direct physical meaning; proficiently predict non-linear, high rate viscoelastic behavior; and offer insight into the underlying physiological factors driving mechanical behaviors due to their mechanistic nature (Arruda 2011). Statistical mechanics models have been used to model multiple finite deformation states in elastic polymers (Boyce and Arruda 2000; Boyce 1994) and, more recently, in biological materials such as skin, cardiac wall, ligament, tendon, and cell cytoskeleton (Bischoff 2000, 2004; Kühl 2005; Ma 2010; Palmer and Boyce 2008). Recently, a statistical mechanics model was used to predict the non-linear response of knee AC compressed at 2.5% and 10% strain/sec (Brown 2009). The ability of a statistical mechanics formulation to model AC behavior under physiological strain rates has not yet been examined.

2.5 Summary

Knee OA is a musculoskeletal disease with widespread impact. Its debilitating physical and economic effects, limited treatment options, and rising prevalence among otherwise healthy young adults warrant immediate action to better understand, prevent, and treat this condition. Ostensibly, abnormal knee mechanics serve a critical role in the development and progression of OA. However, without thorough knowledge of the regional heterogeneity of the mechanical properties of healthy knee AC, the link between knee mechanics and OA remains unclear. Knowledge of the extent to which mechanical properties of healthy knee AC vary across the femoral and tibial surfaces is limited to studies utilizing non-physiological strain rates, sampling at relatively few locations on the joint surface, and/or including osteoarthritic specimens within the study population. Since previous studies utilized very low or very high spatial resolutions without any attempt to identify an optimal level, the spatial resolution required to adequately quantify these variabilities is currently unclear. Beginning with high resolution and simplifying until a minimum requirement is reached would be a reasonable, but not yet attempted, approach to this problem. Moreover, no study has attempted to identify patterns of regional variability in mechanical properties that present across individuals, which, if determined, would remove the limitation posed by requiring subject-specific cartilage properties in theoretical models. Thus, a critical need exists to evaluate the extent and pattern of mechanical variability of healthy human knee AC subjected to a physiologically relevant strain rate.

Likewise, computational models of the knee joint afford a powerful tool for investigating the link between knee mechanics and OA. However, their success depends on an accurate mathematical description of healthy AC mechanics under physiologically relevant loading conditions. While several analytical AC models are currently used, their ability to predict tissue response to the large strains and high strain rates associated with normal human activity is limited. Additionally, few models incorporate regional heterogeneity, which is likely critical to the development of OA. Consequently, an analytical model for AC that successfully predicts the heterogeneous, large deformation, high strain rate response of AC is required to thoroughly investigate the relationship between knee mechanics and OA.

Chapter 3: General Methods for Experimental Studies

Specific Aims 1 and 2 of this dissertation utilized similar methods, including the same cadaveric knees and mechanical testing techniques. For conciseness, these will be documented herein and referenced in subsequent chapters. For more detail of these methods please see Deneweth et al. (2013).

3.1 Knee Donors

Cadaveric knees were carefully chosen to ensure that healthy AC was used for the studies. Osteoarthritis is associated with increasing age and body mass index (BMI) (Blagojevic 2010; Muthuri 2011a). One in three individuals over the age of 65 has OA (Boyan 2012) and individuals with BMI > 30 kg/m^2 were shown to have a seven-fold higher risk of OA than individuals with BMI < 25 kg/m^2 (Toivanen 2010). Knee OA is also more prevalent among women and African-Americans (Felson 2000; O'Connor 2007; Srikanth 2005). The integrity of knee cartilage also can be compromised by physical trauma or alterations in normal gait patterns (Carter 2004; Muthuri 2011b; Toivanen 2010).

With these factors in mind, inclusion criteria for knee donors were the following:

a. Age between 18 and 55 years old
b. BMI less than 26 kg/m^2
c. Female
d. Caucasian

e. No medical history of OA, osteoporosis, lower limb injury or surgery, disease affecting lower limb coordination or gait

It should be noted that activity level, joint alignment, and genetic factors also might be linked to knee OA risk (McWilliams 2011; Sharma 2001a; Sharma 2001b) and in turn, the mechanical properties of knee AC. Data on these factors, however, were not available from the agencies that provided the cadaveric knees and therefore could not be controlled for directly.

Power analysis of preliminary data indicated that eight subjects should ensure a minimum of 80% power to detect significant differences. Therefore, eight unpaired fresh-frozen Caucasian female cadaveric knees were obtained for the studies related to Aims 1 and 2. Relevant demographic information is listed in Table 3.1. Mean age (± one standard deviation) was 49 ± 4 years and mean BMI was 17 ± 2 kg/m^2.

Table 3.1: Knee donor demographics

Donor	Side	Age (years)	BMI (kg/m^2)	Cause of Death
1	Left	41	19	Cancer, Brain
2	Left	52	20	Cancer, unspecified
3	Left	54	14	Cancer, Small Bowel
4	Right	51	19	Cancer, Lung
5	Right	51	16	Cancer, Lung
6	Right	49	14	Cancer, Breast
7	Left	52	19	Cancer, Appendix
8	Right	44	18	Neurofibrosarcoma

3.2 Mechanical Testing

The mechanical testing apparatus was a custom-built device (J. Deneweth, H. Iyer, K. Lapprich) designed for testing compliant materials at linear speeds up to 1000 mm/sec (Fig. 3.1). It consisted of a high-speed electric linear actuator (SMAC, Carlsbad, CA; positional accuracy: ±0.001 mm), a dynamic load cell (Dytran Instruments, Chatsworth, CA; sensitivity: 120 mV/N), a high-speed video camera (Photron USA, San Diego, CA; maximum frame rate: 5400 HZ), and a transparent acrylic water bath. The load cell was mounted at one end of the bath such that its sensing surface faced inward and was perpendicular to the line of action of the actuator rod. The actuator traveled horizontally directly in line with the load cell and entered the bath through the opposite end. Compression plates (Dytran Instruments, Chatsworth, CA; diameter: 15.78 mm) were attached to the facing ends of the load cell and the actuator rod. The camera was mounted over the water bath to record deformation of the AC specimen. Movements of the linear actuator were synced with force and camera data acquisition using a custom LabVIEW program (National Instruments, Austin, TX). This device has been successfully used to extract the compressive properties of foam (H. Iyer, unpublished Masters thesis, University of Michigan).

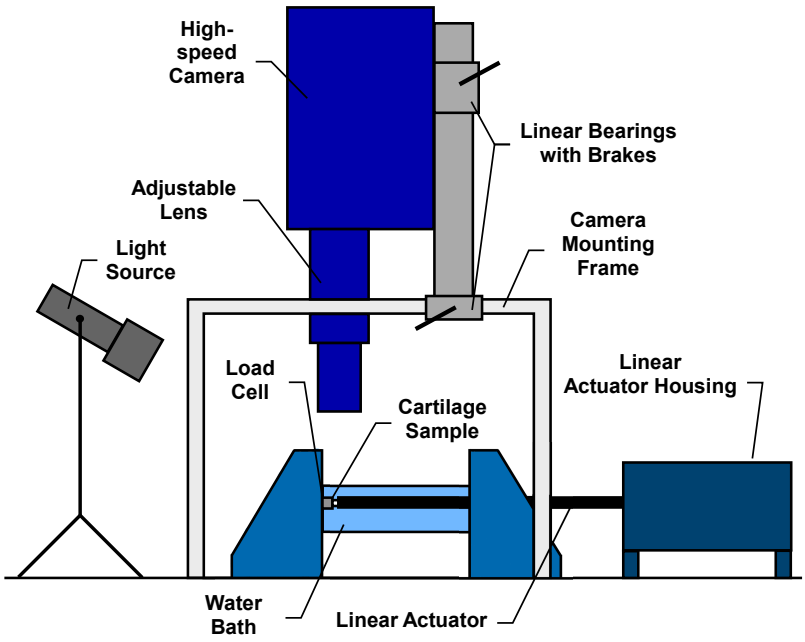

Figure 3.1: Schematic of the mechanical testing device used to test cartilage specimens in unconfined compression. Adapted from Deneweth 2013.

3.3 Parameters of Mechanical Test

Unconfined compression was used to extract the tissue's material properties at each site of interest (Jurvelin 2000; Jurvelin 2003). Since walking is the most common daily activity and gait mechanics are believed to play a role in OA development (Andriacchi 2009), the strain rate and peak strain for the test were selected to represent level-ground walking. For all pre-conditioning and experimental trials, the nominal strain rate was 100% strain/sec (Liu 2010; Mann and Hagy 1980). Peak displacement of the linear actuator was prescribed to equal 20% nominal strain of the AC sample. Each unconfined compression trial started at 0% strain followed by compression to peak strain and an immediate return to 0% strain. The cartilage specimen remained immersed in phosphate-

buffered saline (PBS) solution throughout the testing procedure. Ten pre-conditioning trials were used to ensure a consistent tissue response, based on pilot testing. Subsequently three separate experimental trials were conducted while simultaneous force and video data were collected at 125 Hz. Each test lasted 500 msec with an average of 62 frames of data collected. Several minutes were allowed between trials for the specimen to re-equilibrate with the surrounding solution.

3.4 Strain Analysis of the Tissue

The strain of the AC specimen was determined from digital image correlation (DIC) (Ma 2010; Moerman 2009). Immediately prior to testing, a random speckle pattern was applied along the thickness of the specimen using black India ink (Fig. 3.2). Care was taken to cover the entire surface of the specimen that was viewable by the camera. The speckle pattern was subsequently used to optically track the deformation of the tissue using VIC-2D 2009 software (Correlated Solutions, Columbia, SC) (Ma 2010; Ma 2012).

Strain computation began with defining an area of interest (AOI) in the first video frame of the trial (Fig. 3.3). The AOI was selected based on these criteria:

1. Speckle pattern was present throughout
2. Entire thickness of the specimen was covered
3. Edges of the specimen that curve out of the camera plane were not included
4. Centered near the vertical midline of the specimen

Note: when all criteria could not be met simultaneously, the criteria were prioritized in the order in which they are listed.

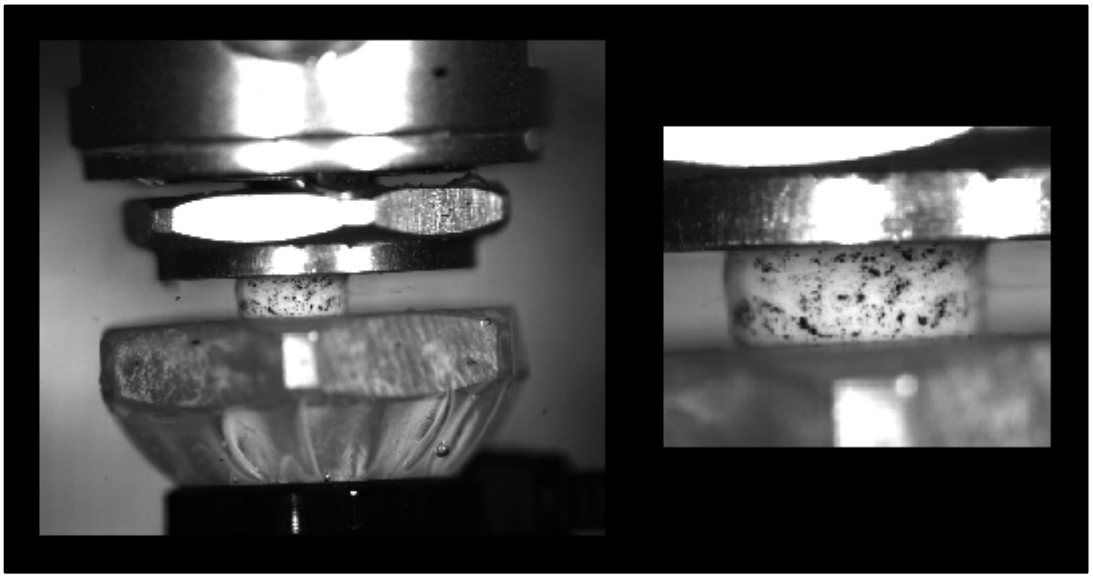

Figure 3.2: Cartilage sample as viewed from overhead camera. The sample is situated between the load cell (top) and actuator (bottom). A speckle pattern has been applied to the side of the sample (black dots). The right-hand image is a close-up view of the cartilage shown at the left.

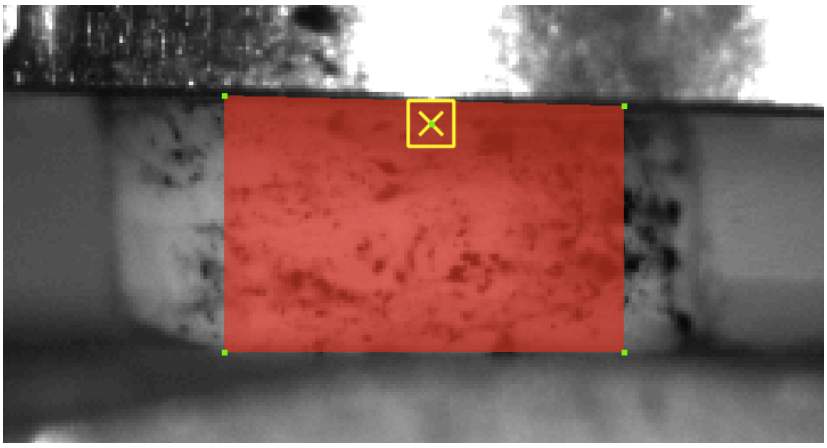

Figure 3.3: Example of the placement of the area of interest (red) and subset box (yellow) for performing digital image correlation strain analysis.

Once an AOI was selected, a subset box, which established the amount of pattern that will be used to track local deformations, was placed near the top and midline of the tissue (Fig. 3.3). The subset box subsequently scanned through the entire AOI, identifying the unique speckle pattern within the subset box at each step. Once it identified local speckle patterns in the first video frame (undeformed sample), it repeated the scanning process for each subsequent frame. Speckle patterns in the current frame were correlated with the previous frames to compute local strains. The software parameters for the analysis were selected to maximize the tracking resolution and minimize untracked areas:

a. Subset box
    i. Box size: 11 (pixels)
    ii. Step size: 1 (pixel)
b. Correlation:
    i. Interpolation: Optimized 8-tap
    ii. Criterion: Normalized squared differences
    iii. Subset weights: Gaussian weights,
    iv. Search: Exhaustive search, Incremental correlation
c. Strain computation:
    i. Filter size: 15 (pixels)
    ii. Filter: Decay filter
    iii. Tensor type: Lagrange

The software computed local deformations of the speckle pattern throughout the AOI for each frame of the trial and converted them to local Lagrangian strains (Fig. 3.4). The local strains were exported to Matlab (Mathworks, Natick, MA) to be converted to average axial strain for the proximal, middle, and distal thirds of the tissue (Fig. 3.5). Strain was found to be

inhomogeneous throughout the thickness of the tissue, so the average axial strain was used for all analyses (Fig. 3.5).

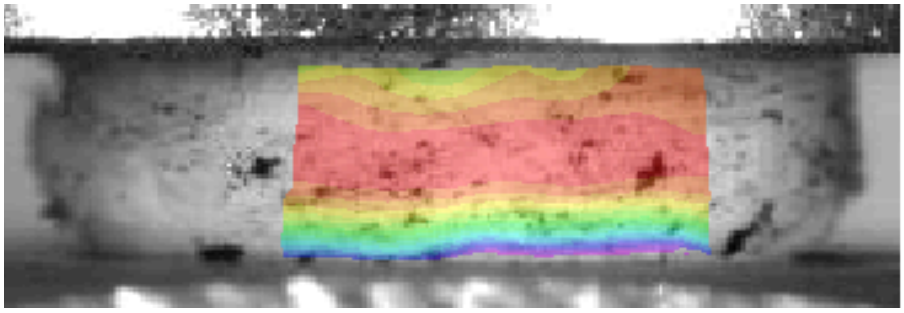

Figure 3.4: Contour map of local axial strain computed in VIC-2D along the thickness of the specimen. Colors indicate relative strain: red – least compression, purple – most compression.

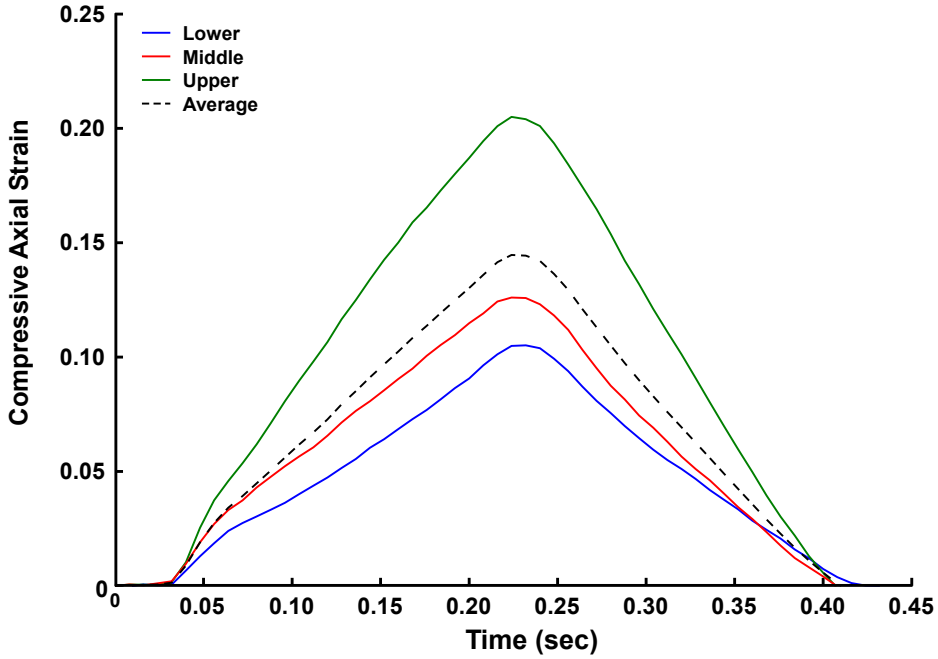

Figure 3.5: Axial compressive strain gradient for a cartilage specimen. Colored lines represent average local strain for the upper, middle, and lower thirds of the tissue. The average strain (dashed line) for the whole tissue was used to compute the stress-strain response curves and the moduli.

3.5 Determination of Cartilage Modulus

The non-linear nature of AC necessitated that the modulus be computed at a predetermined level of stress or strain. Since the mechanical test was strain-driven, a constant physiological strain of 10% was selected for modulus calculations. The modulus of each AC specimen was computed from the loading portion (rise) of the nominal stress-strain curve using Matlab. Nominal strain for each video frame was obtained as detailed in Section 3.4. Nominal stress was calculated by dividing the force of the current frame by the undeformed cross-sectional area of the specimen. The raw nominal stress was plotted versus the raw nominal strain for each trial. An exponential equation, $y = Ae^{bx}$, was fit to the raw data to smooth any noise in the nominal stress curve (Fig. 3.6).

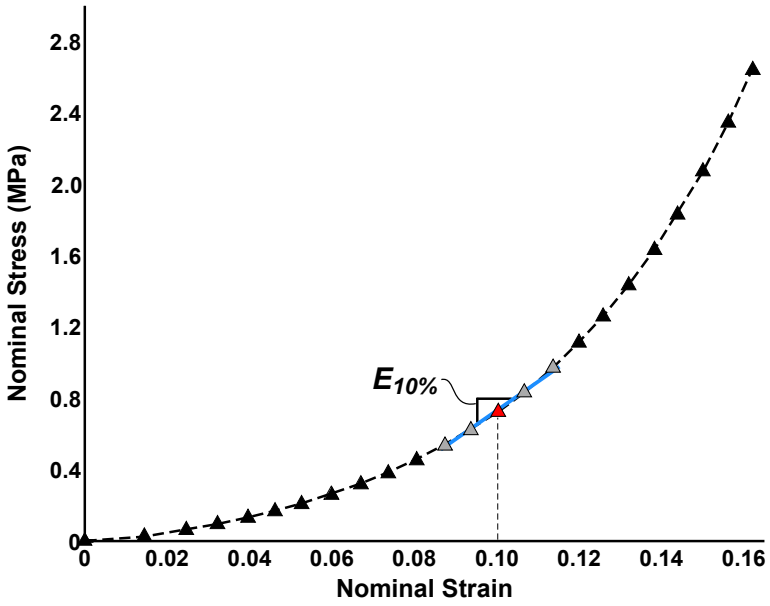

Figure 3.6: Calculation of $E_{10\%}$. The dashed line and triangles represent the smoothed stress-strain curve and its discrete data points, respectively. A line of best fit (blue) was drawn through Point A (red triangle) and the four data points surrounding it (gray triangles). $E_{10\%}$ was computed as the slope of the blue line.

The tangent modulus at 10% strain, $E_{10\%}$, was calculated by fitting a line to the smoothed stress-strain curve at 10% strain. First, the data point whose strain (x-value) was nearest to but not less than 10% strain was identified. This point was subsequently referred to as Point A with coordinates (x_a, y_a). Then, the relative x distance of A from 10% strain was calculated as:

$$d_{rel} = \frac{x_a - 0.10}{x_a - x_{a-1}} \tag{3.1}$$

The number of data points used to compute the modulus line was determined from d_{rel} according to Table 3.2. The line of best fit to the selected points was calculated (Fig. 3.6), and $E_{10\%}$ was defined as the slope of this line.

Table 3.2: Criteria for selecting data points to compute $E_{10\%}$.

	Number of points before (x_a, y_a)	Number of points after (x_a, y_a)	Total number of points including (x_a, y_a)
$0 \leq d_{rel} < 0.25$	2	2	5
$0.25 \leq d_{rel} < 0.75$	2	1	4
$0.75 \leq d_{rel} < 1.00$	3	1	5

* (x_a, y_a) is the smoothed stress-strain datapoint whose compressive strain is closest to but not less than 10% strain.

Chapter 4: Heterogeneity of Tibial Plateau Cartilage in Response to a Physiological Compressive Strain Rate

A manuscript based on the research presented in this chapter has been previously published:

Deneweth JM, Newman KE, Sylvia SM, McLean SG, Arruda EM (2013). Journal of Orthopaedic Research **31**(3):370-75.

4.1 Abstract

Knowledge of the extent to which tibial plateau AC displays non-uniform mechanical topography under physiologically relevant loading conditions is critical to evaluating the role of biomechanics in knee OA. Cartilage explants from 21 tibial plateau sites of eight non-osteoarthritic female cadaveric knees (age: 41-54; BMI: 14-20) were tested in unconfined compression at 100% strain/sec. The elastic tangent modulus at 10% strain ($E_{10\%}$) was calculated for each site and averaged over four geographic regions: not covered by meniscus (I); covered by meniscus – anterior (II); covered by meniscus – exterior (III); and covered by meniscus – posterior (IV). A repeated-measures mixed model analysis of variance was used to test for effects of plateau, region, and their interaction on $E_{10\%}$. Effect sizes were calculated for each region pair. $E_{10\%}$ was significantly different ($p < 0.05$) for all regional comparisons, except I – II and III – IV. The regional pattern of variation was consistent across individuals. Moderate to strong effect sizes were evident for regional comparisons other than I – II on the lateral side and III – IV on both sides. Healthy tibial AC exhibits significant

mechanical heterogeneity that manifests in a common regional pattern across individuals. These findings provide a foundation for evaluating the biomechanical mechanisms of knee OA.

4.2 Introduction

Knee OA has been suggested to develop via joint biomechanical mechanisms (Andriacchi 2009; Andriacchi 2004; Astephen 2008; Deneweth 2010; Fleming 2005; Ristanis 2003; Sharma 2001b). Altered knee biomechanics, due to injury or malalignment for example, may shift the AC contact pattern from regions well-adapted to specific loading patterns to regions poorly suited for such loads, inducing a deleterious AC stress state (Andriacchi 2006; Carter 2004; Chaudhari 2008). Recent research supports this tenet; individuals with increased anterior tibial translation following anterior cruciate ligament injury demonstrated strong signs of early AC degeneration (Haughom 2012). A clear link between knee mechanics and OA initiation within the human joint, however, remains to be established.

Detailed knowledge of the mechanical response of healthy tibiofemoral joint AC is critical in ascertaining a direct link between abnormal knee mechanics and OA. While OA presents on both the tibial and femoral surfaces, the unique interplay between the tibial plateau and the overlaying menisci potentiates large AC mechanical variability (Shepherd and Seedhom 1999a) and provides a logical starting point for such an investigation. Tibial AC appears to exhibit inhomogeneity across its surface (Swann and Seedhom 1993; Thambyah 2006;

Young 2007), but the extent to which it manifests under physiological load states is largely unknown. Studies that provided detailed mapping of human tibial AC mechanics used measurement techniques that do not reflect the short loading periods (i.e. 15-300 msec) and high strain rates (i.e., 50-1000%/sec) experienced by knee AC *in vivo* (Liu 2010; Swann and Seedhom 1993). Those that have examined AC mechanics under more physiologically relevant conditions did not provide detailed data for the entire tibial surface or included test specimens with OA (Barker and Seedhom 2001; Shepherd and Seedhom 1999a; Thambyah 2006; Young 2007). The accuracy with which these findings can be extrapolated to model and interpret the response of the entire AC surface under *in vivo* loading conditions remains uncertain.

If biomechanical mechanisms of knee OA are to be successfully understood, then there is a critical need to assess tibial AC mechanics for non-osteoarthritic human tissue under physiological loading conditions, across the entire tibial surface, and with high spatial resolution. Additionally, if these data could be utilized to develop a universal template of AC mechanics, current *in-vivo* screening and treatment modalities designed to combat OA progression would be greatly enhanced by removing the need for subject-specific tissue properties. The aim of this study, therefore, was to determine the extent to which non-arthritic human proximal tibial AC exhibited regional mechanical properties under physiologically relevant loading. We hypothesized that (1) the mechanical properties of AC covering the proximal tibia are spatially heterogeneous across

the tibial plateau, and (2) the mechanical inhomogeneity of proximal tibial AC manifests in a consistent regional pattern across individuals.

4.3 Methods

4.3.1 Knee Donors

Cadaveric knees were used to obtain the AC samples. Inclusion criteria are documented in **Section 3.1** and demographic data for the donors of the eight knees used in this study is listed in Table 3.1.

4.3.2 Cartilage Samples

To obtain the AC explants, each knee was dissected to expose the tibial articular surface. The inner boundary of each meniscus was outlined on the cartilage surface with black India ink, indicating its position in the unloaded knee at 0° of knee flexion, and then removed. A 4 x 3 grid pattern was drawn onto each plateau using black India ink such that a maximum amount of the plateau fell under the grid. The typical grid cell measured five millimeters mediolateral by eight millimeters anteroposterior. Full thickness cylindrical AC explants without subchondral bone were extracted from the center of 21 cells (Fig. 4.1) of the grid using a 4-mm diameter round-hole hand punch (McMaster-Carr, USA) and a surgical scalpel (Lewis 1998). Explants were not removed from regions of fibrillated cartilage, as identified by an India ink test (Meachim 1972). Each explant was stored in PBS solution at -20°C until testing (Krishnan 2003; Ronken

2012), which has been found to maintain the mechanical integrity of the tissue (Szarko 2010).

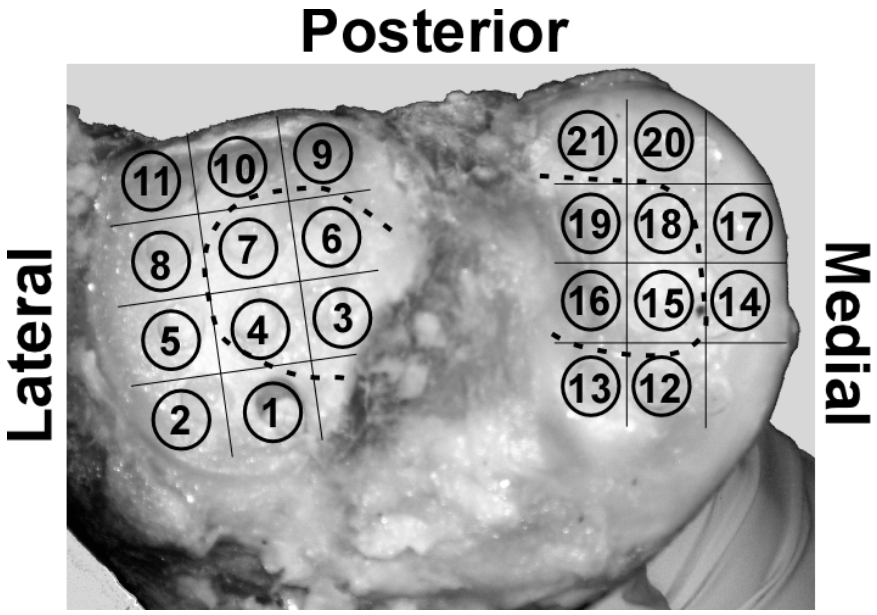

Figure 4.1: Numbered test sites on the tibial plateau from which cartilage explants were procured. Solid lines represent the applied grid pattern used to define the test sites. Dashed lines denote typical inner margins of the menisci.

4.3.3 Mechanical Testing Procedure

Diameter and thickness measurements were obtained using digital vernier calipers (resolution: 0.01 mm, Mitutoyo America Corporation, Aurora, IL) once the explant had completely thawed in the PBS bath. Sample thicknesses ranged from 0.9 - 4.4 mm. A speckle pattern was applied to the cylindrical surface of the cartilage sample using black India ink, as detailed in **Section 3.4**. The AC explants were tested using the device described in **Section 3.2**. The explant was situated between the force sensor and actuator rod under a minimal (0.2 N) tare load and allowed to equilibrate for 10 minutes (Jurvelin 2003). Testing proceeded

as detailed in **Section 3.3** with ten pre-conditioning cycles and three experimental trials of 100% strain/sec unconfined compression.

4.3.4 Data Analysis

The average nominal stress and strain was computed for each experimental trial according to the methods outlined in **Section 3.4** (VIC-2D 2009, Correlated Solutions, Columbia, SC). $E_{10\%}$, the elastic modulus at 10% strain, was subsequently calculated from the nominal stress-strain curve (details can be found in **Section 3.5**). The mean and standard deviation of $E_{10\%}$ at each (n = 21) site was determined. Based on pilot data and published methods for quantifying regional variations in tibial geometry (Eckstein 2008; Swann and Seedhom 1993), we hypothesized that the medial and lateral plateaus each could be divided into four explicit regions: not covered by meniscus; covered by meniscus – anterior; covered by meniscus – exterior; and covered by meniscus - posterior. Therefore, the 21 test sites were grouped into these four regions (Fig. 4.2) and the region-based means and standard deviations of $E_{10\%}$ were calculated.

4.3.5 Statistical Analysis

The mean regional values of $E_{10\%}$ were submitted to a repeated-measures mixed model analysis of variance (ANOVA) to test for the effects of plateau (medial or lateral), region (n=4), and the interaction of plateau*region (n=8). Bonferroni-adjusted pairwise comparisons were made for all main effects. An

alpha level of 0.05 denoted significance. The mixed model analysis was conducted using SAS 8.0 statistical software (SAS Institute Inc., Cary, NC). The effect size between two regions on the same plateau was evaluated using Cohen's d (Cohen 1988):

$$d_{AB} = \frac{\bar{E}_{10\%,B} - \bar{E}_{10\%,A}}{s_P} \tag{4.1}$$

where d_{AB} was the effect size between Regions A and B and $\bar{E}_{10\%,A}$ was the mean value of $E_{10\%}$ for Region A. s_P was the pooled standard deviation of Regions A and B calculated as:

$$s_P = \sqrt{\frac{{s_A}^2(n_A - 1) + {s_B}^2(n_B - 1)}{n_A + n_B}} \tag{4.2}$$

where n_A is the number of samples in Region A. The cut-off levels of d_{AB} for small, moderate, and strong effect sizes were 0.2, 0.5, and 0.8, respectively.

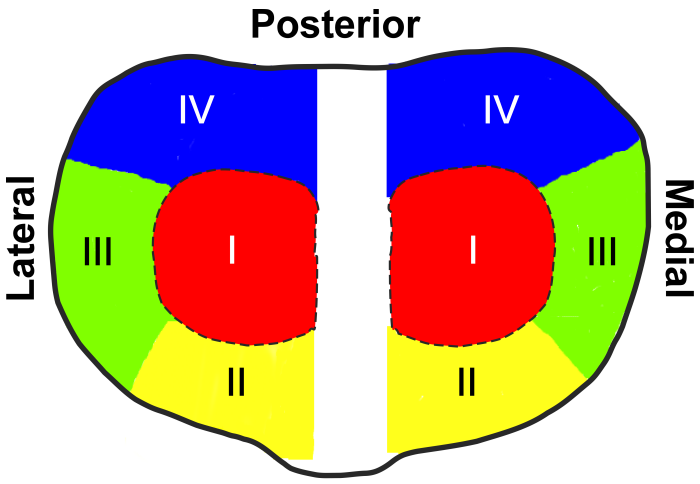

Figure 4.2: For regional analysis, the tibial plateau was divided into the medial and lateral compartments. Each compartment was divided into four regions: I - not covered by meniscus and II - IV anterior, exterior, and posterior one-thirds of the meniscus-covered area, respectively.

4.4 Results

4.4.1 $E_{10\%}$ by Test Site

Of the 168 explants, 40 were excluded due to surface fibrillation identified by staining with India ink, damage incurred during extraction, or an inability to elicit peak strains greater than 10%. For the remaining explants, the stress-strain response under 100% strain/sec loading varied considerably (Fig. 4.3). Laterally, $E_{10\%}$ ranged from 4.69 MPa in the center of the plateau to 20.40 MPa on its posterior edge (Fig. 4.4). Similarly for the medial plateau, $E_{10\%}$ ranged from 7.01 MPa in the center to 30.83 MPa at the posterior margin (Fig. 4.4).

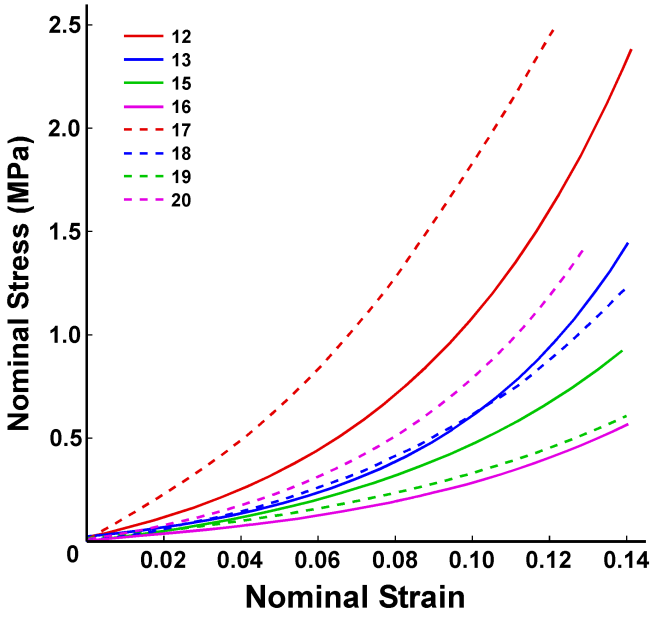

Figure 4.3: Sample stress-strain curve for eight cartilage explants taken from different sites on the same medial plateau. Under a strain rate of 100% strain/sec, the explants demonstrated large differences in overall stiffness despite being from the same knee. The explants from meniscus-covered sites generally displayed steeper responses compared to sites not covered by meniscus.

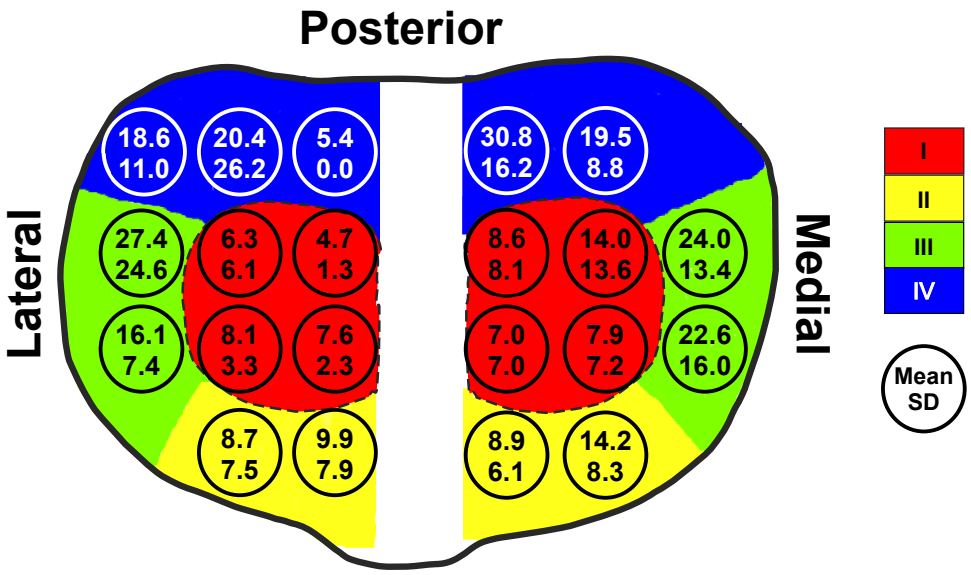

Figure 4.4: Mean and standard deviation of $E_{10\%}$ (MPa) across the tibial plateau. The color mapping identifies the four regions into which the site data were grouped for statistical analysis. Dashed lines denote the inner margins of the menisci and circles indicate test sites.

4.4.2 $E_{10\%}$ by Region

Mixed model analysis revealed that when the 21 sites were grouped into the four pre-defined regions statistically significant differences in $E_{10\%}$ were evident (Fig. 4.5). A significant main effect of region was found, $F(3,20) = 14.71$, $p < 0.0001$. Planned comparisons revealed that region I had a significantly lower value of $E_{10\%}$ compared to region III and region IV ($p < 0.001$ for both cases). Similarly, region II was significantly less stiff than regions III and IV ($p = 0.003$ and $p < .001$, respectively). No significant differences were present between regions I and II ($p = 1.00$) and regions III and IV ($p = 1.00$). Examining the effect sizes for these two comparisons (Table 4.1), the mean differences between III and IV were weak or small, whereas between I and II the difference was moderate on the medial plateau and nearly moderate on the lateral plateau.

There was no significant effect on $E_{10\%}$ due to medial or lateral plateau, $F(1,7) = 1.61$, $p = 0.245$, and no interaction of region*side, $F(3,17) = 0.15$, $p = 0.928$.

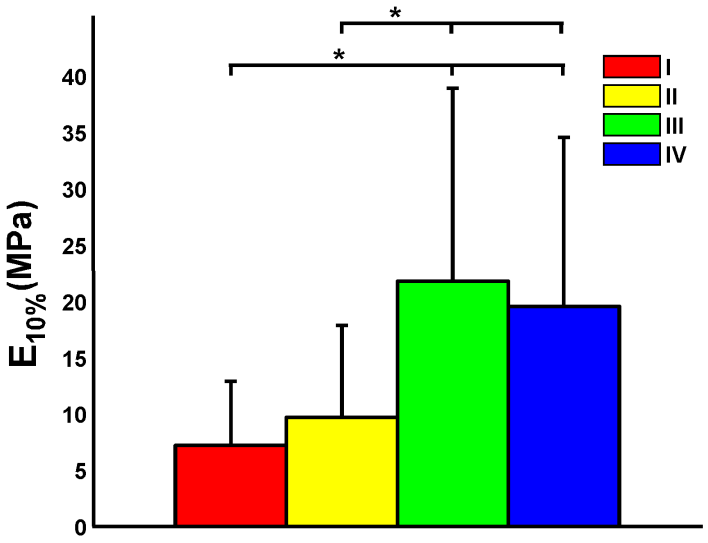

Figure 4.5: Mean $E_{10\%}$ (MPa) across the four pre-defined regions of the tibial plateau. Bars represent one standard deviation. Statistically significant ($p < 0.05$) differences between regions are indicated by *. Regions I and II were similar in magnitude and significantly less stiff than regions III and IV, which did not differ significantly from each other.

In order to examine the consistency of the regional differences across knees, the regional patterns of $E_{10\%}$ in each of the eight knees tested were compared qualitatively. Since no statistically significant differences were observed in $E_{10\%}$ between plateaus, data from both plateaus were averaged for this analysis (Fig. 4.6). A consistent pattern was evident across the eight knees, where regions I and II were similar to each other and substantially less stiff than regions III and IV, which were also similar to each other.

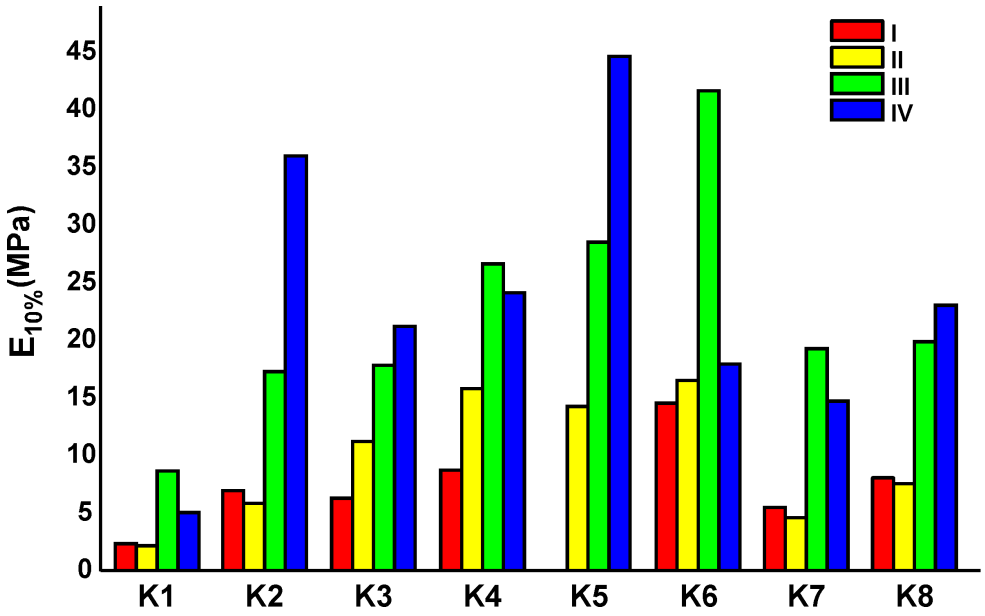

Figure 4.6: Mean $E_{10\%}$ (MPa) across the four pre-defined regions of the tibial plateau for each knee. K1 indicates Knee 1. A consistent pattern is evident across all eight knees, with regions I and II softer than regions III and IV. No data is available for region I of K5 due to compromised cartilage quality in that area of the plateau.

Table 4.1: Mean, sample size (n), confidence interval (CI), and effect size (d_{AB}) for difference in $E_{10\%}$ (MPa) between regions

		I – II	I – III	I – IV	II – III	II – IV	III – IV
Lateral	**Mean**	2.40	15.49	13.29	13.09	10.89	-2.20
	n	33	33	31	30	28	28
	95% CI	(-1.55, 6.36)	(6.53, 24.45)	(5.08, 21.49)	(2.73, 23.44)	(1.23, 20.54)	(-15.77, 11.37)
	d_{AB}	0.43	1.23	1.21	0.95	0.88	0.13
	Effect	Small	Strong	Strong	Strong	Strong	Weak
Medial	**Mean**	4.04	15.49	18.79	11.46	14.75	3.29
	N	38	41	43	25	27	30
	95% CI	(-0.88, 8.96)	(9.14, 21.85)	(12.72, 24.85)	(1.93, 20.99)	(5.65, 23.85)	(-6.78, 13.37)
	d_{AB}	0.60	1.62	1.97	1.00	1.31	0.24
	Effect	Moderate	Strong	Strong	Strong	Strong	Small

4.5 Discussion

Characterizing the response of healthy tibial AC to physiological loading rates is critical to determining and counteracting the mechanism(s) of knee OA development and progression. This study uniquely addressed this need by quantifying the tissue's stress-strain response under a physiologically relevant strain rate at 21 sites across eight non-osteoarthritic human tibial plateaus. Study outcomes confirmed that tibial AC exhibits non-uniform, region-specific properties. Furthermore, these regional mechanical variations are consistent across knee specimens, indicating that they may represent universal trends for the study population.

The loading parameters used (100% strain/sec and 20% peak strain) were consistent with those recently observed for *in-vivo* AC deformation during the stance phase of gait (Liu 2010). AC displayed values of $E_{10\%}$ that ranged from 1.0 – 80.0 MPa, which agrees well with the work of previous authors (Shepherd and Seedhom 1999a; Young 2007). Thus, the reported stress-strain behaviors reflected those likely to occur under true physiological loading conditions. The lateral and medial tibial plateaus were divided into 11 and 10 test sites, respectively, to ensure that the most locations could be consistently sampled on each plateau. A large variation in $E_{10\%}$ was evident across the surface, with the stiffest locations exhibiting $E_{10\%}$ nearly five times larger than $E_{10\%}$ at the most compliant sites.

Significant differences in $E_{10\%}$ were observed when averaged and compared across four respective regions of the medial and lateral plateaus.

Reducing the 21 tibial surface sites into these regions afforded more tractable and clinically relevant inferences regarding relationships between AC contact patterns and tissue mechanics. For the medial and lateral plateaus, regions I (i.e., not covered by meniscus) and II (i.e. anterior third of the meniscus-covered area) consistently displayed the lowest average $E_{10\%}$. Regions III and IV (i.e., exterior and posterior meniscus-covered, respectively) were stiffer than I and II, but were minimally different from each other in terms of $E_{10\%}$. These findings suggest that much of the variability in the mechanical response of tibial AC can by adequately represented by three, rather than four, distinct regions, contrary to our initial hypothesis. These regions, listed in order of increasing stiffness, are: meniscus-uncovered, anterior meniscus-covered, and exterior-posterior meniscus-covered. This result indicates that significant variability exists not only between meniscus-covered and meniscus-uncovered regions but also within the meniscus-covered area.

The regional pattern of $E_{10\%}$ does not appear to be subject-specific in the study population. Additionally, the plateau (lateral or medial) from which the explant was taken did not contribute significantly to $E_{10\%}$. Taken together, these findings suggest that the regional mapping presented herein could serve as a template for healthy tibial AC stiffness within this population.

The significant regional variations observed in the AC mechanical response to physiological loads provide new insights for a potential mechanism of OA development. During ambulatory gait, primary AC deformation typically occurs in the center of the plateau where the AC is not covered by meniscus (i.e.,

region I) (Andriacchi 2009; Carter 2004). Since this region was the most compliant, it appears well adapted to sustaining large deformations, such as at heel strike, without concomitant damage to the tissue structure. Adjacent test sites exhibited substantially different tangent elastic moduli, suggesting that a few-millimeter shift from the normal contact pattern may move primary loading to stiffer and perhaps less suitable regions (e.g., regions III and/or IV). Depending on concurrent changes in AC contact area and in the percentage of load born by the menisci, similar magnitude deformations in these regions, which are 3-4 times stiffer than region I, could produce substantially larger stresses in the tissue. Several studies have shown that knees with a surgically reconstructed anterior cruciate ligament display increased anterior tibial laxity and external tibial rotation during demanding functional tasks compared to their uninjured contralateral knee or healthy control knees (Almekinders 2004; Deneweth 2010; Tashman 2007). These altered joint kinematics could shift primary knee joint contact to stiffer, less optimal tibial AC regions (Haughom 2012; Oiestad 2010; Salmon 2006). Further research is needed to determine, given the findings of the present study, whether such kinematic changes identified *in vivo* can indeed promote OA development. Additionally, as osteoarthritic lesions are also highly prevalent on the femur (Wirth 2009) work must be done to characterize the mechanical variability of femoral AC (**Chapter 5**).

Several factors should be considered when interpreting the results of this study. First, the AC mechanical response was characterized using a single parameter, $E_{10\%}$, to afford comparison with previous literature. This parameter,

while insightful, does not fully capture the mechanics of non-linear tissue. A more comprehensive data analysis using non-linear analytical models is forthcoming (**Chapter 7**). Second, the menisci are known to translate as much as ten millimeters posteriorly over the tibia during knee flexion (Thompson 1991). Thus, some of the AC sites may experience both meniscus-uncovered and meniscus-covered loading during the course of the gait cycle rather than the single type of loading that their regional (I-IV) characterization suggests. This may explain some of the variability found in $E_{10\%}$ within each region. Third, as AC is a viscoelastic tissue with strain rate dependent properties (Oloyede 1992), extrapolation of these findings to describe the response of AC under higher rate loading, such as during running or jumping, must be done with caution. Finally, the applicability of these results to the general population is limited. The sex, race, age, and knee health of the donors for this study were tightly controlled to reduce inter-subject variability. Additionally, the specimens' BMIs were lower than the average population, and activity level and limb alignment information were not available.

Chapter 5: Distal Femoral Cartilage Exhibits Common Spatial Stiffness Patterns In Response To Dynamic Loading

A manuscript related to the research presented in this chapter has been submitted for consideration of publication:

Deneweth JM, Pomeroy SM, Arruda EM, McLean SG (2013). Journal of Biomechanics. *In review.*

5.1 Abstract

Spatial heterogeneity of knee AC mechanical properties has been posited to influence knee OA development. However, the extent of mechanical heterogeneity of distal femoral AC under high strain rate loading is not known. It is also unknown whether the heterogeneity forms a common regional pattern across individuals, which would be valuable to the study of knee OA. We hypothesized that the mechanical stiffness of distal femoral AC significantly varies across the femoral surface in a spatial pattern that depends on mediolateral location and frequency of weightbearing contact. Cartilage explants were obtained from 29 sites on the trochlea (9) and condyles (20) of eight non-osteoarthritic cadaveric femurs and tested in unconfined compression at a walking-like strain rate of 100% strain/sec. Mean elastic tangent modulus at 10% strain ($E_{10\%}$) was determined for each site. Statistical analyses examined whether variability in $E_{10\%}$ could be explained by spatial location on the distal femur. $E_{10\%}$ varied by over 400% across the distal femoral surface in a consistent regional manner. Within the trochlea, $E_{10\%}$ of the lateral aspect was significantly higher

than $E_{10\%}$ of the central and medial regions. Condylar $E_{10\%}$ was significantly lower in the anterior weightbearing region compared to the posterior portion of the condyle. Taken together, these results indicate that distal femoral AC exhibits large variations in its mechanical stiffness that follow distinct patterns in the trochlea and condyles and that these patterns are consistent across individuals. Identification of common mechanical patterns may reveal insight into the development of OA across the distal femur.

5.2 Introduction

Articular cartilage serves an essential role in healthy knee function by establishing nearly frictionless joint articulation and dissipating joint loads (Mow and Guo 2002). Deterioration of AC leads to OA, a debilitating disease commonly characterized by significant pain, swelling, and loss of mobility (Buckwalter 2005). The cause of knee OA remains unclear but joint contact mechanics are believed to play a significant role in the disease process (Andriacchi and Mundermann 2006). Since the loading pattern within the knee joint is non-uniform (Feller 2007; Koo and Andriacchi 2007), knee AC is posited to possess similarly non-uniform mechanical properties (Andriacchi 2009; Swann and Seedhom 1993). A shift in the joint contact pattern due to an abnormal mechanical profile, therefore, could alter the strain pattern in the AC and initiate osteoarthritic degeneration. Understanding the extent to which joint mechanics influences OA development relies on developing a clear understanding of the mechanics of knee AC under loading scenarios relevant to daily living, i.e. normal

gait. Regional variations in the elastic tangent modulus of healthy human tibial AC have been detailed in **Chapter 4**. A regional mechanical analysis, however, has not been published for AC covering the distal femur, the other major articulating surface of the knee.

The degree of mechanical non-uniformity in healthy human distal femoral AC, particularly when subjected to a physiologically relevant loading rate, is not well known. Since knee OA may be linked to abnormal gait mechanics (Andriacchi 2009), examining AC's mechanical properties under a strain rate consistent with that experienced *in vivo* during normal gait would lend important insight into the disease process. Comparison of the two articulating regions of the distal femur, the trochlea that articulates with the patella and the condyles that articulate with the tibia, indicates that trochlear AC tends to be more compliant than condylar cartilage (Barker and Seedhom 2001; Shepherd and Seedhom 1999a). A mapping of the two-second creep modulus at 50 sites across the distal femur suggested that substantial mechanical variability also occurs within the trochlea and condylar regions (Swann and Seedhom 1993). However, detailed examination of mechanical variability within either region has not yet been undertaken at a physiological strain rate.

The proximal one-third of the trochlea and the anterior portion of the condyles primarily contact the opposing articulating surface between 0° and 30° knee flexion (Goodfellow 1976; Li 2005a; Seedhom 1979), which is also the range of motion for level-ground walking (Mann and Hagy 1980). Consequently these regions can be classified as more-frequently weightbearing and the

remaining area of each surface as less-frequently weightbearing (Froimson 1997; Garg and Walker 1990; Goodfellow 1976). In the tibia, the more-frequently weightbearing center of the plateau tends to have more compliant AC compared to the less-frequently weightbearing periphery (**Chapter 4**). It is plausible that a similar situation occurs with the femur. Additionally, the distal femur may have non-uniform joint contact patterns mediolaterally that could create mediolateral mechanical gradient (Garg and Walker 1990; Goodfellow 1976; Koo and Andriacchi 2007, 2008).

Since OA lesions manifest in unique patterns within the trochlea and condyles (Bae 2010; Cohen 2003; Seedhom 1979), knowledge of the mechanical heterogeneity of each region could reveal important insight into the corresponding OA disease processes through improved clinical understanding of the AC's mechanical susceptibilities and more accurate computational knee models. Thus, the aim of this study was to determine the extent to which non-arthritic human distal femoral AC exhibits regional mechanical properties under physiologically relevant loading. We hypothesized that (1) the mechanical properties of AC covering the distal femur are spatially heterogeneous across the femoral trochlea and condyles, and (2) the mechanical inhomogeneity of distal femoral AC manifests in a consistent regional pattern across individuals.

5.3 Methods

5.3.1 Knee Donors

Cadaveric knees were used to obtain the AC samples. Inclusion criteria are documented in **Section 3.1** and demographic data for the donors of the eight knees used in this study is listed in Table 3.1.

5.3.2 Cartilage Samples

Each knee was dissected free of all tissue, including the patella and patellar tendon, and disarticulated from the tibia to expose the distal femoral surface. Samples were not removed from regions of fibrillated AC identified by an India ink test (Meachim 1972). A 3 x 3 grid pattern was drawn onto the trochlear surface using black India ink such that a maximum amount of the region fell under the grid (Fig. 5.1) (Swann and Seedhom 1993). The typical grid cell measured 10 mm mediolateral by 13 mm proximodistal. Similarly, each condyle was covered with a 2 x 5 grid pattern, with grid cells approximately measuring 12 by 15 mm (Fig. 5.1). Full thickness cylindrical AC explants without subchondral bone were extracted from the center of the 29 grid cells using a 4-mm diameter round-hole hand punch to isolate the sample from the surrounding AC and a surgical scalpel to remove the sample from the subchondral bone (Lewis 1998). Samples were stored in PBS solution at -20°C until testing (Krishnan 2003; Ronken 2012).

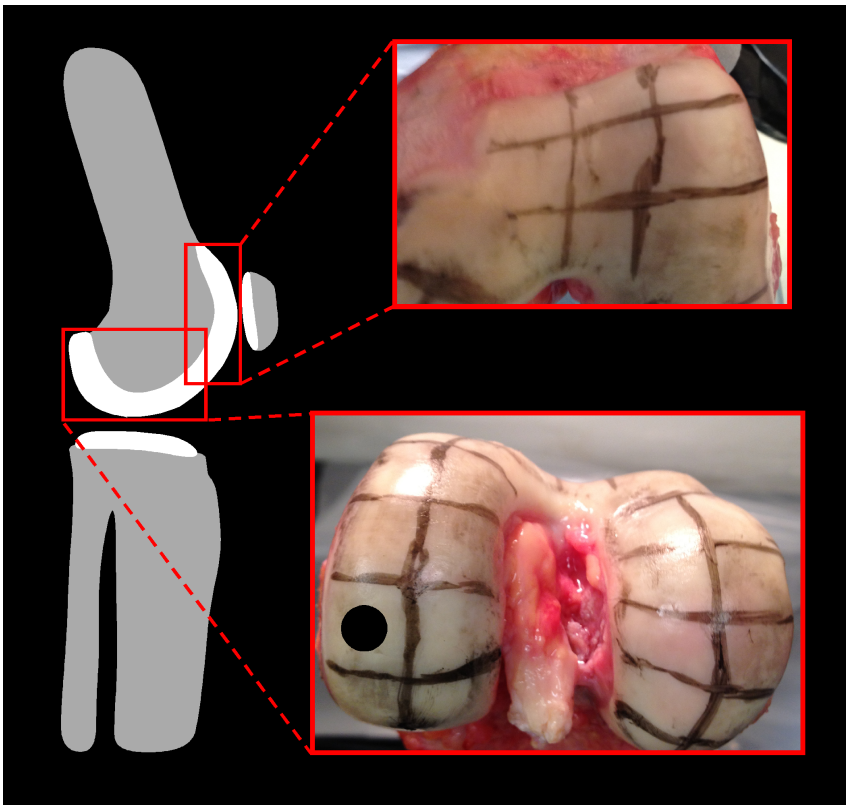

Figure 5.1: Example of grid pattern drawn onto the trochlea (upper) and condyles (lower) of a cadaveric femur. The knee schematic (left) is drawn in the sagittal plane with red rectangles indicating the regions shown in the photographs, white indicating cartilage, and gray indicating bone. Photographs (right) show coronal views of the knee taken from an anterior position with the patella removed. Explants were extracted from the center of each grid cell; the black circle indicates the typical location and relative size of the cartilage explant.

5.3.3 Mechanical Testing Procedure

Diameter and thickness measurements were obtained using digital vernier calipers (resolution: 0.01 mm, Mitutoyo America Corporation, Aurora, IL) once the explant had completely thawed in the PBS bath. Sample thicknesses ranged from 1.00 – 2.95 mm, which falls within the published range of knee cartilage thickness (Cohen 1999; Shepherd and Seedhom 1999b). A speckle pattern was

applied to the cylindrical surface of the AC sample using black India ink, as detailed in **Section 3.4**. The AC explants were tested using the device described in **Section 3.2**. The explant was situated between the force sensor and actuator rod under a minimal (0.2 N) tare load and allowed to equilibrate for 10 minutes (Jurvelin 2003). Testing proceeded as detailed in **Section 3.3** with ten pre-conditioning cycles and three experimental trials of 100% strain/sec unconfined compression.

5.3.4 Data Analysis

The average nominal stress and strain was computed for each experimental trial according to the methods outlined in **Section 3.4** (VIC-2D 2009, Correlated Solutions, Columbia, SC). $E_{10\%}$ was subsequently calculated from the nominal stress-strain curve (**Section 3.5**). The mean and standard deviation of $E_{10\%}$ at each (n = 29) site was determined. For regional analysis, the trochlea was divided into six sub-regions: the medial, central, and lateral weightbearing (WB) and the medial, central, and lateral less weightbearing (LWB) areas (Fig. 5.2). WB was defined as the area contacting the patella between 0° and 30° knee flexion, and LWB corresponded to cartilage in contact with the patella beyond 30° knee flexion (Feller 2007; Garg and Walker 1990; Goodfellow 1976). Similarly, the condyles were divided into four sub-regions: medial and lateral WB and LWB (Fig. 5.2) (Li 2005a). Mean $E_{10\%}$ was calculated for the trochlea, condyles, and the ten sub-regions of each knee.

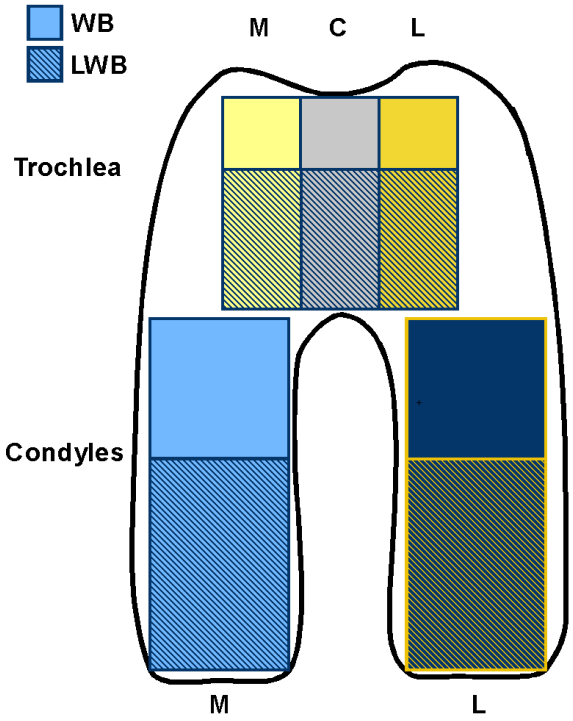

Figure 5.2: For regional analysis, the trochlea was divided into six sub-regions and the condyles were divided into four sub-regions (black outlines). M - medial, C - central, L - lateral, WB - frequent weightbearing, LWB - less-frequent weightbearing.

5.3.5 Statistical Analysis

A repeated-measures ANOVA was conducted to evaluate the effect of primary region (trochlea or condyles) on $E_{10\%}$. To analyze the sub-regions, a repeated-measures mixed model ANOVA was performed to test for the main effects of side [medial, lateral, (central)] and contact frequency (WB, LWB) and the interaction of the two factors on $E_{10\%}$. The trochlear and condylar regions were analyzed separately. Bonferroni-adjusted pairwise comparisons were made for all significant effects. The alpha level for significance was set at 0.05. All statistical analyses were conducted with SAS 8.0 software (SAS Institute Inc.,

Cary, NC). Due to the large number and complex nature of regions being evaluated, effect sizes were not computed.

5.4 Results

5.4.1 $E_{10\%}$ by Test Site

Twenty-three (9.90%) cartilage samples were excluded from analysis due to damage to the AC surface or peak strains less than 10%. $E_{10\%}$ of the remaining samples varied considerably across the femoral surface (Figs. 5.3 – 5.4). Within the trochlea, mean $E_{10\%}$ ranged from 9.17 MPa to 32.95 MPa, while on the condyles, mean $E_{10\%}$ ranged from 16.59 MPa to 41.37 MPa (Fig. 5.4).

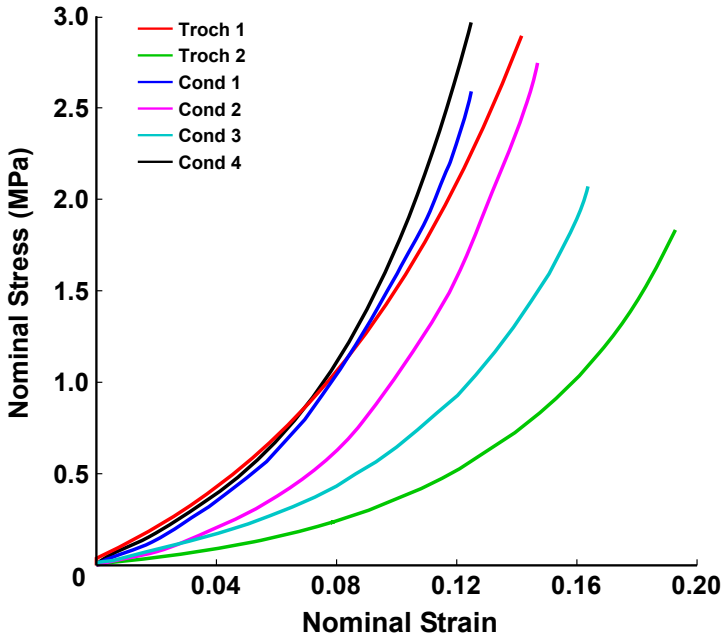

Figure 5.3: Sample stress-strain curves at several sites on the trochlea (Troch) and condyles (Cond) within the same distal femur. When compressed at a 100% strain/sec, the explants demonstrated large differences in overall stiffness despite being from the same knee.

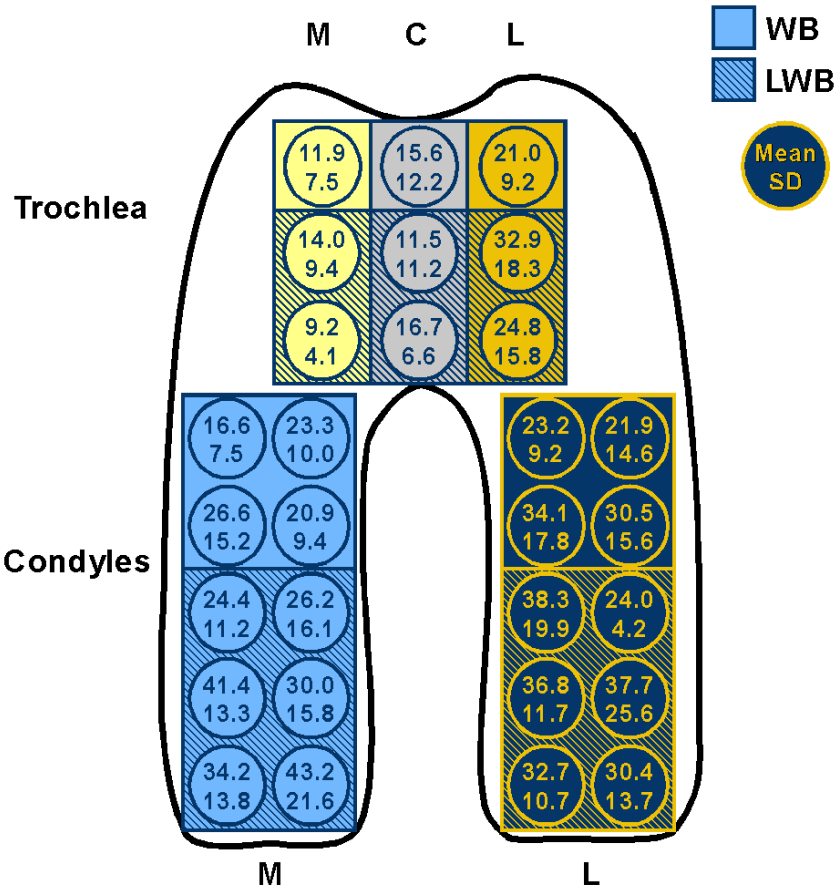

Figure 5.4: Mean and standard deviation of $E_{10\%}$ (MPa) across the distal femur. Solid lines encase the ten sub-regions for statistical analysis. Circles denote test sites. M - medial, C - central, L - lateral, WB - frequent weightbearing, LWB - less-frequent weightbearing.

5.4.2 $E_{10\%}$ by Region

A significant effect of primary region on $E_{10\%}$ was present, $F(1,7) = 39.48$, $p < 0.001$. Mean $E_{10\%}$ of the trochlea (16.45 ± 6.27 MPa) was significantly lower than mean $E_{10\%}$ of the condyles (30.20 ± 6.63 MPa).

Significant sub-regional dependence was also evident within the trochlea and condyles. In the trochlea, there was a significant main effect of side on $E_{10\%}$, $F(2,13) = 9.55$, $p < 0.01$. Planned comparisons indicated that mean $E_{10\%}$ of the

lateral region (26.06 ± 14.90 MPa) was significantly higher compared to the medial (11.57 ± 7.18 MPa, $p < 0.01$) and central (14.46 ± 10.13 MPa, $p < 0.05$) regions (Fig. 5.5). No significant difference was evident between the medial and central regions ($p = 0.93$). There was no main effect of contact frequency, $F(1,7) = 0.25$, $p = 0.63$, with mean $E_{10\%}$ for WB (15.46 ± 9.96 MPa) approximately equal to mean $E_{10\%}$ for LWB (17.10 ± 13.18 MPa). No significant interaction of side*contact frequency was present, $F(2,10) = 1.10$, $p = 0.37$. Region means within each knee are documented in Fig. 5.6 to highlight consistency across individuals.

The condyles displayed a pattern of regional dependence that was directly opposite to the trochlear pattern (Fig. 5.7). There was a significant main effect of contact frequency on $E_{10\%}$, $F(1,7) = 17.55$, $p < 0.01$. Mean $E_{10\%}$ was lower in WB (24.47 ± 13.14 MPa) compared to LWB (34.01 ± 16.24 MPa). There was no significant main effect of side, $F(1,7) = 2.55$, $p = 0.15$. Mean $E_{10\%}$ of the medial condyle (29.09 ± 15.46 MPa) was approximately equal to mean $E_{10\%}$ of the lateral condyle (31.18 ± 16.03 MPa). No significant interaction occurred, $F(1,7) = 0.56$, $p = 0.48$. Mean values for the condylar regions of each knee are shown in Fig. 5.8.

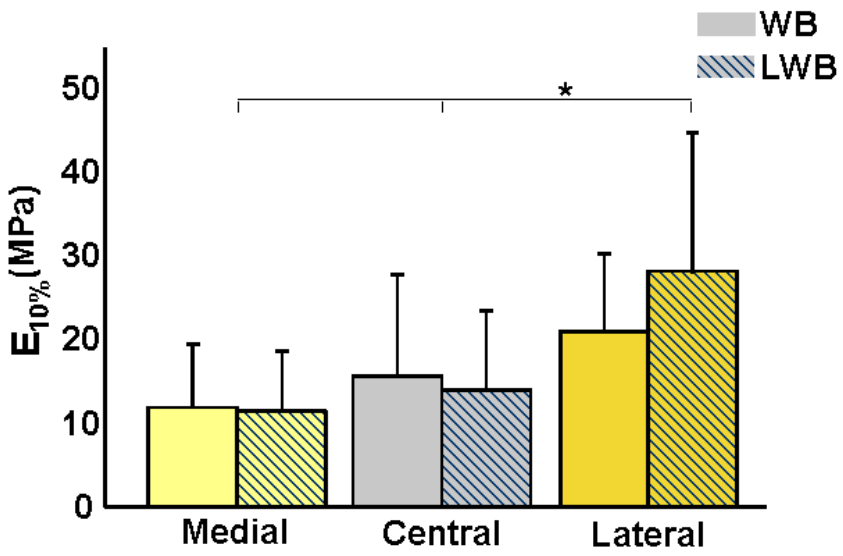

Figure 5.5: Mean $E_{10\%}$ (MPa) for the trochlear sub-regions. Bars indicate one standard deviation and asterisks denote $p < 0.05$. The lateral sub-regions had a significantly higher $E_{10\%}$ compared to the central and medial sub-regions. The weightbearing (WB) and less weightbearing (LWB) sub-regions were not significantly different.

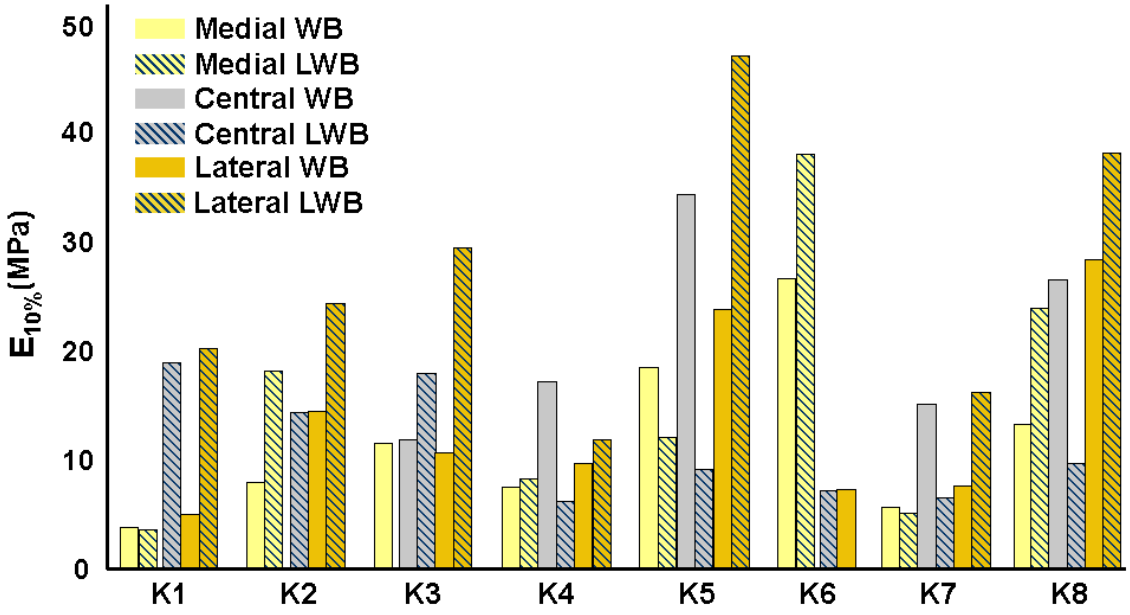

Figure 5.6.: Mean $E_{10\%}$ (MPa) of the trochlear regions within each knee (K1 – K8). WB - weightbearing, LWB - less weightbearing. Missing bars due to compromised cartilage quality in that region.

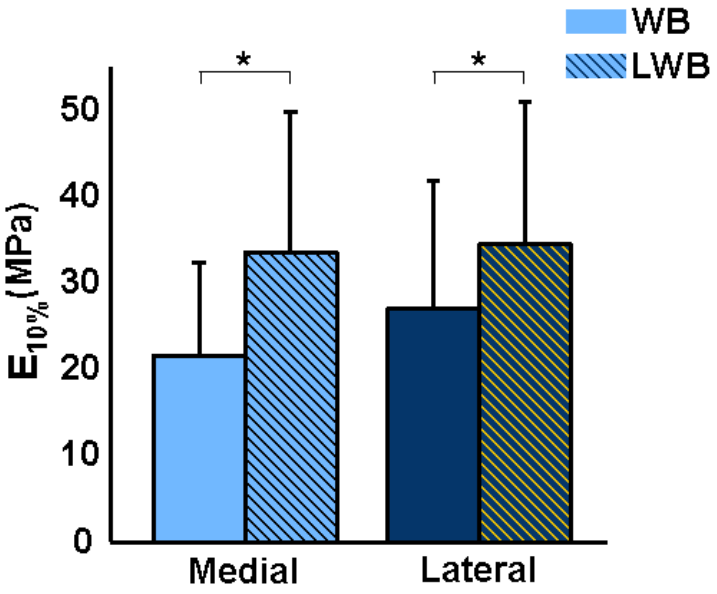

Figure 5.7: Mean $E_{10\%}$ (MPa) for the condylar sub-regions. Bars indicate one standard deviation and asterisks denote $p < 0.05$. $E_{10\%}$ of the weightbearing (WB) sub-regions was significantly less than $E_{10\%}$ of the less weightbearing (LWB) sub-regions. No mediolateral difference was present.

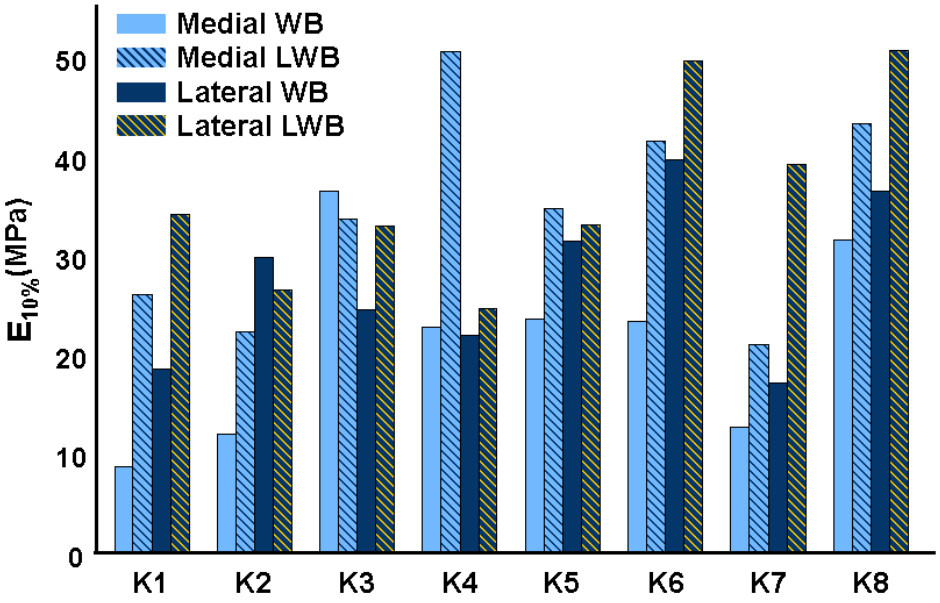

Figure 5.8: Mean $E_{10\%}$ (MPa) of the trochlear regions within each knee (K1 – K8). WB - weightbearing, LWB - less weightbearing.

5.5 Discussion

Developing a thorough knowledge of the regional mechanical properties of healthy human femoral AC is central to identifying the mechanism of knee OA initiation. The current study sought to fill this critical knowledge gap by subjecting AC specimens from 29 repeatable sites across eight femurs to unconfined compression at a strain rate analogous to normal gait. The results of this study appear to represent the first detailed regional mapping of healthy human distal femoral AC mechanics elicited under a strain rate analogous to gait. In particular, the study extends beyond current literature by examining specific patterns of variability of $E_{10\%}$, the elastic tangent modulus at 10% strain, within the trochlea and condylar regions. In doing so it demonstrated that substantial regional mechanical non-uniformities are present within human femur AC and that these non-uniformities follow similar patterns across individuals.

The trochlear and condylar regions displayed relative differences in $E_{10\%}$ that agreed well with previous work (Shepherd and Seedhom 1999a; Swann and Seedhom 1993). The absolute values of $E_{10\%}$ were higher in the present study compared to these previous works and this difference was likely due to lower strain rate used by Swann et al. (1993) and the low sampling resolution used by Shepherd et al. (1999). Cartilage is a viscoelastic tissue that is highly strain rate dependent with its stiffness increasing with increasing strain rate (Oloyede 1992; Shepherd and Seedhom 1999a). Femoral AC also exhibits substantial mechanical variability within the trochlea and condyles, as demonstrated by the

current study. Consistently sampling a more compliant location on the femur may lead to underreporting of the tissue stiffness.

In the trochlea, $E_{10\%}$ was significantly higher in the lateral sub-regions compared to the central or medial sub-regions. During common physical activities, the lateral structures of the knee and the laterally tilted angle of the quadriceps combine to produce a predominant lateral pull on the patella (Goodfellow 1976; Powers 1998). This action is almost entirely counterbalanced by the prominent lateral aspect of the trochlea (Goodfellow 1976; Han 2005). The large imbalance of stress placed on the lateral aspect of the trochlea throughout the range of knee flexion likely results in the significantly higher lateral modulus observed in the WB and LWB sub-regions.

Level ground walking, the most frequent joint loading activity, produces stance-phase knee flexion angles that rarely exceed 30° (Mann and Hagy 1980; Seedhom 1979), which suggested that differences in $E_{10\%}$ would present between the WB and LWB trochlear regions. However, we determined no such statistical difference. Further examination of the data by region revealed that six of the eight subjects did exhibit higher $E_{10\%}$ in LWB (Fig. 5.9). Of the remaining two, one exhibited nearly equal average moduli across the WB and LWB regions and the other exhibited WB moduli four times larger than LWB. While loading occurs less frequently in the LWB region it typically corresponds to higher patellofemoral joint forces, such as during stair ascent or descent, deep knee bends, or rising from a chair (Goudakos 2009; Seedhom 1979). The higher LWB modulus found in the majority of subjects may arise from the higher prevalent

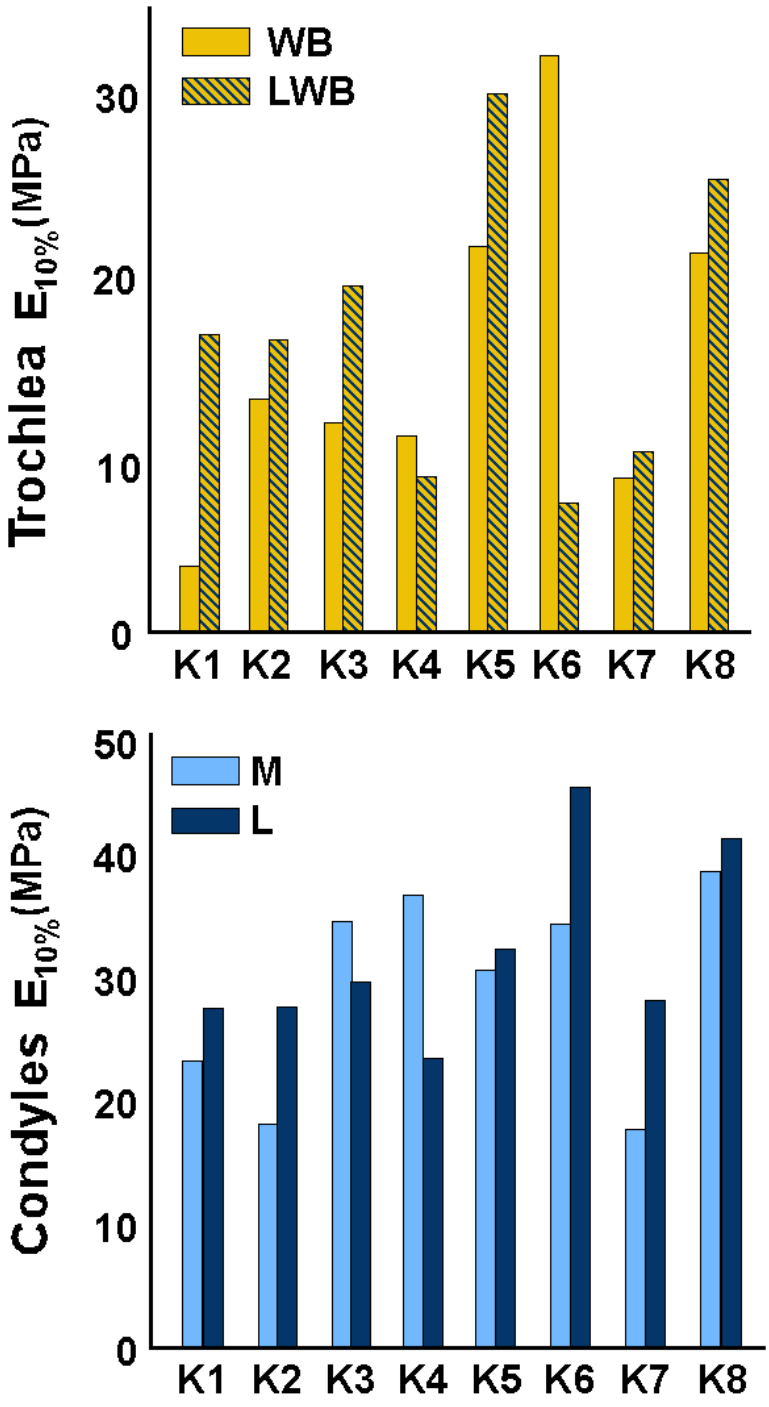

Figure 5.9: Mean $E_{10\%}$ (MPa) by knee (K). (Upper) Weightbearing (WB) and less weightbearing (LWB) sub-regions of the trochlea. (Lower) Medial (M) and lateral (L) sub-regions of the condyles.

stresses of this region. The lack of a consistent trend across all subjects may be due to daily activity factors, such as lower limb range of motion, that were not controlled for in this study.

The non-uniform properties observed for the trochlea region provide important preliminary insights into OA development in the patellofemoral joint. The cartilage in the central region was found to be relatively soft, even in the LWB area, despite the relatively high stresses it is likely to experience (Goodfellow 1976; Goudakos 2009). Likewise, osteoarthritic AC lesions in the trochlea typically originate in the central LWB region and only extend mediolaterally as the disease progresses (Bae 2010; Seedhom 1979). An alteration in the joint mechanics that shifts primary contact from the lateral trochlea to the central trochlea, as seen in many osteoarthritic knees (Herzog 1998), could plausibly increase the stress within central AC to levels that it cannot sustain without damage. Further work is necessary to evaluate this hypothesis.

Significant mechanical heterogeneity was also present on the femoral condyles. The LWB region exhibited significantly higher $E_{10\%}$ than the WB region. At heel strike during walking, the femur and tibia are aligned in full extension. The cartilage contact path begins anteriorly on the condyles but is posterior on the condyle when the joint load peaks (Liu 2010; Mann and Hagy 1980; Shelburne 2005). Higher tibiofemoral joint forces occur during less common tasks, e.g., running or deep knee bends, and these tasks are also associated with deeper knee flexion angles (Bingham 2008; Mann and Hagy 1980). Thus the WB AC

experiences frequent lower-magnitude loading while the LWB AC undergoes infrequent high-magnitude loading, which may explain its lower relative $E_{10\%}$ (Carter 2004).

Unlike the trochlear region, no mediolateral difference was determined in the condyles. During walking the tibiofemoral joint center of rotation is located in the lateral compartment, suggesting transmission of larger loads through the lateral condyle (Hoshino and Tashman 2012). Similarly, contact stresses appear higher on the lateral condyle compared to the medial condyle (Koo and Andriacchi 2008). However, relative loading of the mediolateral compartments is also influenced by lower limb alignment (Koo and Andriacchi 2008) and tibial rotation (Kenawey 2011), which were not controlled for in this study. Post-hoc examination revealed that only two of the eight specimens had higher medial condyle modulus (Fig. 5.9). Of these two contradictory knees, Knee 4 also exhibited an altered trochlear WB-LWB relationship that suggests it may have demonstrated atypical habitual knee joint mechanics. Future work should further clarify whether lateral compartment AC is generally stiffer than medial AC.

Osteoarthritic cartilage lesions tend to manifest on the lateral condyle in the posterior, or LWB portion (Bae 2010; Gulati 2009). On the medial condyle, however, lesions appear more anteriorly (Bae 2010; Gulati 2009). These two regions represent the stiffest and softest areas of the condyles, respectively, based on the results of the present study. It is unclear why lesions would manifest in such disparate regions but it suggests that AC properties alone cannot predict OA development. Joint mechanics that could alter and promote

debilitative loading patterns in both regions, such as excessive tibial rotation (Deneweth 2010), must be considered as well in future research efforts.

Several limitations apply to the current study that should be considered. Study data came from middle-aged, non-overweight Caucasian female specimens, which limits extrapolation to other demographic groups. Also as noted, lower limb alignment, lower limb range of motion, and habitual activity levels, which may all influence AC mechanics, were not examined in this study. Accounting for these factors in future studies may reveal further mechanical distinctions in femoral AC. The sub-region classifications used herein were based on general mechanical profiles and known variations in AC morphology (Froimson 1997; Garg and Walker 1990; Goodfellow 1976; Koo and Andriacchi 2008; Koo 2011; Li 2005a; Quinn 2005). These classifications were adopted due to the lack of existing analysis of AC mechanics within the trochlea and condyles. While other classifications may have revealed different sub-regional differences, our current selection appeared most intuitive and relevant to normal joint mechanics. Lastly, $E_{10\%}$ represents a linear description of a non-linear material (Mow and Guo 2002). While the stress-strain curves exhibited similar curvature such that a curve with a higher modulus at 10% strain also exhibited a higher modulus at other strains, work has been completed (**Chapter 8**) to expand analyses to include non-linear parameters that may provide a more complete assessment of AC mechanics.

Chapter 6: Evaluation of Hyperelastic Models for the Non-Linear and Non-Uniform High Strain Rate Mechanics of Proximal Tibial Cartilage

A manuscript based on the research presented in this chapter has been accepted for publication:

Deneweth JM, McLean SG, Arruda EM (2013). Journal of Biomechanics. *In press.*

6.1 Abstract

Accurate modeling of the high strain rate response of healthy human knee AC is critical to investigating the mechanism(s) of knee OA and other cartilage disorders. Osteoarthritis has been suggested to originate from regional shifts in joint loading during walking and other high strain rate physical activities. Tibial plateau AC under compression rates analogous to walking exhibits a non-linear and location-dependent mechanical response. A constitutive model of AC that efficiently predicts the non-linear and non-uniform high strain rate mechanics of tibial plateau AC is important for computational studies of OA development. A transversely isotropic hyperelastic statistical chain model has been developed. The model's ability to simulate the 100% strain/sec unconfined compression response of healthy human tibial plateau AC has been assessed, along with two other hyperelastic statistical chain models. The transversely isotropic model exhibited a superior fit to the non-linear stress-strain response of AC. Furthermore, the model maintained its predictive capability after being reduced

from four degrees of freedom to one. The remaining material constant of the model, which represented the local collagen density of the tissue, demonstrated a regional dependence in close agreement with physiological variations in collagen density and AC modulus in human knees. The transversely isotropic eight-chain network of freely jointed chains with a region-dependent material constant represents a novel and efficient approach for modeling the complex response of human tibial AC under high strain rate compression. The anisotropy and microstructural variations of the AC matrix dictate the model's response, rendering it directly applicable to computational modeling of the human knee.

6.2 Introduction

Deterioration of knee AC leads to severe joint debilitation in the form of OA (Buckwalter 2005). Identifying the mechanism(s) that causes healthy AC to degenerate into this diseased state is of high priority. While computational knee models enable the systematic and controlled evaluation of potential OA disease mechanisms (Wilson 2005b), the utility of these models' results relies on the accuracy of the modeled AC.

Articular cartilage poses a modeling challenge due to its complex physiology and equally complex mechanical response. It consists of a solid phase of cartilage cells (chondrocytes) embedded within an extracellular matrix and a fluid phase of water and soluble ions (Poole 2001). The extracellular matrix is composed mainly of cross-linked type II collagen fibrils and negatively charged proteoglycan macromolecules. The interaction of the solid and fluid phases

creates a non-linear poroviscoelastic response to compressive loading (Mow 1984). Extensive work has been done to model this behavior (Boschetti 2006; Hayes 1972; Lai 1991; Mak 1986; Wilson 2004). The short-term, high strain rate response of AC, however, depends predominantly on the flow-independent, intrinsic viscoelasticity of the matrix (Bader and Kempson 1994), which results from the collagen meshwork and its entrapment of high-swelling aggrecan macromolecules (Maroudas 1976). The collagen network in the STZ is particularly important in the tissue's response to high-rate loading (Mizrahi 1986). These data suggest that the mechanical response of knee AC to high-rate loading (e.g., walking) (Liu 2010) may be represented by using the collagen meshwork and its anisotropy as the main input parameters. This unique approach would afford representation of the non-linear elastic response of cartilage with a low number of material constants to facilitate implementation in a computational model of the entire knee joint.

The structural properties of the STZ are non-uniform across the tibial plateau, which in turn may promote heterogeneous mechanical properties. The regions of the plateau covered by meniscal tissue, for example, tend to have a thicker STZ, more tangentially oriented collagen fibrils, and a higher collagen density, compared to regions not covered by meniscal tissue (Clark 1991; Eyre 2006). Individual collagen fibrils are primarily tensile elements. Thus when the collagen network is compressed, fibrils oriented perpendicular to the loading axis will stretch and resist the deformation, while fibrils oriented parallel to the loading axis will provide minimal load support. Therefore, regions with large amounts of

tangentially oriented collagen fibrils, such as meniscus-covered regions, are expected to exhibit larger compressive stiffness compared to other regions, which has been supported experimentally (Barker and Seedhom 2001; Shepherd and Seedhom 1999a; Young 2007). The regional variability, however, may be more complex; we have demonstrated that AC elastic moduli beneath the external and posterior portions of the menisci exceeded 300% of AC not covered by the meniscus or beneath the anterior third of the meniscus (**Chapter 4**). Insight into knee AC behavior and the development of OA, therefore, appear better served by modeling both the non-linear and non-uniform elastic response of the STZ.

Statistical mechanics models offer the ability to predict finite deformations of hyperelastic materials with relatively few material constants (Boyce and Arruda 2000). These mechanistic models are particularly powerful because they offer insight into the underlying physiological factors driving mechanical behaviors (Ma 2010). A material is represented as a cross-linked network of flexible molecular chains (Arruda and Boyce 1993). The chains, which can be analogized to “entropy springs,” produce significant forces when stretched but have minimal resistance to compression, much like collagen fibrils. As the material is deformed, the chains rotate and stretch to accommodate the deformation, altering the statistical entropy of the chain network and producing network stress.

Statistical mechanics models have accurately modeled multiple finite deformation states in elastic polymers (Boyce and Arruda 2000; Boyce 1994)

and, more recently, in biological materials (Bischoff 2004; Ma 2010; Palmer and Boyce 2008). Since the driver of knee AC's short-term response, the collagen network, can be analogized to a statistical chain network, these models are strong candidates for modeling the short-term response of AC (Brown 2009). However, the ability of the model to replicate the high strain rates associated with walking or the non-uniform mechanical properties of tibial AC remains unknown. The aim of this study, therefore, was to develop a transversely isotropic statistical mechanics model to simulate non-arthritic human proximal tibial AC mechanics under physiologically relevant loading and compare it to existing isotropic statistical mechanics models. We hypothesized that (1) the transversely isotropic statistical mechanics model would accurately simulate the tibial AC stress-strain response elicited under physiological loading, (2) the transversely isotropic model would perform superiorly to isotropic statistical mechanics models, and (3) the parameters of the transversely isotropic model would exhibit regional dependency similar to that determined in **Chapter 4**.

6.3 Methods

6.3.1 Statistical Mechanics Models for Articular Cartilage

Three statistical mechanics model—isotropic eight-chain network of freely jointed chains (FJC), isotropic eight-chain network of MacKintosh chains (MAC), and transversely isotropic eight-chain network of freely jointed chains (TI) were used to simulated proximal tibial AC. Statistical mechanics models have two key components: the mathematical description of the chains and the manner in which

the chains are assembled to form a network. The freely jointed chain model (Kühn and Grun 1942) and the MacKintosh chain model (MacKintosh 1995) were each implemented within an isotropic eight-chain network (Arruda and Boyce 1993; Palmer and Boyce 2008) to produce the FJC and MAC models, respectively. Additionally, the freely jointed chain was placed in a transversely isotropic eight-chain network (Bischoff 2002) to develop the TI model.

6.3.1.1 Freely Jointed Chain

The freely jointed chain is a highly flexible unconstrained rotating chain comprised of N rigid segments of length l (Kühn and Grun 1942) (Fig. 6.1). One end of the chain is fixed at the origin and the other end occupies a volume dv at a location $\boldsymbol{r}$ with probability $p(\boldsymbol{r})$. $p(\boldsymbol{r})$ is determined from:

$$\ln p(\boldsymbol{r}) = p_0 - N\left(\frac{r}{Nl}\beta_r + ln\frac{\beta_r}{\sinh \beta_r}\right) \tag{6.1}$$

where p_0 is a constant, $r = |\boldsymbol{r}|$, $\beta_r = \mathcal{L}^{-1}(r/Nl)$, and $\mathcal{L}(x) = \coth x - 1/x$ is the Langevin function. The inverse Langevin is commonly computed from the Padé approximation (Cohen 1991):

$$\mathcal{L}^{-1}(x) = x\frac{(3 - x^2)}{(1 - x^2)} + O(x^6) \tag{6.2}$$

The position of one link relative to the previous link is uncorrelated, such that all link angles have equal probability. Consequently the chain is highly flexible and its resting end-to-end length r_0 is much less than it's contour length $L = Nl$. Elongating the freely jointed chain to vector length $\boldsymbol{r}$ requires a tensile force, f_{chain} (Arruda and Boyce 1993):

$$f_{Chain} = \frac{k\Theta}{l}\beta_r \approx \frac{k\Theta}{l}\frac{r}{L}\frac{(3-\left(\frac{r}{L}\right)^2)}{(1-\left(\frac{r}{L}\right)^2)} \tag{6.3}$$

where the Padé approximation has been used to simplify the inverse Langevin, k is Boltzmann's constant (1.38065 x 10^{-23} $J \cdot K^{-1}$), and Θ is the absolute temperature. The force-extension response of the change is non-linear; the force remains low for small stretches and then rapidly increases as the stretch approaches $\sqrt{N}$, typically referred to as the locking stretch (Fig. 6.2).

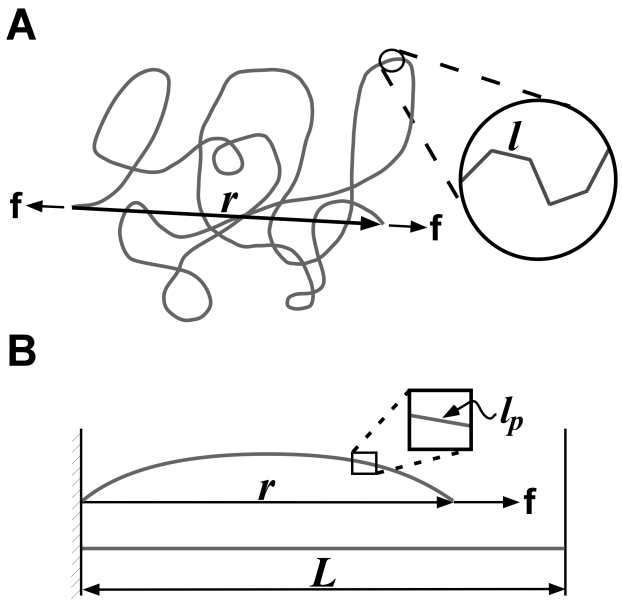

Figure 6.1: Schematics of the two statistical chain models used to model tibial cartilage. The application of tension (f) stretches the chain to vector length r. (A) The highly flexible freely jointed chain, composed of N rigid links of length l. (B) The semi-flexible MacKintosh chain with contour length L and persistence length l_p. Adapted from Palmer 2008.

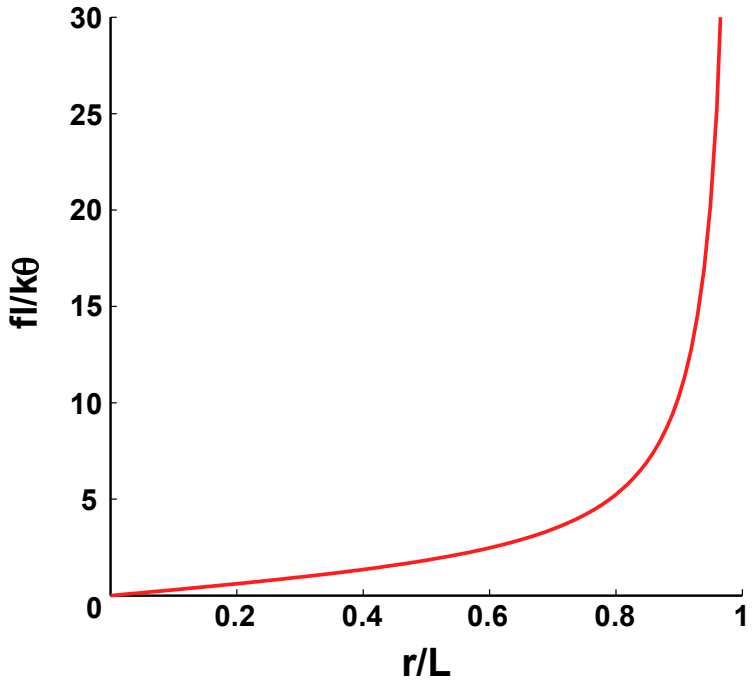

Figure 6.2: Force-extension response of the freely jointed chain model.

6.3.1.2 MacKintosh Chain

The MacKintosh chain describes a semi-flexible statistical chain with significant bending rigidity (MacKintosh 1995). Like the freely jointed chain, chain tension is a function of $L = Nl$. However, the chain is also described by an additional parameter, the persistence length l_P(Fig. 6.1B). The persistence length represents the length of the chain over which it appears straight. In turn, it governs the bending rigidity of the chain; as l_P increases, the bending rigidity also increases (Fig. 6.3). Since the MacKintosh is semi-flexible $l_P \approx L$ (Fig. 6.1B). The chain exhibits an average end-to-end resting length r_0 and an average vector length under no applied tension $r_{f=0}$. L, l_P, and $r_{f=0}$ are related by (Palmer and Boyce 2008):

$$r_{f=0} = L(1 - \frac{L}{6l_P}) \tag{6.4}$$

The tension developed in the chain when it is extended to an end-to-end length r can be written as:

$$f_{chain} = \frac{k\Theta}{l_p}\left(\frac{1}{4(1-{}^{r}/_{L})^2}\right)\left(\frac{{}^{L}/_{l_p} - 6(1-{}^{r}/_{L})}{{}^{L}/_{l_p} - 2(1-{}^{r}/_{L})}\right) \tag{6.5}$$

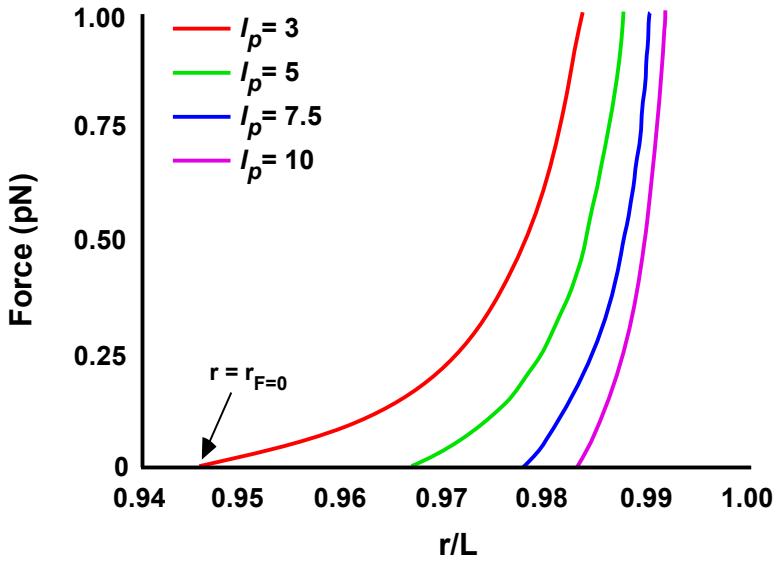

Figure 6.3: Force-extension response of the MacKintosh chain as a function of the persistence length, l_p (μm). L = 1.02 μm.

6.3.1.3 Isotropic Eight-Chain Network (FJC and MAC)

The isotropic eight-chain network treats a unit cell of material as a cube with sides aligned along the principal axes of stretch (Fig. 6.4) (Arruda and Boyce 1993). Eight statistical chains originate from the center of the cube and extend to

each corner. Incorporating Eq. (6.3) into the isotropic eight-chain network yields the strain energy, U_{FJC}, for the FJC model:

$$U_{FJC} = nk\Theta N\left\{\frac{\lambda_{chain}}{\sqrt{N}}\beta_{chain} + ln\frac{\beta_{chain}}{sinh(\beta_{chain})}\right\} \tag{6.6}$$

where n is the chain density, $\lambda_{chain} = \left({\lambda_1}^2 + {\lambda_2}^2 + {\lambda_3}^2\right)^{1/2}/\sqrt{3}$, λ_i is the principal stretch in the i^{th} direction (i = 1, 2, 3), and β_{chain} is the inverse Langevin ($\mathcal{L}^{-1}$) of $\lambda_{chain}/\sqrt{N}$ (Arruda and Boyce 1993).

Cartilage behaves as a nearly incompressible material under high strain rates (Wong 2000) and is frequently modeled as incompressible (Ateshian 2007; Brown 2009; Mow 1980). The deformation gradient for uniaxial compression or tension of an incompressible material is:

$$\mathbf{F} = \begin{bmatrix} \lambda & 0 & 0 \\ 0 & {}^{1}/_{\sqrt{\lambda}} & 0 \\ 0 & 0 & {}^{1}/_{\sqrt{\lambda}} \end{bmatrix} \tag{6.7}$$

where λ is the axial stretch. Substituting Eq. (6.7) into Eq. (6.6), taking the derivative of Eq. (6.6) with respect to λ, and solving for the unknown hydrostatic pressure yields the nominal stress in the axial direction (Arruda and Boyce 1993):

$$T_{o1_{FJC}} = \frac{nk\theta}{3}\frac{\sqrt{N}}{\lambda_{chain}}\mathcal{L}^{-1}\left(\frac{\lambda_{chain}}{\sqrt{N}}\right)\left(\lambda - {}^{1}/_{\lambda^2}\right) \tag{6.8}$$

where

$$\lambda_{chain} = [(\lambda^2 + 2/\lambda)/3]^{1/2} \tag{6.9}$$

The stress response depends on two material constants: $C_R = nk\theta$, an independent parameter that reflects the chain density per unit volume of the material, and N, the contour length of the chain.

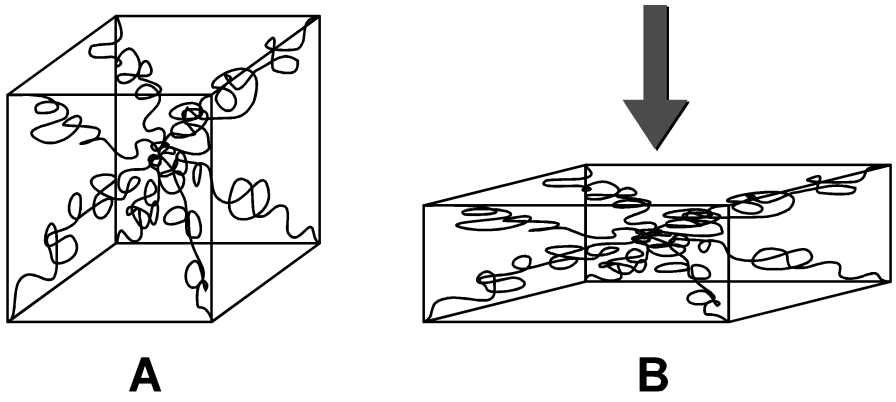

Figure 6.4: Eight-chain isotropic network model (A) undeformed and (B) in unconfined compression. The chains rotate and stretch to accommodate the deformation.

Similarly, the MAC strain energy is defined as (Palmer and Boyce 2008):

$$U_{Mac} = nk\Theta\left\{\frac{L}{4l_p y} + \ln(y) - \ln\left(L - 2l_p y\right)\right\} \tag{6.10}$$

$$y = 1 - \frac{r}{L} = 1 - \frac{r_0\lambda_{chain}}{L} \tag{6.11}$$

where n, k, Θ, and λ_{chain} are defined identically to the FJC model. Assuming $r_0 = r_{f=0}$, the axial nominal stress is:

$$\mathrm{T}_{o_1 MAC} = \frac{nk\Theta}{3l_p}\frac{r_{f=0}}{\lambda_{chain}}\left[\frac{1}{4\left(1 - {r_{f=0}\lambda_{chain}}/{L}\right)^2}\right]\left[\frac{{L}/{l_p} - 6\left(1 - {r_{f=0}\lambda_{chain}}/{L}\right)}{{L}/{l_p} - 2\left(1 - {r_{f=0}\lambda_{chain}}/{L}\right)}\right](\lambda - 1/\lambda^2) \tag{6.12}$$

Since $r_{f=0}$ is a function of l_p and L [Eq. (6.4)], the response depends on only three material constants: $C_R = nk\theta$, l_p, and L.

6.3.1.4 Transversely Isotropic Eight-Chain Network (TI)

An orthotropic eight-chain network was developed to simulate the anisotropic non-linear behavior of soft tissue (Bischoff 2002). The model

incorporates orthotropic anisotropy into the traditional eight-chain framework by replacing the cubic unit cell with a rectangular prism of unequal, unitless sides a, b, and c (Fig. 6.5). The material will exhibit the highest tensile modulus in the direction of the largest dimension. Incompressibility is not assumed in the model but a bulk compressibility term is included to maintain near-incompressibility (Bischoff 2002). The total strain energy of the orthotropic eight-chain configuration of freely jointed chains, U_{Ortho}, is (Bischoff 2002):

$$U_{Ortho} = U_0 + \frac{nk\Theta}{4}\left(N\sum_{i=1}^{4}\left[\frac{\rho^{(i)}}{N}\beta_\rho^{(i)} + ln\frac{\beta_\rho^{(i)}}{sinh\,\beta_\rho^{(i)}}\right] - \frac{\beta_P}{\sqrt{N}} ln\left[\lambda_{\mathbf{a}}^{a^2}\lambda_{\mathbf{b}}^{b^2}\lambda_{\mathbf{c}}^{c^2}\right]\right) + \cdots \quad (6.13)$$

$$\ldots + \frac{B}{\alpha^2}\{cosh[\alpha(J-1)] - 1\}$$

and

$$\beta_\rho^{(i)} = \mathcal{L}^{-1}(\rho^{(i)}/N) \quad (6.14)$$

$$\beta_P = \mathcal{L}^{-1}(P/N) \quad (6.15)$$

$$P = \frac{1}{2}\sqrt{a^2 + b^2 + c^2} = \sqrt{N} \quad (6.16)$$

where U_0 is a constant, $\rho^{(i)}$ is the deformed length of the i^{th} chain, P is the undeformed chain length, $\lambda_{\mathbf{a-c}}$ are the stretches along the principal material axes, J is the ratio of the deformed volume to the original volume, B controls the bulk compressibility near $J = 1$, and α is a constant that governs the curvature of the hydrostatic pressure versus volume curve for large volume changes. If small volume changes are assumed, i.e., in the case of near incompressibility, α is typically set to unity.

This model can be simplified to a transversely isotropic model by setting the in-plane dimensions b and c equal to one another and assuming that the

stretches in these two principal directions are equal (i.e., $\lambda_{\mathbf{b}} = \lambda_{\mathbf{c}} = \lambda_2$) (Fig. 6.6). This yields the strain energy for the TI model:

$$U_{TI} = U_0 + \frac{nk\Theta}{4}\left(N\sum_{i=1}^{4}\left[\frac{\rho^{(i)}}{N}\beta_\rho^{(i)} + ln\frac{\beta_\rho^{(i)}}{sinh\,\beta_\rho^{(i)}}\right] - \frac{\beta_P}{\sqrt{N}}ln\left[\lambda_{\boldsymbol{a}}^{a^2}\lambda_{\boldsymbol{b}}^{2b^2}\right]\right) + \cdots \qquad (6.17)$$

$$\ldots + \frac{B}{\alpha^2}\{cosh[\alpha(J-1)] - 1\}$$

and

$$\rho = \frac{1}{2}\sqrt{a^2{\lambda_1}^2 + 2b^2{\lambda_2}^2} \qquad (6.18)$$

$$P = \sqrt{N} = \frac{1}{2}\sqrt{a^2 + 2b^2} \qquad (6.19)$$

$$\lambda_2 = \sqrt{\frac{J}{\lambda_1}} \qquad (6.20)$$

Taking the derivative of the Eq. (6.17) to λ, and solving for the unknown hydrostatic pressure yields the nominal stress in the axial direction:

$$T_{0_1 TI} = \frac{nk\theta}{4\lambda_1}\left(a^2\left[\frac{{\lambda_1}^2\beta_\rho}{\rho} - \frac{\beta_P}{\sqrt{N}}\right] - b^2\left[\frac{{\lambda_2}^2\beta_\rho}{\rho} - \frac{\beta_P}{\sqrt{N}}\right]\right) \qquad (6.21)$$

Please refer to Appendix B for a detailed derivation of Eq. (6.21). Four material constants are required: $C_R = nk\theta$; a, the unit cell dimension along the direction of compression (1-direction); b, the unit cell dimension perpendicular to the direction of compression (2- and 3- directions); and J. As the ratio of b:a, i.e., the degree of transverse isotropy, increases, the initial slope of the stress-strain curve decreases and the material stiffens rapidly at lower strains (Fig. 6.7).

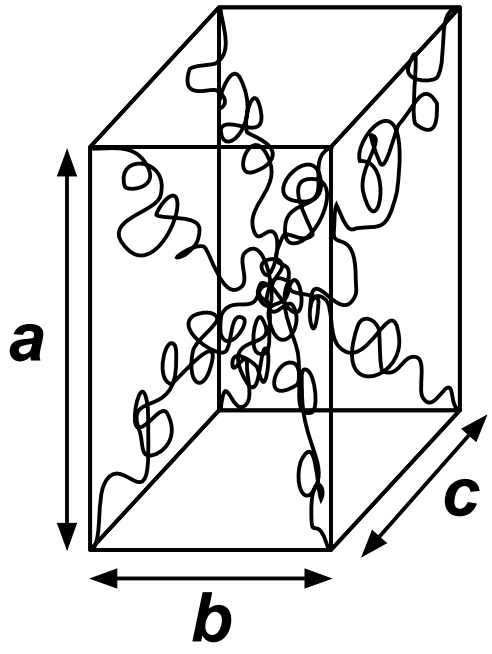

Figure 6.5: Schematic of the eight-chain orthotropic network model. The unequal dimensions a, b, and c produce an anisotropic deformation response that is stiffest in the direction of the largest dimension. Adapted from Bischoff 2002.

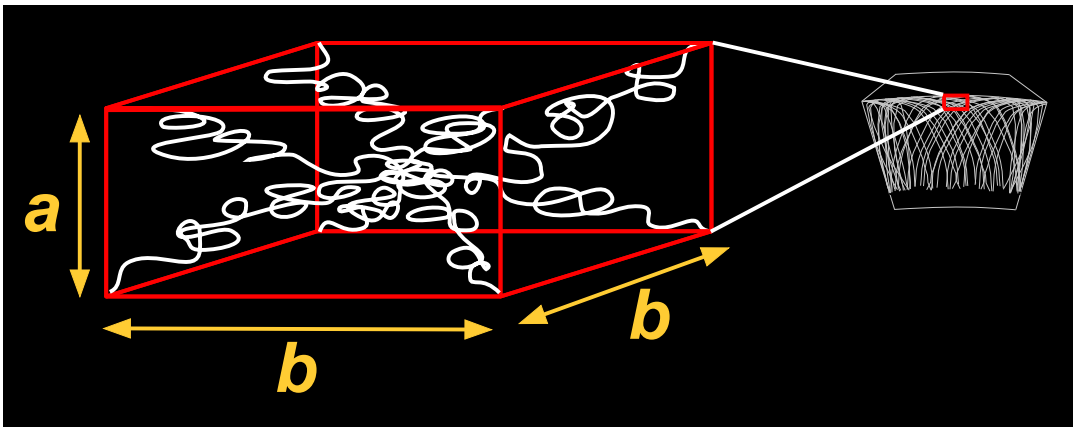

Figure 6.6: The TI model replicated the transverse isotropy of the STZ by setting the in-plane dimensions (*b)* equal to each other while keeping the dimension along the compression axis (*a*) different.

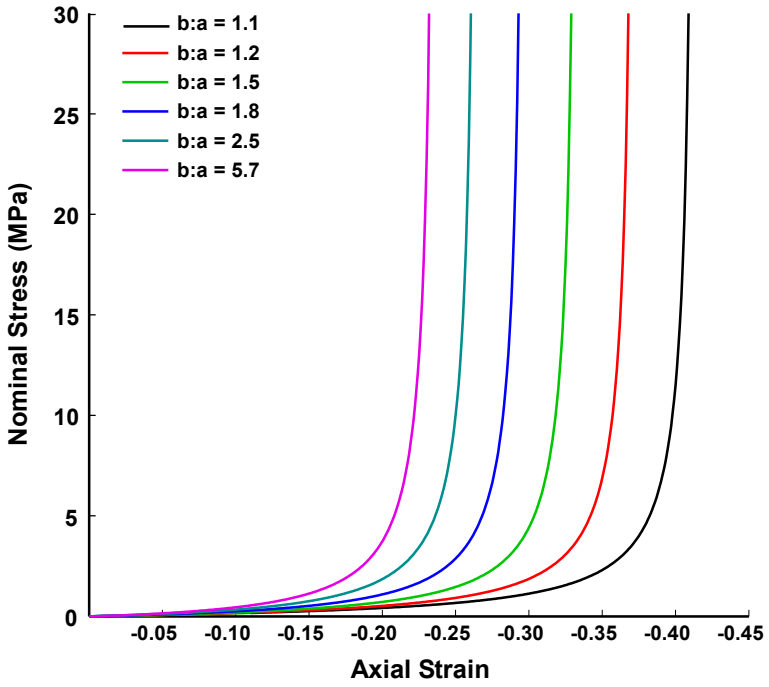

Figure 6.7: Unconfined compression response of the TI model for several values of $b{:}a$. C_R = 0.134 MPa, N = 1.3, J = α = 1.

6.3.2 Experimental Data

The three models were simulated against the nominal stress-strain data obtained in a separate study (**Chapter 4).** Data from Subject 1 was excluded because it was missing data for several test sites. Donor demographics from the knees used in this study (K2-K8) are can be found in Table 3.1.

6.3.3 Model Simulations

Each analytical model was implemented in Matlab (Mathworks, Natick, MA). The unknown material constants were determined for each model using a built-in numerical non-linear optimization scheme (lsqcurvefit.m) to minimize the

squared difference between the model-predicted stress and the observed experimental stress (Coleman and Li 1996). Inputs to the model were the experimental strain, experimental stress, and initial guesses at the unknown parameters. Outputs were the parameter values that provided the best fit to the experimental data and the predicted stress computed with these values. The unknown parameters were C_R and N for the FJC model; C_R, l_P, and L for MAC; and C_R, a, b, and J for TI. All parameters were constrained to be nonnegative as they represented lengths, moduli, or a volume ratio. Additional constraints to the TI model were $0.05 \leq a : b \leq 20$ with $a, b \geq 1$ to agree with experimentally determined anisotropy (Jurvelin 2003; Wang 2003; Woo 1976) and $J \leq 1$ (Chegini and Ferguson 2010; Korhonen 2002).

6.3.4 Determination of Best-Fitting Model

To determine the most successful model, the final experimental trial for each sample was submitted to the three model optimization schemes. Goodness of fit was calculated as:

$$R^2 = 1 - \frac{\sum_i (\sigma_{exp_i} - \sigma_{pred_i})^2}{\sum_i (\sigma_{exp_i} - \bar{\sigma}_{pred})^2} \tag{6.22}$$

where σ_{exp_i} is the experimental stress corresponding to the i^{th} strain data point, σ_{pred_i} is the i^{th} predicted stress, and $\bar{\sigma}_{pred}$ is the mean predicted stress.

6.3.5 Analysis of Regional Dependence

The formulation with the highest mean R^2 was used to evaluate whether it

could predict location-specific dependence via the parameter C_R. The model was modified such that all parameters except C_R were assumed constant across the tibial surface. This adjustment was made to isolate the effect of C_R and to evaluate the viability of the simplest version of the model. The values of the fixed model parameters were determined from the results of the first set of simulations. The modified model was simulated against all available data trials using the same non-linear optimization scheme detailed in the Section 6.3.5.

Simulations with excellent fit to the data, $R^2 \geq 0.97$, were used for regional analysis. Regional heterogeneity of C_R was evaluated by dividing the medial and lateral tibial plateaus into the same four regions used to evaluate the experimental data (**Chapter 4**): not covered by meniscus (I), and the anterior (II), exterior (III) and posterior (IV) thirds of the meniscus-covered area (Fig. 4.2). The mean regional values of C_R were computed for each region of each knee.

6.3.6 Statistical Analysis

Mean C_R values were submitted to a repeated-measures mixed model ANOVA to test for the effects of plateau side (medial or lateral, *n*=2), region (*n*=4), and the interaction of side*region (*n*=8) in SAS 8.0 (SAS Institute Inc., Cary, NC). Bonferroni-adjusted pairwise comparisons were made for all main effects.

The effect size of each pairwise comparison was evaluated using Cohen's d, Eq. (4.1) (Cohen 1988). The values 0.2, 0.5, and 0.8 denote the cut-off levels of d for small, moderate, and strong effect sizes, respectively (Cohen 1988). Only

simulations with $R^2 \geq 0.97$ were included in the statistical analyses. An alpha level of 0.05 denoted significance for all statistical measures.

6.4 Results

6.4.1 Determination of Best Fitting Model

The MAC configuration performed poorly ($R^2 = 0.900$, Table 6.1, Fig. 6.8). FJC and TI, in contrast, provided excellent model fits across the entire data set ($R^2 = 0.995$ and 0.999, respectively) (Table 6.1, Fig. 6.8). FJC and TI fit the small subset of linear stress-strain responses equally well (Fig. 6.8). However, TI was superior in fitting the non-linear stress-strain curves that were associated with the majority of samples (Fig. 6.8). It was concluded that the TI model best captured the tibial AC stress-strain response, and it was used for subsequent analyses.

6.4.2 Analysis of Regional Dependence

The TI model was modified such that a and b were fixed at representative values of 1.00 and 1.33, respectively, based on the low variation in a and b in the first set of simulations (Table 6.1). Additionally, AC was assumed to be incompressible such that J = 1.00. Implementing the TI model with a = 1.00, b = 1.33, and J = 1.00 produced a good fit to the data (R^2 = 0.983, Fig. 6.8). Twelve percent of the simulations were excluded for R^2< 0.970. The mean values of C_R for the remaining simulations are reported in Table 6.2.

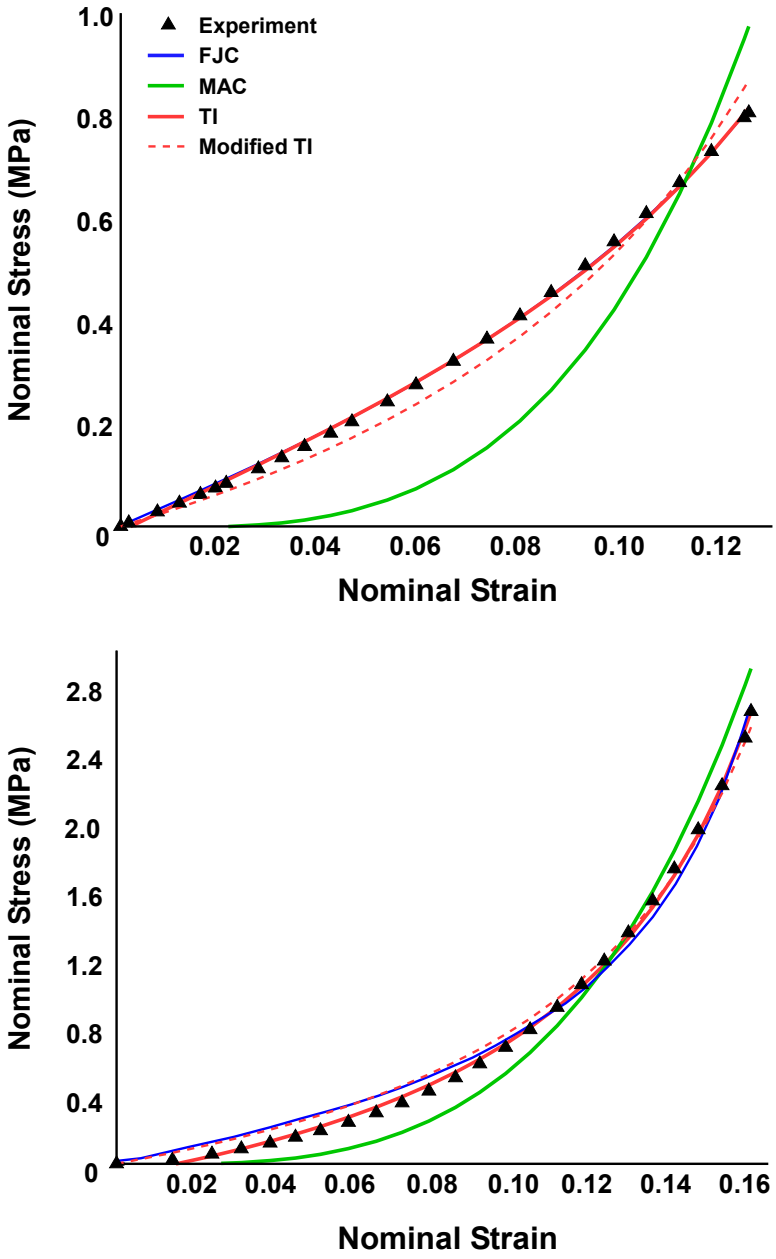

Figure 6.8: Representative simulation results for the FJC, MAC, TI, and Modified TI models for (upper) nearly linear and (lower) non-linear stress-strain responses. In the nearly linear case, the FJC and TI curves fall approximately on top of one another. In the non-linear case, TI supplies a superior fit to FJC, particularly for low strains. The MAC model poorly fits the data in both situations.

Table 6.1: Mean and standard deviation (SD) of parameter values and goodness of fit (R^2) for the FJC, MAC, and TI simulations of tibial AC.

	FJC			MAC				TI				
	C_R	N	R^2	C_R	l_p	L	R^2	C_R	a	b	J	R^2
Mean	113.34	1.048	0.995	3017.08	4.76	2.215	0.900	207.88	1.010	1.315	0.978	0.999
SD	106.94	0.014	0.003	3006.73	1.28	0.547	0.124	168.66	0.055	0.057	0.046	0.001

Units for C_R: kPa

A significant main effect on C_R was found for region, $F(3,17) = 11.16$, $p < 0.001$, Fig. 6.9. A pairwise comparison of mean C_R by region revealed significant differences ($p < 0.05$) between regions I and III, I and IV, II and III, and II and IV (Fig. 6.9, Table 6.2). The relative pattern of variability across regions was similar across subjects (Fig. 6.10). The mean difference of C_R between each pair of regions exhibited moderate to strong effect sizes except for I-II and III-IV on the lateral plateau and III-IV on the medial plateau (Table 6.3).

No significant main effect of side was determined, $F(1,6) = 3.12$, $p = 0.13$, which indicated that mean C_R was statistically the same between the medial and lateral plateaus (Fig. 6.9). The small effect size between the medial and lateral plateaus ($d = 0.32$) confirmed this finding. No statistically significant interaction of region*side was determined, $F(3,14) = 0.55$, $p = 0.65$.

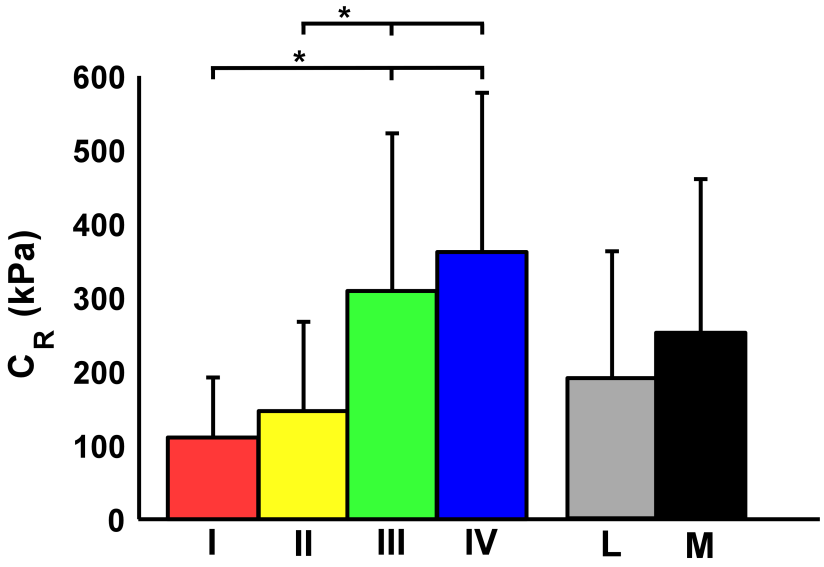

Figure 6.9: Mean C_R of the modified TI simulations for the four regions (I – IV) and the lateral (L) and medial (M) plateaus. Bars represent one standard deviation. Asterisks (*) denote statistically significant differences ($p < 0.05$). C_R of regions I and II were similar in magnitude and significantly lower than regions III and IV, which did not differ significantly from each other.

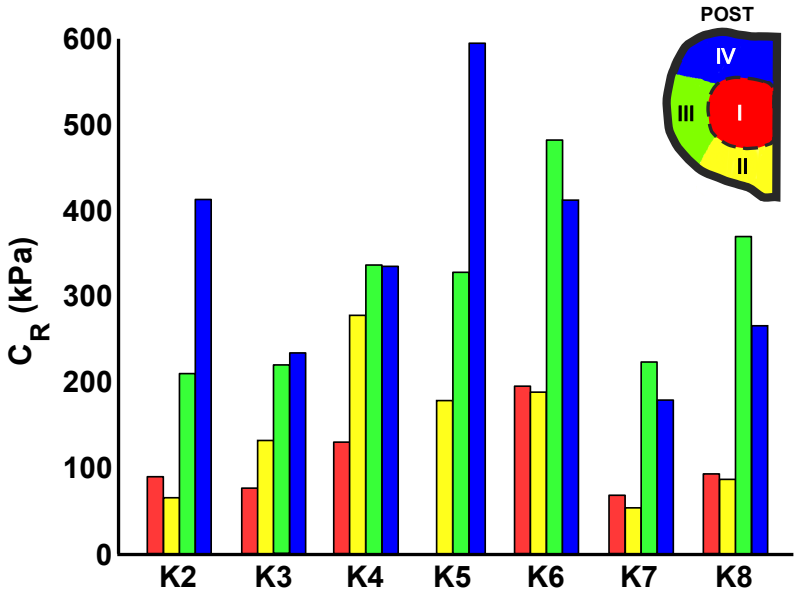

Figure 6.10: Mean regional C_R of the modified TI simulations by knee (K2 – K8). No data are available for region I of K4 because $R^2 < 0.97$. Region values have been averaged across sides due to the lack of a statistically significant difference between the medial and lateral plateaus. The relative pattern of regional differences manifests similarly across the seven knees.

Table 6.2: Mean C_R for the TI model (a = 1.00, b = 1.33, J = 1.00) by knee and region. Blank cells reflect missing experimental data or R^2 < 0.97.

	LATERAL PLATEAU				MEDIAL PLATEAU				BOTH PLATEAUS			
Knee	**I**	**II**	**III**	**IV**	**I**	**II**	**III**	**IV**	**I**	**II**	**III**	**IV**
1	145.08	47.88	211.24	446.68	52.55	82.29	208.16	395.81	89.57	65.08	209.70	412.77
2	-	48.30	162.51	157.21	76.31	215.62	276.27	272.24	76.31	131.96	219.39	233.90
3	141.77	138.49	266.48	336.25	106.18	556.00	406.23	333.28	129.91	277.66	336.35	334.77
4	-	272.34	341.18	579.15	-	84.38	301.26	605.14	-	178.3	327.87	594.75
5	122.73	199.84	519.00	139.76	249.35	176.47	445.13	548.00	195.06	188.16	482.07	411.92
6	55.62	53.33	171.14	67.75	74.02	-	275.49	400.89	67.89	53.33	223.31	178.80
7	96.56	86.47	226.63	254.27	87.32	-	512.32	272.96	92.86	86.47	369.47	265.48

Table 6.3: Inter-region statistics for C_R (kPa) of the TI model (a = 1.00, b = 1.33, J = 1.00).

REGIONS			LATERAL PLATEAU				MEDIAL PLATEAU			
A	B	*p*	Mean B – A	95% CI	Cohen's *d*	Effect Size	Mean B – A	95% CI	Cohen's *d*	Effect Size
I	II	1.000	8.82	(-48.92, 66.56)	0.12	Small	76.83	(-13.18, 166.84)	0.70	Moderate
I	III	0.004	159.04	(38.73, 279.34)	1.01	Strong	240.76	(141.36, 340.17)	1.74	Strong
I	IV	< 0.001	176.09	(68.29, 283.89)	1.38	Strong	305.21	(199.09, 411.34)	2.02	Strong
II	III	0.038	155.22	(20.59, 279.85)	0.90	Strong	163.93	(7.38, 320.49)	0.95	Strong
II	IV	0.008	167.27	(47.77, 286.78)	1.20	Strong	228.38	(61.76, 395.00)	1.22	Strong
III	IV	1.00	-17.06	(-194.12, 160.01)	0.08	Weak	64.45	(-95.23, 224.13)	0.32	Small

Mean B – A: mean difference between regions A and B, calculated by subtracting the mean of region A from the mean of region B
CI: confidence interval

6.5 Discussion

Three common statistical chain network models were evaluated to determine whether these formulations could represent the non-linear, non-uniform elastic response of healthy human tibial AC to a compression rate consistent with walking. Successful use of computational models to investigate the underlying mechanisms of OA development can be enhanced by a constitutive model that reflects physiologically relevant human AC behavior with a minimal number of physically-meaningful material constants (Keenan 2012). The results of this study suggested the transversely isotropic eight-chain network with freely jointed chains (TI) appears to be such a model.

The TI model successfully simulated a wide range of experimentally-determined tibial plateau AC responses (**Chapter 4**). Moreover, its material constants (C_R, a, b, and J) and inherent anisotropy accurately represented AC physiology, which provides insight into the relationship between physiology and mechanics. Physiologically, C_R represents collagen density and mechanically dictates the initial slope of the stress-strain response and influences its tangent modulus. C_R may also reflect the integrity of the collagen matrix, with decreased values indicating a reduced amount of intact collagen fibrils. The large variability of C_R agrees well with the non-uniformity of collagen density in the STZ and AC mechanical properties across the tibial plateau (Clark 1991; Young 2007). The central regions of the joint, which tend to experience compressive loading (Andriacchi 2009; Bevill 2008) and have a lower collagen density (Clark 1991), also demonstrated lower mean C_R. In contrast, the posterior and lateral peripheral

regions, which more frequently undergo shear loading (Andriacchi 2009; Bevill 2008) and have a higher collagen density (Clark 1991), exhibited higher mean C_R. This suggests C_R as a useful parameter for incorporating region-dependent mechanics.

The ratio $a : b$ represents the degree of transverse isotropy in the tissue. The more the STZ collagen molecules align parallel to the surface, the greater the expected anisotropy. Meniscus-covered regions tend toward a higher density of parallel-aligned collagen compared to the meniscus-uncovered regions (Clark 1991). In the present study, however, $a : b$ remained relatively consistent across the tibial plateau. Considering the larger variability of C_R, this finding may indicate that collagen density rather than alignment contributes more to the unconfined compression response of the tissue. On average $b > a$, which is expected if the in-plane tensile stiffness was greater than axial tensile stiffness. Lastly, J indicates the compressibility of the tissue. J remained nearly constant at 0.978, which agreed with expectations (Wong 2000).

The TI model was successfully simplified to an incompressible model with a single material constant without compromising its ability to replicate tibial plateau AC mechanics. The material constant that remained, C_R, varied regionally in accordance with the experimental findings presented in **Chapter 4**. This suggested that regional mechanical dependence of the TI model can be established by representing the meniscus-uncovered, anterior meniscus-covered, and exterior-posterior meniscus-covered regions with separate C_R values while holding a, b, and J fixed (Fig. 6.11). This represents a unique and

powerful approach to modeling human AC: the constitutive relation is driven by the anisotropy and physiological variations (i.e., collagen density) of the STZ matrix, which makes the model highly applicable to the human knee joint. Since a regional shift in the joint loading pattern has been suggested to initiate knee OA (Andriacchi 2009), a tibial AC constitutive model that successfully captures regional stiffness variations could offer unique insight into the mechanisms of disease development compared to current models. Further, its ability to capture the non-linearity of the tissue with a single material constant is desirable for use in whole joint computational models.

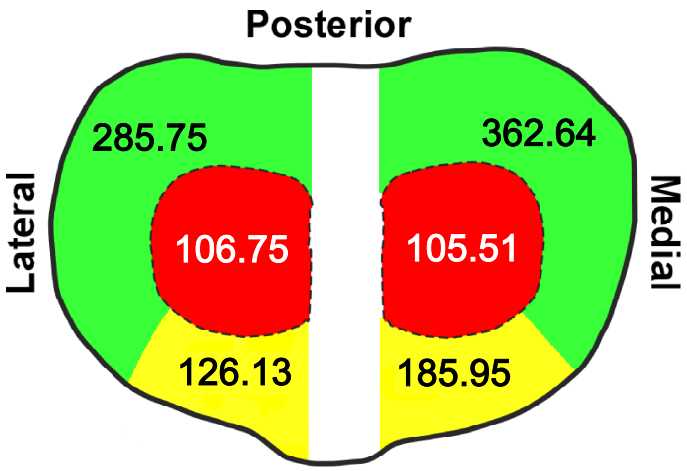

Figure 6.11: Mean C_R (kPa) for the uncovered (red), meniscus-covered anterior (yellow), and meniscus-covered exterior-posterior (green) regions. These regions are suggested for implementing spatial-dependent stiffness into the TI cartilage model.

The TI model can be readily implemented into one of the many commercial finite element packages that permit user-defined hyperelastic materials. These routines typically require the model's strain energy [Eq. (6.17)],

its derivatives, and parameter values. To model the heterogeneity in human AC, C_R (i.e., $nk\theta$) must be defined as a function of position across the AC surface, while J, a, and b can be assigned the values used in the second part of this study. An appropriate scenario for using the TI model is a material with known transverse anisotropy and a mechanical response that is largely dominated by non-linear, recoverable deformation.

The single loading configuration used to examine the model and the narrow demographic from which experimental data was obtained currently limits the results of this study. The ability of the model to simulate tibial AC was determined by fitting it to a set of unconfined compression data. However, it may be advantageous for the model to represent multiple deformation states with a single set of parameters. Therefore, future work should examine whether the TI model can represent AC across the spectrum of potential deformation states. Similarly, the model has been found to be successful with knee AC from Caucasian females within a narrow age and BMI range. Thus, application of these results to other populations, such as males, is not warranted at this time and requires further investigation. Finally, a complete model of tibiofemoral joint AC is desirable for investigating OA development as the disease affects both tibial and femoral AC. The immediate next step of this research is to expand the TI model to describe femoral AC (**Chapter 7**). Despite these limitations, however, the results of this study provide a novel and promising method for modeling knee AC that could substantially advance research towards determining and preventing OA.

Chapter 7: Evaluation of Hyperelastic Models for the Non-Linear and Non-Uniform High Strain-Rate Mechanics of Distal Femoral Cartilage

A manuscript based on the research presented in this chapter has been submitted for consideration of publication:

Deneweth JM, Arruda EM, McLean SG (2013). Journal of Biomechanical Engineering. *In review.*

7.1 Abstract

Knee AC exhibits complex mechanical behavior, even under high strain rates, which poses a challenge to developing accurate and efficient AC models. In particular, the tissue's stress-strain response is non-linear and the stiffness of the response is location-dependent. Recently, a statistical chain network representing the transverse isotropy of the collagen matrix in the STZ of AC has been developed. The model successfully simulated the 100% strain/sec unconfined compression response of human proximal tibial AC. Moreover, the model represented known spatial variations in the elastic modulus through a single parameter. Given the success of the model, we desire to determine whether these outcomes are equally applicable to healthy human distal femoral AC so that a complete model of tibiofemoral joint AC can be developed. The transversely isotropic model was employed along with two other statistical network models to determine which model best simulated recently-obtained unconfined compression data for healthy distal femoral AC. The transversely

isotropic model fit the data excellently (R^2 = 0.999). The model was subsequently simplified to depend on a single parameter and reapplied to the dataset. The modified model maintained an excellent fit to the data (R^2 = 0.999), and its single parameter varied in a statistically similar regional pattern (p < 0.05) to the experimentally-obtained elastic modulus of the tissue. Outcomes suggest that this model is suitable for modeling the spatially-varying, non-linear mechanics of healthy human distal femoral AC. Implementation of this constitutive relation within computational models of the knee will provide novel insight into the relationship between joint mechanics, AC loading, and knee OA development.

7.2 Introduction

Knee OA afflicts 14% of the US population over the age of 26 and 37% of the population over age 60, yet it remains a poorly understood disease (Lawrence 2008). Computational knee models afford a powerful research tool for investigating how the disease initiates and progresses (Bae 2012; Pena 2006; Shirazi and Shirazi-Adl 2009). Computational studies in which joint kinematics and kinetics are systematically varied and the effect on AC stress is determined can indicate which loading patterns are most likely to initiate and/or promote OA. However, the effectiveness of these models depends on the accuracy of the constitutive relations describing the many structures making up the knee. In the case of OA, in which the AC is heavily affected, the AC material model is particularly important (Wilson 2005b).

Selection of a material model requires balancing multiple criteria, such as correct mechanical response for loading conditions of interest, use of parameters with physical meaning that reveal insights into underlying mechanisms, and computational efficiency, e.g., short running time and minimal number of parameters (Hubbard 1993; Taylor and Miller 2006). For the study of OA, appropriate loading conditions are those associated with walking and other activities of daily living (Andriacchi 2009; Andriacchi and Mundermann 2006). During level ground walking knee AC undergoes compressive strains at a relatively high strain rate of 100%/sec and peak strains near 20% (Liu 2010; Mann and Hagy 1980), which can be challenging deformation parameters for popular AC models, e.g., the linear biphasic model and its derivatives (Armstrong 1984; DiSilvestro 2001; Taylor and Miller 2006).

The tissue's viscoelastic and non-linear high strain rate response limits the applicability of linear elastic models (Li and Gu 2011; Mow 1984). However, a highly complex AC model could be avoided by focusing on the flow-independent, intrinsic viscoelasticity of the AC solid matrix, which dominates the mechanical response to high strain rates (Bader and Kempson 1994; DiSilvestro 2001; Maroudas 1976; Mizrahi 1986). Hyperelastic statistical chain network models have successfully modeled high strain rate, finite deformations of biological tissues, such as aortic valve, skin, myocardium, tendon, ligament, and actin cytoskeleton (Bischoff 2002, 2004; Kühl 2005; Ma 2010; Palmer and Boyce 2008). The physical structure of these models is analogous to the collagen network that forms the backbone of the AC matrix (Hasler 1999; Jeffery 1991).

These models require a small number of physically-meaningful parameters, enabling them to be executed in short computational times (Bischoff 2002; Boyce and Arruda 2000; Palmer and Boyce 2008). Taken together, these findings indicate that a statistical chain network model would be viable model for high strain rate loading of human femoral AC.

Recently, it was determined that a transversely isotropic eight-chain network with freely jointed chains (TI model) could simulate the 100% strain/sec uniaxial compression response of healthy human tibial plateau AC with high accuracy (R^2 = 0.999) (**Chapter 6**). The transverse isotropy of the model reflects the anisotropy of the STZ of AC (Clark 1991; Jeffery 1991), which is the zone that most influences the AC matrix's response (Mizrahi 1986). High accuracy was maintained when the model was reduced to dependence on a single parameter that represented the density of the solid collagen matrix. Experimentally-determined regional variations in the tissue elastic modulus were captured by this single parameter. Consequently this material model would be highly useful for evaluating the role of regional loading patterns on the development of OA (Andriacchi and Mundermann 2006; Chaudhari 2008). It is plausible that a similar model would be equally effective at modeling the femoral AC of the knee.

The 100% strain/sec unconfined compression response of healthy distal femoral AC has been recently documented (**Chapter 5**). Similar to tibial AC, significant regional variations in the elastic modulus were determined across the femoral surface. With this in mind, the aim of this study was investigate the ability of the TI model to simulate non-arthritic human distal femoral AC under

physiologically relevant loading compared to existing isotropic statistical mechanics models. The goal was to provide a complete material model for healthy human tibiofemoral joint AC that can be readily implemented into whole knee computational modeling schemes. We hypothesized that (1) the transversely isotropic statistical mechanics model would accurately simulate the femoral AC stress-strain response elicited under physiological loading, (2) the transversely isotropic model would perform superiorly to isotropic statistical mechanics models, and (3) the parameters of the transversely isotropic model would exhibit regional dependency similar to that determined in **Chapter 5**.

7.3 Methods

7.3.1 Statistical Mechanics Models

The isotropic eight-chain network of freely jointed chains (FJC), isotropic eight-chain network of MacKintosh chain (MAC), and transversely isotropic eight-chain network of freely jointed chains (TI) presented and employed in **Chapter 6** were also used in the current study to simulate distal femoral AC. Please refer to **Section 6.3.1** and **Appendix B** for additional details of the models.

7.3.2 Experimental Data

Unconfined compression data from a separate study (**Chapter 5**) were used for model simulations. Demographic data related to this dataset is presented in Table 3.1 (K2-K8).

7.3.3 Model Simulations

Simulations were conducted in Matlab (Mathworks, Natick, MA) to find the set of model parameters that optimized the modeled stress to the experimental stress. A detailed description of the methods can be found in **Section 6.3.3**.

7.3.4 Determination of Best-Fitting Model

To determine the most successful model, the final experimental trial for each sample was submitted to the three model optimization schemes. Goodness of fit determined from the R^2 value [Eq. (6.22)], with higher values indicating a better fit.

7.3.5 Analysis of Regional Dependence

The formulation with the highest mean R^2 was used to evaluate whether it could predict location-specific dependence via the parameter C_R in a similar manner to that described in **Section 6.3.5**. The model was modified such that all parameters except C_R were assumed constant across the femoral surface. The values of the fixed model parameters were determined from the results of the first set of simulations. The modified model was simulated against all available data trials using the same non-linear optimization scheme used in **Section 7.3.3**.

Simulations with excellent fit to the data, $R^2 \geq 0.97$, were used for regional analysis. The distal femur was divided into two primary regions (trochlea and

condyles), six sub-regions within the trochlea, and four sub-regions within the condyles, similar to the regional divisions used experimentally (**Chapter 5**) (Fig. 5.2). The trochlear sub-regions were: medial WB, medial LWB, central WB, central LWB, lateral WB, and lateral LWB. The condylar sub-regions were: medial WB, medial LWB, lateral WB, and lateral LWB. WB and LWB areas represented femoral AC contacting the opposing joint surface between 0° and 30° knee flexion and beyond 30° knee flexion, respectively (Feller 2007; Garg and Walker 1990; Goodfellow 1976; Li 2005a). Mean C_R was computed for the primary regions and the sub-regions.

7.3.6 Statistical Analysis

Mean C_R of the trochlea and condyle primary regions were compared via repeated-measures ANOVA. For the sub-regions, the main effect of side [medial, lateral, (central)] and contact frequency (WB, LWB) and the interaction of side*contact frequency on C_R were evaluated with repeated-measures mixed model ANOVA. Statistical analyses were conducted separately for the trochlea and condyles. In the case of significant main effects or interactions ($p < 0.05$), Bonferroni-adjusted pairwise comparisons were made. All statistical analyses were conducted with SAS 8.0 software (SAS Institute Inc., Cary, NC). Due to the large number of regions being evaluated, effect sizes were not computed.

7.4 Results

7.4.1 Determination of Best Fitting Model

The TI model consistently provided the best fit to the experimental data (R^2 = 0.999), followed by the FJC (R^2 = 0.995), and MAC models (R^2 = 0.906) (Fig. 7.1). The MAC model tended to underestimate the stress at low strain and overestimate it at high strain, whereas the FJC model slightly overestimated the stress at low strains but matched the stress at high strains. The mean and standard deviations for each model's parameters are presented in Table 7.1. The TI model was used for the analysis of regional dependence as it had the highest R^2.

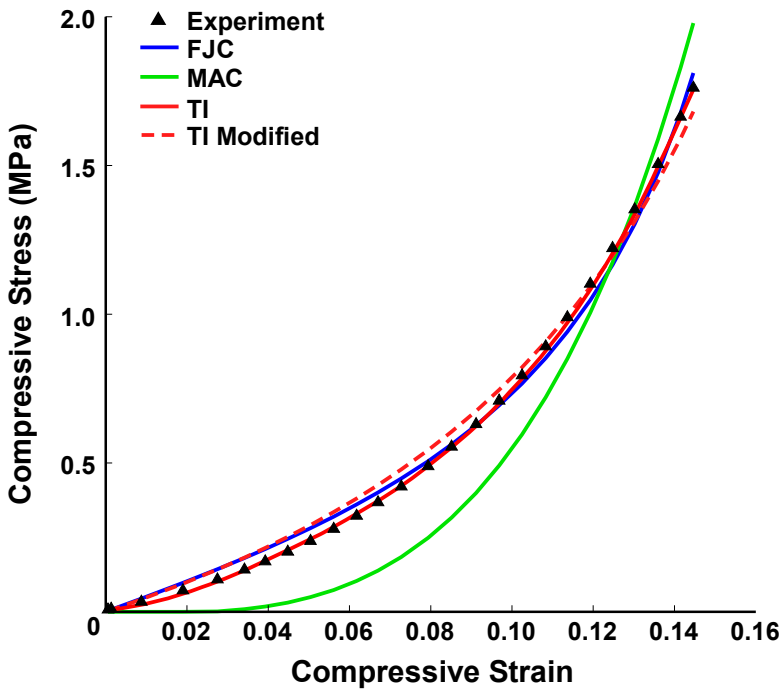

Figure 7.1: Example of unconfined compression data (triangles) and simulated fits of each model. TI Modified is the TI model with all parameters fixed except C_R. The TI model was most successful in fitting the experimental data.

Table 7.1: Mean and standard deviation (SD) of parameter values and goodness of fit (R^2) for the FJC, MAC, and TI simulations of femoral AC.

	FJC			MAC				TI			
	C_R	N	R^2	C_R	L	l_P	R^2	C_R	b	J	R^2
Mean	0.053	1.143	0.995	5.045	4.207	5.792	0.906	0.370	1.348	0.994	0.999
SD	0.047	1.390	0.005	2.667	0.907	0.902	0.075	0.615	0.248	0.005	0.001

Units for C_R: MPa

7.4.2 Analysis of Regional Dependence

The TI model was modified such that only C_R could vary by establishing the following parameter conditions: $a = 1.000$ (from best-fit analysis), b = 1.348 (mean for best-fit analysis), $J = 1.000$ (incompressible). The goodness of fit remained high when the TI model was implemented with these modifications (R^2 = 0.981, Fig. 7.1). For regional analysis, 20.28% (100 out of 493 total) of simulations were excluded due to $R^2 < 0.970$.

Mean C_R is tabulated by knee and sub-region in Table 7.2. C_R was significantly lower for the trochlea (0.533 ± 0.476 MPa) compared to the condyles (0.696 ± 0.517 MPa), $F(1,6) = 10.42$, $p < 0.05$. Within the trochlea, there was a significant effect of side on C_R, $F(2,12) = 10.79$, $p < 0.01$ (Fig. 7.2). Pairwise comparisons determined no statistically significant difference between the medial and central one-thirds ($p = 1.00$). However, C_R of the lateral sub-region was significantly larger than C_R of the medial and central sub-regions ($p < 0.01$ for both cases). This pattern was consistent across knees (Fig. 7.3). No statistically significant effect of contact frequency [$F(1,6) = 0.74$, $p = 0.422$] nor of the interaction of side*contact frequency [$F(2,8) = 0.98$, $p = 0.418$] was found for the trochlea.

On the condyles, side did not have a significant main effect of C_R although a trend of the lateral side being stiffer than the medial side was evident, $F(1,6) = 4.07$, $p = 0.090$. However, a significant main effect of contact frequency was determined, with WB sub-regions demonstrating significantly lower C_R than LWB

regions, $F(1,6) = 10.48$, $p < 0.05$ (Fig. 7.2 – 7.3). No significant interaction of side*contact frequency was determined.

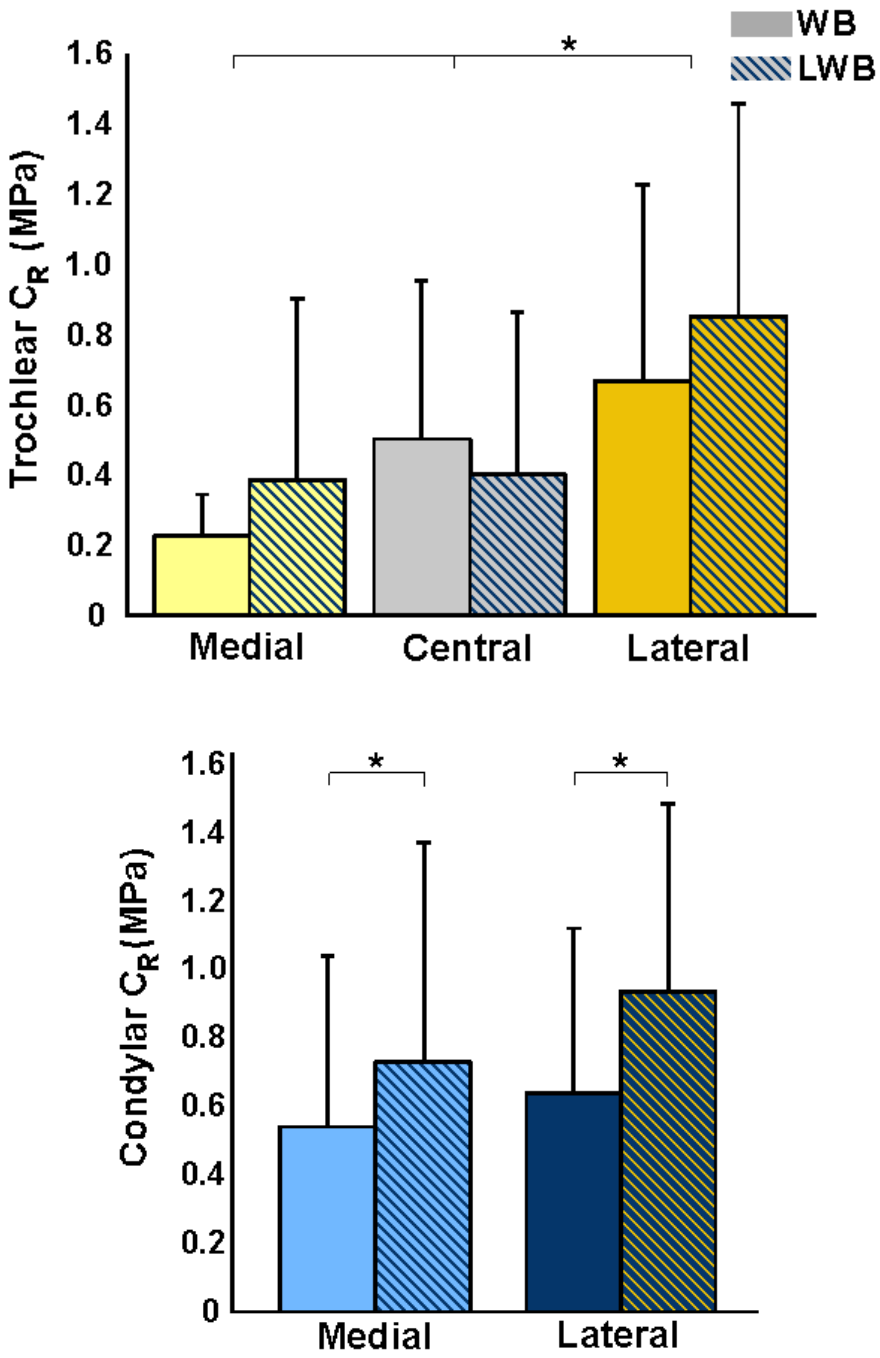

Figure 7.2: Mean C_R by sub-region for the trochlea (upper) and condyles (lower). Bars indicate one standard deviation. Hatching indicates less weightbearing regions.

Table 7.3: Mean C_R for the TI model (a = 1, b = 1.348, J = 1) by knee and sub-region. Blank cells reflect missing experimental data or R^2 < 0.97. Blank cells reflect missing experimental data or R^2 < 0.97.

	TROCHLEA						CONDYLES			
Knee	**M WB**	**C WB**	**L WB**	**M LWB**	**C LWB**	**L LWB**	**M WB**	**L WB**	**M LWB**	**L LWB**
1	0.094	0.085	0.244	0.107	0.125	0.272	0.228	0.335	0.270	0.707
2	0.217	0.462	0.404	0.158	0.480	0.617	0.504	0.614	0.617	1.465
3	-	1.349	1.658	1.532	1.389	1.811	1.620	2.163	1.658	1.862
4	0.130	0.320	-	0.324	0.078	0.379	0.215	0.375	0.208	0.543
5	0.189	-	0.196	0.300	0.191	0.550	0.598	0.535	0.439	0.634
6	0.411	0.604	0.963	0.121	0.122	1.594	0.358	0.595	0.657	1.008
7	0.314	0.194	0.521	0.144	0.404	0.733	0.256	0.483	0.607	0.332

M – medial; C – central; L – lateral; WB – weightbearing; LWB – less weightbearing

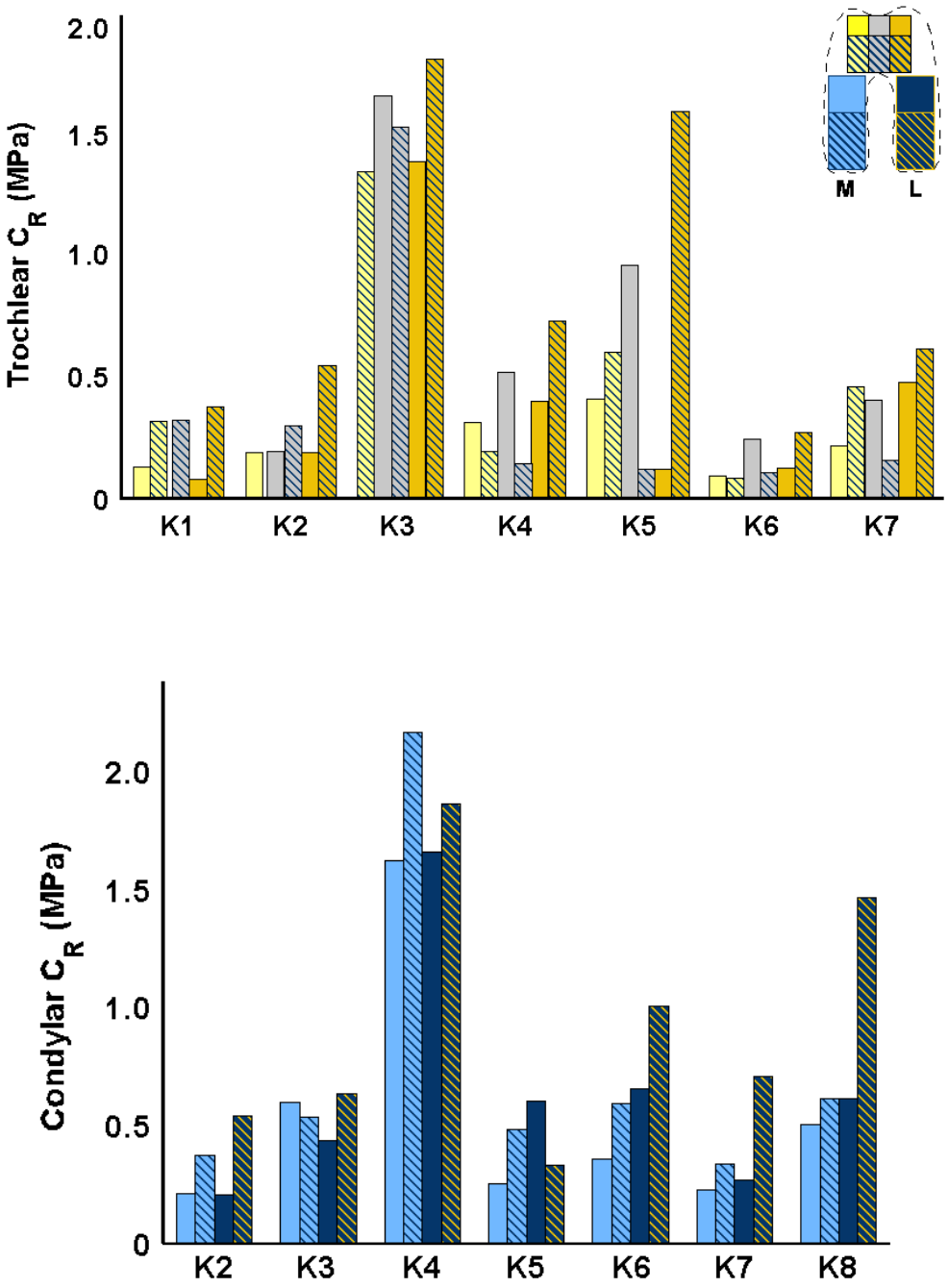

Figure 7.3: Mean C_R (MPa) across the sub-regions of the trochlea (upper) and condyles (lower) of each knee (K2 – K8). Colors indicate mediolateral position and hatching indicates less weightbearing regions (inset). Missing bars indicate that all specimens in region had OA or R^2 < 0.97.

7.5 Discussion

Variations in the mechanical properties of tibiofemoral AC have been suggested to play an important role in the initiation of OA (Andriacchi 2004). However, few AC models currently incorporate region-dependent mechanical properties. The TI model examined herein manifested similar regional mechanical variations to those shown experimentally for healthy human femoral AC via the parameter C_R. In the modified TI model a = 1, b = 1, J = 1, and C_R was selected to optimize the simulated stress to the experimental stress. Model simulations against the entire experimental dataset produced values of C_R that varied regionally within each knee in a similar fashion to regional variations in the AC elastic modulus (**Chapter 5**). Specifically, C_R of the condyles was significantly higher than C_R of the trochlea. Within the trochlea, C_R of the lateral sub-regions were significantly higher than the central and medial sub-regions, and no dependence on contact frequency was present. Within the condyles, C_R was higher in the less weightbearing regions compared to the weightbearing regions, but no mediolateral differences were present. This result indicates that implementing a spatially-dependent C_R in the TI model would allow the spatial heterogeneity of the AC mechanical response to be modeled efficiently within whole joint computational schemes.

The advantage of using the TI model to represent the mechanical response of human knee AC is that its physical design directly relates to the structure of the AC solid matrix. Thus, the mechanistic nature of the model enables exploration of the effect of various physiologically-based input

parameters on the AC stress-strain response. In the context of knee AC, C_R represents the volume density of intact collagen fibrils. Areas with fewer collagen fibrils or with increased damage to existing fibrils (e.g., due to OA) will exhibit a lower C_R. The effect of C_R is reflected in the initial modulus of the stress-strain curve; lower C_R dictates a lower initial modulus (Arruda and Boyce 1993).

The ratio $a{:}\,b$ indicates the extent of transverse isotropy, with $a{:}\,b > 1$ occurring when the collagen fibers are more frequently aligned in the direction of compression and $a{:}\,b < 1$ indicating that the collagen fibers are preferentially oriented in the plane perpendicular to the compression axis (Bischoff 2002). Collagen fibers in the STZ of knee AC align primarily parallel to the tissue's surface (Clark 1991; Jeffery 1991). The results of this study agree well with this finding as $a{:}\,b$ was less than one across for all test sites. If a depth-dependent AC response is desired, the model could be extended to the entire thickness of the tissue by allowing $a{:}\,b$ to vary with depth: $a{:}\,b < 1$ in the STZ, $a{:}\,b \approx 1$ in the MZ where the collagen fibers transition from their parallel orientation at the surface to their radial orientation near the subchondral bone, and $a{:}\,b > 1$ in the DZ near the subchondral bone (Jeffery 1991).

The final parameter of the model is J, which governs the compressibility of the tissue. If the tissue is incompressible, meaning that it deforms without changing total volume, $J = 1$. Articular cartilage is composed mainly of water and thus is nearly incompressible (Ateshian 2007; Wong 2000). In the present study J remained nearly constant across regions and knees, which agrees well with the physiology of the tissue and with previous findings for modeling tibial AC

(**Chapter 6**). Therefore, we feel confident that J can remain fixed near 1.00 for modeling healthy knee AC. Likewise, changes in the water composition of the tissue or the ability of the tissue to maintain its hydrostatic pressure (e.g., due to severe matrix damage) could be modeled with a decrease in J, although this must first be validated.

The mean R^2 for the TI model with all parameters fixed except C_R was very high, but 20% of the simulations were subsequently rejected for $R^2 < 0.97$. Post-hoc repeated-measures ANOVA determined that mean b for high-rejection test sites (50% or more rejected trials) was 1.287, which was significantly lower than mean b for low-rejection sites (b =1.325), $F(1,6) = 325.95$, $p < 0.001$. This finding suggests that the model is particularly sensitive to b in regions with less anisotropy than average (i.e., lower b). Nonetheless all rejected simulations demonstrated $R^2 > 0.90$, which is generally accepted as a high goodness of fit. When the regional analysis for C_R was repeated with all simulations included, observed regional variations in C_R remained the same. Consequently, the modified TI model would be an excellent method for modeling the high strain rate response of femoral AC.

Several potential limitations may have impacted the generalizability of study outcomes. The experimental data used for this study, for example, were taken from a restricted demographic. Therefore, the extent to which these results can be applied to the general population is unclear. Further work must be done to validate the model against datasets from other demographics and, if necessary, to determine relevant parameter values for these groups. The model also has

only been evaluated for AC loaded in unconfined compression, but other deformation states, e.g., shear, may also be relevant to AC degeneration (Anderst and Tashman 2009; Setton 1995). Eight-chain networks have successfully modeled multiple deformation states for polymers (Arruda and Boyce 1993; Boyce and Arruda 2000), but this has not been examined with AC. Additional research into the extent to which the current model parameters can successfully simulate other important deformation states should now be conducted. Despite these limitations, the TI model appears to be highly valuable for modeling of AC within whole knee computational models. Use of the TI model will provide new insights into diseases associated with the non-uniform mechanical properties of the tissue without compromising the efficient dynamics of the overall model. If such steps are taken, efforts to implement and validate the TI model using a region-dependent C_R, within a valid knee joint model, should initially be undertaken.

The TI model as proposed in this paper can feasibly be implemented within any commercial finite element package that permits user-defined hyperelastic materials (e.g., Abaqus, Dassault Systèmes, France). The model's strain energy Eq. (6.17) would be supplied along with its derivatives and parameter values. The strain energy can be simplified by using constant values for all parameters except C_R (i.e., $nk\theta$): $\alpha, a, J, B = 1$; and b =1.348. To model the heterogeneity in human AC, C_R must be defined as a function of position across the cartilage surface (Fig. 7.4).

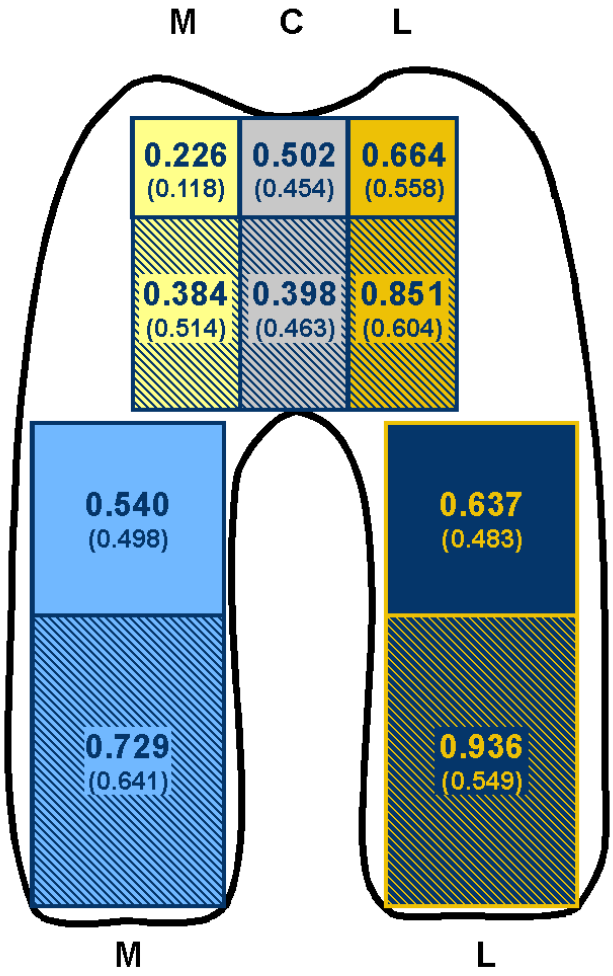

Figure 7.4: Mean C_R for each sub-region of the femur as determined by the Modified TI model. These values can be used to implement region-dependent mechanical properties into the TI network model of femoral cartilage. Solid areas indicate weightbearing sub-regions and hatched areas indicate less weightbearing sub-regions. M - medial, C – central, L – lateral.

Chapter 8: Summary and Future Directions

8.1 Introduction

The overarching goal of this dissertation was to gain a more detailed understanding of the non-uniform dynamic mechanical properties of healthy human knee AC and to subsequently develop a constitutive relation to successfully model these mechanics. Achievement of this goal would result in fundamental knowledge of AC mechanics that is critical to illuminating the elusive relationship between knee joint mechanics and OA development. With 10% of the world population suffering from OA and rate of occurrence continually increasing, these data are essential to preserving quality of life and long-term health of a large number of otherwise healthy individuals. The four major self-contained studies presented in this dissertation represent three key specific aims, designed to build sequentially on each other to achieve this goal. A brief synopsis of the key outcomes of each study is provided below, clearly demonstrating that overall study objectives were achieved. Methodological limitations and translational applications are also presented, which provide possible future directions for this critical baseline research.

8.2 Summary

In **Chapter 4**, the elastic tangent modulus at 10% strain ($E_{10\%}$) was determined at 21 locations across the tibial plateau. This represented the first high-resolution, high strain rate mechanical mapping of non-arthritic tibial AC. Moreover, it is the first study to attempt to identify regional mechanical patterns across individuals. The key outcome of this study was that $E_{10\%}$ significantly varied between regions. Although absolute values of the elastic tangent modulus differed between knees, the relative regional differences within knees remained consistent. Specifically, the pattern within the medial and lateral plateaus was (in order of increasing stiffness): central plateau, anterior periphery, and exterior and posterior periphery. While previous work has suggested that the meniscus-covered periphery has uniform mechanical properties, these results indicate a major paradigm shift: significant mechanical differences exist within the meniscus-covered AC. In fact, the anterior meniscus-covered AC exhibits mechanics much more similar to the central region than to the rest of the meniscus-covered area. The results of this study indicate that healthy human tibial plateau AC does have non-uniform mechanical properties.

Chapter 5 built on the work of Chapter 4 by documenting the spatial mechanics of femoral AC of the knee. In this case, $E_{10\%}$ was evaluated at nine locations on the trochlea and 20 locations on the condyles. Substantial differences were evident among these 29 locations within each knee. As with Chapter 4, to our knowledge this study represented the first high resolution, high strain rate mapping and the first attempt to identify regional patterns of healthy

human distal femoral AC mechanical properties. Examination of $E_{10\%}$ for the sub-regions determined that, similar to the tibia, the relative regional differences within knees were consistent, although absolute values differed between individuals. Within the trochlea, the lateral one-third exhibited a significantly higher modulus than the central and medial one-thirds. No significant differences, however, occurred between the upper one-third of the trochlea (i.e., the area that is most frequently weightbearing) and the lower two-thirds of the trochlea, which is less frequently weightbearing. Interestingly, the condyles exhibited an opposite regional pattern to the trochlea, which may indicate that knee joint motions impact AC health in these regions differently.

The results Chapters 4 and 5 clearly indicate that modeling tibiofemoral joint AC as a spatially uniform material is insufficient in applications where AC stress or strain is an output of interest. Therefore, **Chapters 6 and 7** sought to develop and evaluate a material model that could incorporate the regional mechanical non-uniformity of knee AC. In the course of this work, other modeling issues were also addressed: permitting high strain rate loading, replicating the non-linearity of the AC stress-strain response, producing accurate results for the unconfined compression configuration, maintaining physiological relevance, and minimizing model complexity and simulation time. To this end, a transversely isotropic statistical chain network model was developed and compared to existing isotropic statistical chain network models. Several key outcomes were determined from these studies. First, the model was highly effective in modeling the high strain rate, non-linear unconfined compression responses of both tibial

and femoral AC samples from across the entire joint surface. Second, the model also performed superior to the isotropic models. Third and most critically, the model captured regional variations in AC mechanics through changes in a single parameter (C_R). When all other parameters of the model were held fixed, adjusting C_R alone permitted the model to maintain an excellent fit to the experimental data, regardless of spatial location on the joint. Relative differences in this parameter between regions of each knee followed an identical pattern to that presented in **Chapters 4 and 5** for $E_{10\%}$. These outcomes suggest the transversely isotropic eight-chain network as a novel alternative to current modeling approaches for high strain rate, unconfined compression. It uniquely addresses the need to model spatially-varying AC mechanical properties, which is largely absent from current AC models.

8.3 Limitations

The studies in this dissertation represent significant advances in the identification and modeling of knee AC mechanics. However, several limitations should be considered when interpreting the outcomes of this research.

8.3.1 Limitations of Experimental Data

The population from which knee AC samples were taken was not representative of the general population. All knee donors were female, Caucasian, middle-aged, underweight, and suffering from various cancers at time of death. Further work is required to determine whether current outcomes apply

equally to other population demographics, such as males and overweight individuals.

Limited information was available for each knee donor: age, BMI at death, cause of death, and a brief medical history. Thus, factors that may influence cartilage health, such as physical activity and BMI throughout life, static and dynamic lower limb alignment, and any unreported surgeries or injuries were not accounted for in these studies. Additionally, side effects of cancer and cancer-related treatments (most individuals were on several prescription medications at the time of death) may have caused physical side effects to these individuals that influenced AC mechanics, such as weight loss and reduced physical activity. Such subject-specific factors likely contributed to the absolute differences in moduli values between knees, with some knees exhibiting higher overall moduli compared to other knees. Consequently, repeated-measures ANOVA was employed for statistical analysis to account for variance due to these between-subject effects. Therefore, the relative moduli differences between regions are generally applicable to the population represented by the study. Absolute values, however, varied substantially between individuals and the mean regional values presented in Chapters 4 and 5 should be applied outside the current test population with caution.

Extensive care was exercised to ensure AC samples were not arthritic, including stringent exclusion criteria for knee donors, rejection of knees that revealed extensive AC damage upon dissection, and application of the India ink test to identify arthritic tissue not apparent to the naked eye. In some knees,

however, a few samples had to be excluded for osteoarthritic damage. In these cases, the rest of the AC that was not osteoarthritic based on the India ink test was included in the study. These steps were necessarily undertaken because obtaining perfect AC even in relatively young individuals is nearly impossible. However, AC adjacent to osteoarthritic areas may also be degenerative and thus early arthritic AC may have been included in the study. To improve confidence in our methods, some excluded samples were tested and found to be an order of magnitude less stiff than healthy AC samples, including samples adjacent to arthritic areas. Therefore, we feel fairly confident that the presence of unhealthy AC within the study data was minimal at most. Nonetheless, these methods can be improved in future work by incorporating histological tests in addition to macroscopic examination to ensure the health of each AC sample.

Cartilage mechanics were determined by testing each sample in an unconfined compression configuration. This configuration was chosen because it is frequently used in the mechanical characterization of biological materials including AC, (Armstrong 1984; Bader 1992; Ballyns and Bonassar 2011; Brown and Singerman 1986; Cohen 1998a; Erne 2005; Fortin 2000), and it permitted examination of local tissue mechanics without a confounding influence of the surrounding material. Additionally, analysis of the data is straightforward and requires no assumptions of geometry, Poisson's ratio, or incompressibility that are required by other testing configurations (Korhonen 2002). However, use of this method required extracting each sample from the surrounding AC, which would disrupt the integrity of the collagen matrix at the sample's periphery and

may have affected the results. However, as the main interest of Chapters 4 and 5 was relative differences in AC mechanics, rather than absolute values, and all samples were extracted in an identical fashion, we feel that the use of unconfined compression does not compromise the results of these studies.

Mechanical testing utilized walking-like parameters, 100% strain/sec and 10% nominal strain, to determine the elastic modulus. These parameters were selected based on the limited data currently available regarding *in-vivo* AC deformation. It is likely that the entire AC surface does not experience identical strains or strain rates given the complex loading pattern of the joint, but these local variations are currently unknown. As knowledge of spatial *in-vivo* AC deformation improves, these analyses can be revised to improve understanding of the regional AC mechanical properties most relevant to common joint loading patterns. However, the stress-strain curves presented in Chapters 4 and 5 had similar curvature, suggesting that relative differences at 10% strain would remain consistent at higher or lower strains. This was similarly confirmed by Chapters 6 and 7 in which the stress-strain response was dictated by C_R, which controls the initial modulus (i.e., small strain response) of the curve. Therefore, the results of this dissertation still provide highly valuable initial insight into the regional properties of knee AC.

Articular cartilage mechanics were evaluated with nominal stress and strain rather than true stress and strain, which is typically preferred for large strains (>5%) (Rees 2006). The linear actuator used for this study can currently only produce constant strain rate tests, which precludes a true strain rate test

because it requires continuous updating of the strain rate during testing. Therefore, we felt that it was most appropriate to report data as nominal stress-strain. This decision was additionally supported by several factors: the peak strains for each test remained near the small strain regime, the study focused on relative and not absolute values in moduli, and the nearly-incompressible nature of healthy AC permits conversion from nominal stress-strain to true stress-strain via:

$$\sigma = s(1 + e) \tag{8.1}$$

$$\varepsilon = \ln(1 + e) \tag{8.2}$$

where σ is true stress, s is nominal stress, ε is true strain, and e is nominal strain. Furthermore, both the data and the model used nominal stress and strain, so there is no loss of accuracy. Regardless of these facts, work is underway to address the limitation of a constant strain rate within the testing protocols.

A final important limitation of the experimental studies pertains to the classification of regions. Spatial regional analysis of knee AC mechanics is not present in the literature. Therefore, the tibial and femoral regions adopted herein were based on regional variations in knee AC thickness and physiology and the non-uniform joint contact during walking and other activities. Particularly with respect to the “weightbearing” and “less weightbearing” classifications, data defining these regions is currently limited due to the minimal knowledge of *in-vivo* AC deformations. It is plausible that different or additional regional classifications would yield different outcomes. However, we feel our chosen regions are intuitive, based on known physiology and joint mechanics, permit ease of

identification on MRI, and relate to distinct and informative spatial mechanical patterns.

8.3.2 Limitations of Modeling Approach

As with all theoretical formulations of biological phenomena, several assumptions were made in modeling the knee AC that must be considered in applying the results. The model assumed that the AC was perfectly transversely isotropic, that this transverse isotropy was uniform across the width of the tissue, and the tissue was perfectly incompressible. The structure of the collagen matrix, however, is highly complex (Cohen 1998b; Jeffery 1991; Moger 2009). While its collagen fibers have a preferential direction in the STZ that appears similar to transverse isotropy, this alignment changes throughout the tissue depth (Jeffery 1991) and the degree of anisotropy may vary across the width of the tissue (Clark 1991). Likewise, healthy AC is nearly incompressible under high strain rate loading due to its high water content, but not perfectly incompressible. Compressibility, however, is influenced by loading rate, water content, proteoglycan density, and relative ionic concentrations in the fluid (Bader 1992; Lu and Mow 2008; Mow and Guo 2002). Nonetheless, even with incorporation of these assumptions the model fit a wide range of data with excellent accuracy, which largely justifies these assumptions.

The most valuable type of theoretical model can model multiple deformation states of the same material with a single set of parameters. It also can successfully simulate datasets other than the one against which it was

validated. The AC model developed herein was validated against a single series of unconfined compression experiments. Cross-validation has not yet been conducted against other deformation states or experimental data sets. Our current work represents a significant step in model development and proof of concept, but is currently confined, therefore, to this testing configuration and dataset. This limitation does not invalidate the model, but it does indicate a critical avenue of further model development. Likewise, the AC constitutive model has been developed with the goal of implementing it within a larger computational model of the knee. We suggest in Section 8.4 a method for executing this task. However, this work, while highly feasible, has not yet been undertaken. Immediate steps will be undertaken to develop and validate a full knee model that represents dynamic tibiofemoral AC behaviors via this TI constitutive model.

8.4 Implications and Future Directions

8.4.1 Experimental studies

The results of **Chapters 4 and 5**, taken together, have important implications for understanding OA development. Recent technological advances have enabled *in-vivo* measurement of joint AC contact during dynamic movements (Anderst 2005; DeFrate 2004). While changes in spatial contact paths and frequency of loading can be identified with these techniques, the extent to which such alterations would affect the stresses in the AC is unclear. Incorporation of the regional tibial and femoral AC mappings developed herein

can address this issue, which would provide essential insight for determining the mechanism(s) of knee OA initiation and progression.

From a practical standpoint, this type of study could be implemented by combining *in-vivo* dynamic joint imaging, i.e., via high-speed bi-plane fluoroscopy (Deneweth 2010; Tashman 2007), or dynamic MRI (Barrance 2006; Carpenter 2009; Logan 2004) in conjunction with static MRI of the unloaded knee joint in full extension. Biplane fluoroscopy or dynamic MRI would be used to determine the path of AC contact as the subject performs a functional task of interest (DeFrate 2004; Kozanek 2009; Liu 2010). Separately, the static MRI would be used to reconstruct a map of the subject's knee AC using 3D medical image segmentation software (Baldwin 2010; Cohen 1999; Liu 2008). The spatial regions evaluated in Chapters 4 and 5 would be defined on the segmented AC surface to provide a high-probability mapping of the relative regional stiffness of a subject's knee AC. Finally, the dynamic joint contact path would be overlain on the relative AC stiffness map. From this, several outcomes can be determined, including the frequency with which each region was loaded during the task and at what phase in the task the loading occurred.

This technique has immediate and critical benefits for studying which regions of knee AC are more frequently loaded in patients at-risk for developing OA (e.g., individuals with injured anterior cruciate ligaments). Additionally, relative differences in regional AC contact patterns can be related to joint kinematics to identify "risky" joint motions that disproportionately load high-modulus regions. Incorporation of joint kinetics with regional AC moduli can be

used to provide even better estimates of AC stress throughout the dynamic task. Taken together, such efforts would afford relations between altered joint contact patterns and potentially detrimental loading conditions for the knee AC to be explored. Further, the ability for explicit clinical interventions to improve these outcomes could be systematically investigated. While alterations in the joint loading pattern have long been postulated to initiate knee OA, little direct evidence exists to confirm that abnormal loading patterns that disproportionately load certain regions of AC are present in high OA-risk populations. Therefore, these additional insights would be highly advantageous to the study of knee OA development and the long-term goal of drastically reducing global OA incidence.

8.4.2 Modeling Studies

Based off the results of **Chapters 6 and 7**, an immediate avenue of future work is to implement the model within a finite element computational scheme. The transversely isotropic eight-chain network developed in this thesis is an anisotropic hyperelastic strain energy function. Such models can be implemented into most commercial finite element packages as a user-defined material model. Implementation, while not trivial, is relatively straightforward. Typically, the strain energy equation (6.17) must be supplied along with its first and second derivatives. Values of all fixed parameters also must be provided. Finally, the material definition must include an algorithm for assigning C_R based on the spatial location of each numerical integration point. Fixed and spatially-dependent parameter values can be taken directly from Chapters 6 and 7. Once

the model is implemented and validated in an independent AC numerical model, it should be incorporated and validated within a whole knee joint model.

A valid knee model with regionally-varying AC affords a baseline for a myriad of investigations examining knee joint function and health. For example, “risky” kinematics, as identified from the research extensions of Chapters 4 and 5 or from other work, can be input into the model and regional AC stress and/or strain can be output to evaluate the likelihood that suggested kinematic profiles could initiate OA development. A number of key morphologic indices have been additionally proposed to contribute to the risk of OA development and/or progression (Bierma-Zeinstra and Koes 2007; Brouwer 2007; Prodromos 2008; Smith 2006). Systematic variations in such factors, e.g. anterior cruciate ligament stiffness or coronal plane knee alignment, can be conducted within knee models with regionally varying AC to identify the relevant contributions of each factor to local AC stress and/or strain and, in turn, OA risk. Surgical and rehabilitative interventions can also be examined with the model to determine the extent to which they return AC stress/strain to “normal” levels. For example, high tibial osteotomy is currently employed to limit medial compartment OA progression (Gomoll 2011; Rossi 2011) by altering the mechanical axis of the knee. It is unclear, however, how changing the mechanical axis of the knee affects the AC loading pattern. Cadaveric methods, which are typically used to study high tibial osteotomy, are hindered by the finite experimental life of the cadaveric knee and cannot indicate cartilage stresses (Javidan 2013; Van Thiel 2011). These issues can be overcome by employing computational simulations within knee joint

models with spatially-varying AC properties, which allow an infinite number of experiments and can predict regional AC stress.

In conclusion, the outcomes of this dissertation substantially advance research into the mechanism(s) of knee OA development through two key outcomes. First, the relative moduli of healthy tibial and femoral AC have been mapped across the joint surface. These data provide critical knowledge into the extensive variability and spatial pattern of knee AC mechanics that is crucial to establishing relations between abnormal knee joint motions and OA initiation. Second, a novel non-linear constitutive relation that successfully models the spatial variations in knee AC moduli has been developed. This model will substantially improve current dynamic computational knee models, particularly for the study of knee OA development, by incorporating locally-dependent moduli without compromising model efficiency or accuracy. The net result of this research ultimately will be an improved quality of life for a large number of otherwise healthy individuals suffering the debilitating consequences of knee OA.

APPENDIX A

Tibiofemoral Joint Kinematics of the Anterior Cruciate Ligament-Reconstructed Knee During A Single-Legged Hop Landing

Jessica M. Deneweth, Michael J. Bey, Scott G. McLean, Terrence R. Lock, Patricia A. Kolowich and Scott Tashman
Am J Sports Med 2010 38: 1820-8.

Tibiofemoral Joint Kinematics of the Anterior Cruciate Ligament-Reconstructed Knee During a Single-Legged Hop Landing

Jessica M. Deneweth,*†‡ Michael J. Bey,† PhD, Scott G. McLean,‡§ PhD, Terrence R. Lock,‖ MD, Patricia A. Kolowich,‖ MD, and Scott Tashman,¶ PhD

From the †Bone and Joint Center, and the ‖Department of Orthopaedic Surgery, Henry Ford Hospital, Detroit, Michigan, the ‡School of Kinesiology, and the §Bone and Joint Injury Prevention and Rehabilitation Center, University of Michigan, Ann Arbor, Michigan, and the ¶Department of Orthopaedic Surgery, University of Pittsburgh, Pittsburgh, Pennsylvania

Background: Abnormal 3-dimensional tibiofemoral joint kinematics have been identified in anterior cruciate ligament-reconstructed knees during functional gait tasks, which is suggested to directly affect risk of knee osteoarthritis. However, the extent to which similar high-risk abnormalities are present during more demanding maneuvers, such as single-legged hopping, is largely unknown.

Hypothesis: When performing a single-legged forward hop landing, the reconstructed knee will demonstrate altered sagittal, frontal, and transverse plane kinematics compared with the contralateral limb.

Study Design: Controlled laboratory study.

Methods: High-speed biplane radiography was used to quantify bilateral 3-dimensional tibiofemoral joint kinematics in 9 subjects with unilaterally reconstructed anterior cruciate ligaments (mean time after surgery, 4 months) during 3 single-legged, forward hop landing trials. Mean subject-based initial foot contact and maximum stance (0-250 ms) values were calculated for each kinematic variable. Two-tailed paired *t* tests were subsequently applied to examine for the main effect of limb (reconstructed vs contralateral).

Results: The reconstructed knees exhibited significantly greater extension ($P = .04$), external tibial rotation ($P = .006$), and medial tibial translation ($P = .02$) than the contralateral knees at initial contact. Reconstructed knees underwent significantly greater maximum flexion ($P = .05$), maximum external tibial rotation ($P = .01$), and maximum anterior tibial translation ($P = .02$). No significant differences existed between limbs for initial contact ($P = .65$) or maximum adduction-abduction ($P = .55$).

Conclusion: Tibiofemoral joint kinematics of the anterior cruciate ligament-reconstructed knee are significantly different from those of the uninjured contralateral limb during a single-legged hop landing. This altered kinematic profile, in conjunction with the large impact loads associated with hopping, may further contribute to the risk of posttraumatic knee osteoarthritis.

Clinical Relevance: Returning to sports involving dynamic single-legged landings at 4 months after anterior cruciate ligament reconstruction surgery may contribute to accelerated knee joint degeneration.

Keywords: anterior cruciate ligament; reconstruction; joint kinematics; osteoarthritis; hopping

Anterior cruciate ligament (ACL) rupture is a common sports injury, representing a significant source of pain, disability, and medical expense. A high percentage of ACL ruptures occur in young, healthy athletes during sports activity.[1,10] In addition to extensive short-term trauma and loss of play, approximately 50% of all ACL ruptures lead to osteoarthritis within 10 to 20 years after the incident injury.[30] Consequently, it is not uncommon for posttraumatic osteoarthritis to afflict persons as young as 30 years old.[41] For patients of such a young age, successful treatment options are limited, often necessitating cessation of strenuous activity.[21]

Surgical reconstruction is the current standard of care for a ruptured ACL in physiologically young, physically active persons. The primary goal of ACL reconstruction is the restoration of normal joint kinematics.[13] Indeed, during "low-demand" gait tasks such as level-ground walking, ACL-reconstructed knees have been found to demonstrate tibiofemoral joint kinematics similar to those of matched

*Address correspondence to Jessica M. Deneweth, 401 Washtenaw Avenue, Ann Arbor, MI 48109 (e-mail: jmden@umich.edu).

One or more authors has declared a potential conflict of interest: This project was supported by grant AR046387 from the National Institutes of Health/National Institute of Arthritis and Musculoskeletal and Skin.

The American Journal of Sports Medicine, Vol. 38, No. 9
DOI: 10.1177/0363546510365531

TABLE 1
Subject Characteristics[a]

Subject No.	Age, y	Sex	Height, in	Weight, lb	Graft Type	Additional Procedures
1	27	M	75	210	HD	Medial meniscal repair
2	22	F	64	155	HS	Partial lateral meniscectomy
3	19	F	67	150	HD	None
4	17	M	66	150	HD	Medial meniscal repair
5	22	M	66	172	HD	Medial/lateral menisci repairs
6	23	F	68	150	HS	None
7	52	M	70	194	AD	None
8	49	M	72	170	AD	Partial medial meniscectomy
9	28	M	71	190	HD	Partial lateral meniscectomy

[a]HD, hamstring tendon autograft double-bundle technique; HS, hamstring tendon autograft single-bundle technique; AD, allograft double-bundle technique.

control knees.[20] Previous research suggests, however, that this goal may not be readily achieved for more demanding tasks, such as those that incorporate rapid deceleration and/or pivoting. For example, during single-legged hopping and single-legged vertical drop landing, ACL-reconstructed knees were found to undergo significantly different knee flexion motion than the uninjured contralateral knees.[22,52,54] Furthermore, Papannagari and colleagues[35] reported that ACL-reconstructed knees underwent significantly more anterior tibial translation and external tibial rotation while performing a single-legged lunge than the healthy contralateral knee. Similarly, during downhill treadmill running, ACL-reconstructed knees have been reported to demonstrate significantly more adduction and external rotation of the tibia relative to the femur than the uninjured contralateral knees.[49] These data strongly suggest that ACL reconstruction fails to restore normal joint kinematics during dynamic movement tasks. Moreover, it has been suggested that abnormal knee joint kinematics play a critical role in the initiation and progression of knee osteoarthritis.[6,9,18]

Patients who elect to undergo surgical reconstruction of a torn ACL most often choose this treatment option because they wish to return to preinjury activity levels, which are typically high.[45] Therefore, it is important to determine the extent to which normal kinematics are restored during movements relevant to this particular patient population. Single-legged hop landings are synonymous with the demanding jumping and cutting movements of high-level competitive sports, such as soccer and basketball.[42] Moreover, single-legged hopping induces larger vertical ground-reaction forces than walking, running, or lunging.[2,22,32,38,54] Although it is likely that the high forces placed on the knee joint by single-legged hopping elicit further kinematic differences between ACL-reconstructed and uninjured contralateral knees,[39] accurate 3-dimensional (3D) kinematic data to support this notion do not exist.

Therefore, the objective of this study was to use dynamic radiostereophotogrammetric analysis (RSA; accuracy, ± 0.1 mm[46,48,49]) to evaluate 3D tibiofemoral joint kinematics in patients with unilateral ACL reconstruction during the landing phase of a single-legged hop. On the basis of previous studies of the ACL-reconstructed knee during dynamic motions,[22,35,49] we hypothesized that the reconstructed knee would demonstrate altered sagittal, frontal, and transverse plane kinematics compared with the uninvolved limb.

MATERIALS AND METHODS

Subjects

We enrolled 9 recreational athletes (6 men and 3 women) who were undergoing primary arthroscopic reconstructive surgery to repair a unilateral ACL rupture (Table 1). Based on previous data comparing ACL-reconstructed and uninvolved limb kinematics for downhill running,[49] we estimated that to achieve 80% power with an alpha level of 0.05, a minimum of 7 subjects would be required. Inclusion criteria were (1) no history of surgery to either limb and (2) no damage to the injured limb other than the ruptured ACL and minor meniscal tears requiring removal of no more than one third of the radial width of the meniscus. All subjects who matched the inclusion criteria and who were undergoing surgery by one of the participating surgeons were contacted to participate in the study. Mean subject age was 28.8 $\pm$ 12.8 years. Mean time from injury to surgery was 9.6 $\pm$ 9.5 months. Mean time from surgery to testing was 4.4 $\pm$ 0.7 months. We obtained informed consent from all subjects, and the appropriate institutional review board for human subject research approved the study protocol.

Surgical Reconstruction

The ACL reconstruction surgery was performed by 1 of 2 surgeons (P.A.K. and T.R.L.). Graft type was not restricted and included single-bundle hamstring tendon autograft (n = 2), double-bundle hamstring tendon autograft (n = 5), and double-bundle allograft (n = 2). For the single-bundle reconstructions, the femoral graft tunnel was drilled using a transtibial guide. For the double-bundle surgeries, the posterolateral femoral tunnel was drilled through an accessory medial portal and the anteromedial femoral tunnel was placed using a transtibial guide. Interference screw

fixation was used in all cases. During the ACL reconstruction procedure, the surgeon inserted small tantalum spheres (1.6-mm diameter) into the distal femur and proximal tibia of both limbs using a cannulated drill.[48] The sphere placement was such that each bone contained 3 noncollinear spheres with a minimum 2-cm separation between spheres. The surgeon did not attempt to place the spheres at specific anatomical landmarks. The tantalum spheres served as internal markers for the dynamic RSA procedure employed in this study. This method has been used extensively and reported in previous studies by our research group.[4,5,47-49]

Testing Procedures

After surgery, all subjects completed the standard rehabilitation protocol of our institution. The rate of rehabilitation was dictated by the patient's progress. Laboratory testing took place once the physician cleared the subject to return to light sports activity, typically 4 to 5 months after surgery. We used dynamic RSA to assess 3D tibiofemoral joint kinematics from biplane radiographic images acquired during the landing phase of a single-legged forward hop. The biplane x-ray system contains 2 x-ray gantries that are configured with their beam paths intersecting at 60° in a plane parallel to the floor. Each gantry contains a 100-kW pulsed x-ray generator (CPX 3100CV; EMD Technologies, Quebec, Canada), a 30-cm image intensifier (Shimadzu AI5765HVP, Kyoto, Japan), and a high-speed digital video camera (Phantom IV, Vision Research, Wayne, New Jersey). This experimental approach has been used in previous studies of knee function and is capable of measuring in vivo joint motion to an accuracy of within ± 0.1 mm.[46,49]

Subjects were positioned in the biplane x-ray system so that the knee of interest would remain in the system's 3D imaging volume throughout the landing phase of a single-legged forward hop. Subjects were required to complete 3 successful 0.5-second forward hop trials for each leg. To perform a successful hop, the subject was required to stand on 1 leg and, at his or her discretion, to jump forward over a 4-cm high obstacle and land at a distance of 30 cm in front of the takeoff position. The subject landed on the takeoff leg and was required to maintain this position for as long as possible. The 0.5-second data collection period was initiated when the subject was in flight before landing and included at least 250 ms of the postimpact phase. While in the air, the subject broke the plane of an optoelectric switch (RadioShack, Fort Worth, Texas), which triggered the biplane x-ray system to begin recording. Radiographs were generated using an exposure of 90 kVp and 160 mA, with the digital radiographic images collected at 170 Hz.

On the same day as laboratory testing, subjects underwent bilateral CT imaging of the tibiofemoral joint. The CT field of view was approximately 28 × 28 cm, slice thickness ranged from 0.6 to 1.25 mm, and in-plane resolution was approximately 0.55 mm per pixel. The 3D bone models of the distal femur and proximal tibia of each knee joint were reconstructed from the CT images, as previously described in detail.[46] First, the 3D center of each implanted tantalum bead was located within the CT volume to within the nearest one-half slice in the CT image stack and to within the nearest pixel within the slice (ImageJ 1.32 J, National Institutes of Health, Bethesda, Maryland). Next the tibia and femur were manually segmented from surrounding tissues. After segmentation, custom software was used to perform feature-based interpolation to create the reconstructed 3D bone model.

Measuring Tibiofemoral Joint Motion

Custom software tracked the 2-dimensional position of each tantalum bead from each of the biplane x-ray images throughout all trials. The 2-dimensional positions were combined to reconstruct the 3D position of each bead,[43] and these positions were subsequently low-pass filtered using a sixth-order zero-lag Butterworth digital filter with a 20 Hz cutoff frequency. Subject-specific local anatomical coordinate systems were created for both the femur and tibia as previously described in detail.[46] The origin of the femoral coordinate system was defined as the 3D point halfway between the center of the medial and lateral femoral condyles. Similarly, the origin of the tibial coordinate system was defined to be the 3D point located halfway between the most medial and lateral aspects of the tibial plateau. Rotations of the tibia relative to the femur were defined with respect to the bone-fixed coordinate systems, and calculated using body-fixed axes in the order flexion-extension, adduction-abduction, and internal-external rotation.[49] Neutral rotations (zero values) were defined as the position where the tibial and femoral coordinate systems were aligned. Anteroposterior and mediolateral displacements of the tibia relative to the femur were also quantified using the position vector from the femoral anatomical origin to the tibial anatomical origin.

Statistical Analysis

For each successful hopping trial, the initial foot contact value and maximum value within the first 250 ms of stance were quantified bilaterally for the 3 rotational and 2 translational kinematic variables described earlier. This interval was selected as it captures the primary loading phase of the knee (ie, achievement of maximum knee flexion angle and peak ground-reaction force and a return toward full extension) during this task. Mean subject-based values for each of these measures were subsequently determined. Two-tailed paired *t* tests were used to examine for the main effect of limb (reconstructed vs contralateral) on each of these dependent measures. An alpha level of 0.05 was used to denote statistical significance.

RESULTS

A number of kinematic differences were observed between the reconstructed and uninvolved limbs for the single-legged hopping task. Specifically, the reconstructed limb

TABLE 2
Means and Standard Deviations for All Dependent Variables Examined[a]

Dependent Variable	Initial Contact		Maximum	
	Recon	Contra	Recon	Contra
Knee flexion, deg	19.08 ± 8.64[b]	26.04 ± 9.60[b]	38.92 ± 10.85[b]	47.69 ± 8.14[b]
Knee adduction (+) / abduction (−), deg	0.87 ± 0.91	0.65 ± 1.76	1.28 ± 1.92	0.94 ± 2.26
Internal (+) / external (−) tibial rotation, deg	0.61 ± 4.30[b]	6.02 ± 4.59[b]	4.84 ± 6.28[b]	9.84 ± 5.70[b]
Lateral (+) / medial (−) tibial displacement, mm	0.89 ± 1.47[b]	2.51 ± 1.30[b]	1.16 ± 1.70	2.65 ± 1.34
Anterior (+) / posterior (−) tibial displacement, mm	9.89 ± 4.14	9.40 ± 4.34	12.00 ± 3.67[b]	10.48 ± 4.21[b]

[a]Recon, reconstructed limb; Contra, uninjured contralateral limb.
[b]$P \leq .05$, side difference.

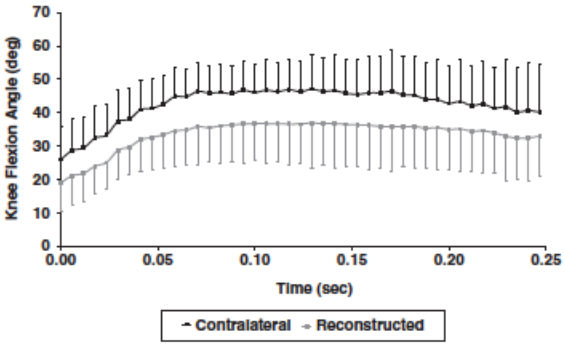

Figure 1. Mean knee flexion angle as a function of time after initial contact. For visual clarity, unidirectional positive and negative standard deviations are represented for the contralateral and reconstructed limbs, respectively. The reconstructed knee was significantly less flexed at initial contact ($P = .04$).

was significantly ($P = .04$) less flexed than the healthy limb at initial contact (Figure 1). Similarly, maximum knee flexion was significant ($P = .05$), with the reconstructed limb exhibiting a smaller maximum flexion angle than the contralateral limb (Table 2).

The reconstructed limb was found to be consistently more adducted than the contralateral limb throughout the landing phase (Figure 2), but the differences were not found to be statistically significant for either initial contact ($P = .65$) or maximum ($P = .55$) angles (Table 2).

The reconstructed limb was less internally rotated throughout the first 250 ms of ground contact (Figure 3), with significantly smaller initial contact ($P = .006$) and maximum ($P = .01$) angles being observed (Table 2)

Bilateral limb differences were evident in mediolateral tibial displacements at initial contact, with the reconstructed limb demonstrating significantly ($P = .02$) less lateral displacement at this time point compared with the contralateral limb (Figure 4 and Table 2). Statistical differences were not observed between limbs, however, for maximum mediolateral displacement values ($P = .08$) (Table 2).

Bilateral limb differences were observed in anteroposterior tibial displacement measures, with the reconstructed limb eliciting significantly ($P = .02$) larger maximum anterior tibial displacement compared with the contralateral limb (Table 2). Although this trend was observed across the entire stance phase, no significant differences were evident between limbs for anteroposterior displacement at initial contact ($P = .23$) (Figure 5 and Table 2).

DISCUSSION

The objective of this study was to determine the extent to which ACL reconstruction may promote 3D kinematic differences between the reconstructed and contralateral (uninjured) limbs during a single-legged hop landing. On the basis of previous studies of the ACL-reconstructed knee during dynamic motions,[22,35,49] we hypothesized that the reconstructed knee would demonstrate altered sagittal, frontal, and transverse plane kinematics compared with the uninvolved limb. As predicted, the reconstructed tibia remained in a more extended, externally rotated, and anteriorly displaced position relative to the femur throughout the hop landing. Significant differences also were evident for mediolateral displacement, while no significant differences occurred for adduction-abduction angle.

The 30-cm forward hopping task provided a reasonably challenging yet safe landing movement for assessing bilateral kinematic differences that were reflective of the athletic ability of the subjects, as well as consistent with the physical constraints of the biplane x-ray system. All subjects were familiar with the hopping task from their postsurgical rehabilitation routine.[24,33] The single-legged hopping task is highly relevant to the athletic demands placed on ACL-reconstructed knees when the patients return to sports activity after surgery.[54] Therefore, we believe that identification of bilateral differences in tibiofemoral joint kinematics during performance of this task is pertinent to elucidating the role of joint mechanics in the development of knee osteoarthritis in this population.

We found that the reconstructed knee was consistently more extended throughout the single-legged hop landing. This observation agrees with previous studies investigating

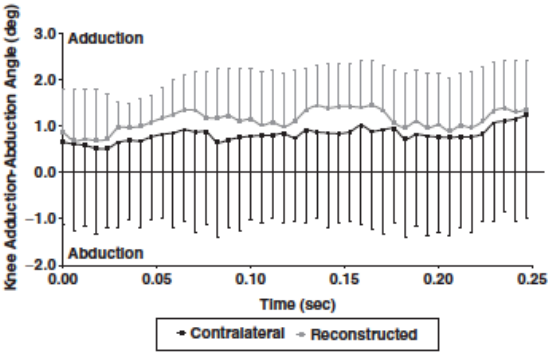

Figure 2. Mean knee adduction-abduction angle as a function of time after initial foot contact. For the vertical axis, positive values indicate adduction and negative values indicate abduction. Unidirectional positive and negative standard deviations are represented for the reconstructed and contralateral limbs, respectively. No significant differences in adduction-abduction angle were detected between limbs at initial contact ($P = .65$).

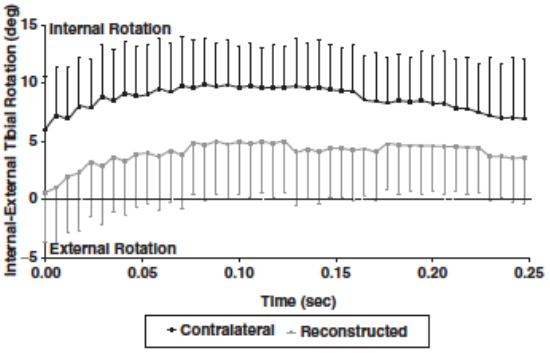

Figure 3. Mean internal-external tibial rotation as a function of time after initial foot contact. For the vertical axis, positive values indicate internal rotation and negative values represent external rotation. Unidirectional positive and negative standard deviations are represented for the contralateral and reconstructed limbs, respectively. The reconstructed tibia was significantly more externally rotated at heel strike ($P = .006$).

single-legged hopping knee mechanics in patients with ACL-deficient and ACL-reconstructed knees.[22,39,42,54] A more extended landing posture may be a strategy that patients with ACL-deficient or ACL-reconstructed knees use to achieve greater knee stabilization, particularly in the presence of increased anteroposterior laxity, as seen in this study.[42,53] Increased extension may also be necessary to prevent knee collapse that may otherwise occur during the deceleration phase because of a relatively weak opposing quadriceps force, a common occurrence following ACL injury.[23,25,34]

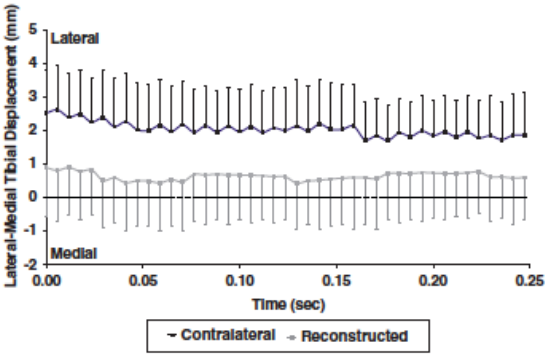

Figure 4. Mean mediolateral tibial displacement relative to the femur as a function of time after initial foot contact. For the vertical axis, positive values indicate lateral translation and negative values indicate medial translation. Unidirectional positive and negative standard deviations are represented for the contralateral and reconstructed limbs, respectively. The reconstructed tibia was positioned significantly less laterally at heel strike ($P = .02$).

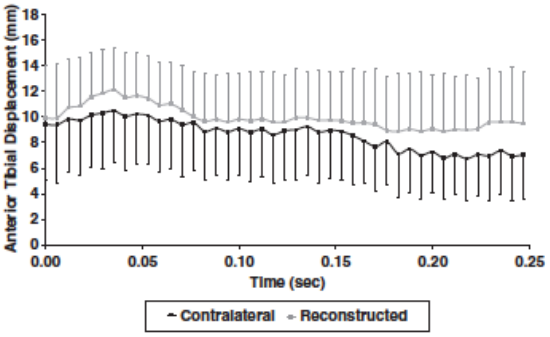

Figure 5. Mean anterior tibial displacement relative to the femur as a function of time after initial foot contact. Unidirectional positive and negative standard deviations are represented for the reconstructed and contralateral limbs, respectively. No significant difference was detected between limbs at initial contact ($P = .23$).

Because we did not measure muscle strength in the current study, however, we can only speculate to the plausibility of this relationship. It should be noted also that, although a minimum jump height was enforced using an obstacle that was 4 cm high, the height of the single-legged hop was not controlled for in the experimental protocol. Therefore, it is possible that the peak hop height achieved by the uninjured limb was larger than the peak height achieved by the injured limb, which would require more energy to be absorbed at impact and more knee joint flexion in the uninjured limb. However, because the task was a forward hop over a relatively small distance rather than a vertical hop, we believe that jump height differences would be relatively minor.

No significant differences in knee adduction were detected in this study, contrary to our hypothesis. Previous studies using identical techniques[49] compared reconstructed and healthy contralateral limbs during downhill running and found the reconstructed limb to be significantly more adducted (mean difference, 1.32°). This difference is much larger than the between-limb differences noted in the present study (0.22° and 0.34° for initial contact and maximum knee adduction angle, respectively). It is commonly proposed that the reconstructed knee has increased knee adduction motions or loads during walking and running gait, increasing risk of osteoarthritis through an altered cartilage loading pattern.[8,17,49] Our current results, however, suggest that at least for single-legged hopping, substantial modifications in cartilage loading patterns via an altered knee abduction-adduction profile are not as likely.

In this study we found that internal-external tibial rotation of the ACL-reconstructed limb did not match that of the uninjured limb during a single-legged hop landing. Specifically, the reconstructed knee was significantly more externally rotated both at initial contact and at maximum internal-external rotation. Tashman and colleagues[49] found similar results when they evaluated 3D knee kinematics during downhill treadmill running using the same techniques as the current study. Further, this bilateral kinematic discrepancy continued to manifest at both 5 and 12 months after surgery. Ristanis et al[40] similarly found that ACL-reconstructed knees had greater axial tibial rotation than healthy control knees during 2 separate tasks: a jump landing followed by a 90° pivot turn and a stair descent followed by a 90° pivot turn. Interestingly, however, Georgoulis and colleagues[20] found no significant differences in stance-phase axial rotation between reconstructed and contralateral knees during level-ground walking. Therefore, it seems plausible that altered internal-external knee rotation patterns may occur in the ACL-reconstructed knee only during more demanding dynamic landing and pivoting tasks, where extreme axial loading states are known to manifest.[12,31] If altered knee internal-external rotations contribute to the risk of osteoarthritis initiation and/or progression, as has been proposed, then the single-legged hop may indeed be a task where this risk is exacerbated.[6,7,44]

It is interesting to note that the current study included 7 subjects who had undergone double-bundle ACL reconstruction surgery, a technique that is believed to better restore healthy internal-external rotation patterns.[55] A post hoc comparison between the single- and double-bundle subjects found no substantial differences in any kinematic variable, including internal-external rotation angles. However, the sizes of the single- and double-bundle subgroups were too small to provide adequate statistical power for this analysis. These double-bundle reconstructions were also performed with the femoral anteromedial tunnel drilled using a transtibial technique, typically resulting in a nonanatomical anteromedial tunnel position high in the femoral notch. More recent double-bundle techniques employ a medial portal drilling approach to place the femoral graft tunnels over the native insertions of the ACL bundles.[37] Kinematics after this anatomical double-bundle reconstruction procedure are currently under investigation.

This study determined that the reconstructed knee experienced larger peak anterior tibial translation than the contralateral knee by an average of 1.52 ± 1.55 mm. Previous studies have reported similar results for walking, double-legged squatting, and single-legged lunging.[11, 29, 35] Papannagari et al[35] found that reconstructed knees translated approximately 2.9 mm more at full extension and 2.2 mm more at 15° of knee flexion when compared with the uninvolved limb for a quasistatic weightbearing single-legged lunge. Logan and colleagues[29] investigated sagittal plane kinematics during quasistatic squatting using open MRI and similarly determined that the anterior tibial position of the involved knee was greater at 0°, 20°, 45°, and 90° of knee flexion. As the ACL is the primary restraint to anterior tibial translation, one of the primary goals of ACL reconstruction is to return anterior laxity, and hence the anteroposterior translational profile, to within the limits of the uninjured knee.[13,16] Our results support the notion that this goal may not be readily achieved using the surgical techniques employed for this study,[3,11,35] which represent commonly used surgical procedures.[13,56]

The reconstructed tibia was more medially translated than the contralateral tibia at initial contact, with this discrepancy being maintained over the first 250 ms of stance. Li and colleagues[27] similarly found that the tibiofemoral contact patterns of ACL-deficient knees during a single-legged weightbearing lunge were consistent with a medial shift of the tibia. Previous research has also shown that the ACL resists medial tibial translation, again suggesting that this medial tibial shift in the reconstructed limb may stem from an ACL graft that is unable to properly restrain knee joint motion.[26,28,36]

The results of this study demonstrate that bilateral differences in tibiofemoral kinematics exist following ACL reconstruction, even for patients who have been cleared to return to light sports activity. These findings may lend insight into the high incidence of early knee osteoarthritis that is common in this patient population.[30,41] Hop landings are representative of the demanding sports activities that many patients with ACL-reconstructed knees perform on a regular basis.[42,45] These activities elicit larger impact-induced joint forces than other movements that have been previously studied in the ACL-reconstructed knee (eg, walking).[2,22,32,38,54] Thus, when a hop landing is performed with the knee in a more extended position, it is likely that the articular cartilage and other surrounding joint tissues are subjected to much higher compressive loads than would be experienced within the uninjured and comparatively more flexed knee.[42]

In the current study, we determined an average difference in external tibial rotation angle between the reconstructed and contralateral knees of 5.41° and 5.00° for initial contact and peak values, respectively. Andriacchi and colleagues[6] have demonstrated that a 5° internal rotational offset of the tibia leads to accelerated cartilage thinning in a finite element model of the tibiofemoral joint. Therefore, it is plausible that an external rotational shift of similar magnitude,

particularly when coupled with a more extended knee position, could lead to similar cartilage changes.

In the present study, the reconstructed knee also showed altered anteroposterior and mediolateral displacements of the tibia relative to the femur. As with a rotational offset, it is likely that these changes alter the manner in which the articular cartilage is loaded.[7,18] The greater anterior displacement of the tibia seen in this study likely creates a posterior shift in the femur's contact location on the tibial plateau. Ironically, a posterior shift in the femur's location of contact on the tibia has been associated with greater cartilage thinning on the anterior tibial plateau.[7] In other words, a decrease in load may be associated with cartilage thinning. In contrast, Li and colleagues[28] have found that shifts in mediolateral tibial position in the ACL-deficient knee shift the point of tibial contact in the medial compartment closer to the medial tibial spine, where cartilage degeneration frequently presents in the ACL-deficient knee. These contradictory findings—that is, that cartilage degeneration occurs in regions where loads are believed to increase or decrease—suggest that the relationship between cartilage loading and cartilage degeneration is highly complex and not well understood. Regardless of the specific mechanism that relates cartilage degeneration and mechanical loading, patients with ACL-reconstructed knees who perform a demanding activity such as hopping may be altering the cartilage loading patterns in a manner that is sufficient to initiate the development of osteoarthritis.[9]

The data from this study also suggest that the manifestation of bilateral kinematic differences appears to be task-specific. In this study, single-legged hopping elicited significant differences in all examined degrees of freedom, except adduction of the tibia relative to the femur. However, in a study of knee kinematics during downhill running[49] that evaluated a similar population using identical methods, significant differences were noted only in the angles of tibial adduction and tibial external rotation. Similarly, Bush-Joseph et al[15] found that sagittal plane kinematics were not significantly different between patients with ACL-reconstructed knees and healthy matched controls for light activities such as walking, but that kinematic profiles did indeed diverge for higher demand activities. Consequently, it is important for future studies aimed at assessing the efficacy of specific ACL reconstruction techniques to assess knee function during high-level activities that are consistent with the goals of the young, athletic patient.

The strength of this study lies in the high accuracy of the methods used to quantify tibiofemoral kinematics. Dynamic RSA eliminates errors due to skin motion associated with surface marker-based techniques, thus allowing for the 3D, dynamic measurement of in vivo knee motion to an accuracy of within ± 0.1 mm.[46] To our knowledge, no prior study has assessed 3D tibiofemoral kinematics during single-legged hopping with this level of accuracy. However, we also acknowledge limitations to this study. In particular, we adopted the uninjured contralateral knee as the control population for the reconstructed knee. Although this method has been employed in several previous studies to examine motion of the ACL-injured knee,[27,29,35] comparisons between injured and contralateral limbs must be made cautiously, given the potential for intraindividual variability and the possibility that the incident injury or surgery may have produced bilateral neuromuscular changes.[14,51] Nonetheless, on the basis of recent work suggesting that intersubject variability exceeds intrasubject variability with regard to tibiofemoral joint morphometric dimensions[19] and gait mechanics,[50] we believe that the use of the uninvolved limb as the control population was justified. Additionally, the sample size was small, and we did not control for surgeon, meniscal injury, graft type, sex, age, rate of rehabilitation, or activity level, although all subjects were recreational athletes. Therefore, extrapolation of these results to the general ACL-reconstructed population must be made with caution. Regardless, the development of posttraumatic osteoarthritis is neither confined to a single reconstructive procedure nor to a single patient demographic. Because this group of subjects represents a typical subset of those with ACL-reconstructed knees and statistically significant trends were consistent across subjects despite the apparent heterogeneity, we are confident in our results.

In conclusion, patients who have undergone unilateral ACL reconstruction perform a single-legged hop landing with significantly different tibiofemoral joint motion in the reconstructed knee as compared with the contralateral knee. This task is a common sports movement that elicits large ground-reaction forces and places substantial demands on the knee joint. For patients with ACL-reconstructed knees who are returning to sports activity, performing this task with the potentially altered knee kinematics demonstrated in this study could result in deleterious consequences for articular cartilage health. Future investigations will be necessary to determine the extent to which this kinematic profile alters the normal loading pattern of the tibiofemoral joint. Additionally, it is important to determine the mechanisms underlying bilateral kinematic differences after ACL reconstruction and to evaluate the ability of clinical interventions, such as a more anatomical graft tunnel placement, to reduce these changes.

REFERENCES

1. Agel J, Arendt EA, Bershadsky B. Anterior cruciate ligament injury in national collegiate athletic association basketball and soccer: a 13-year review. *Am J Sports Med*. 2005;33(4):524-530.
2. Alkjaer T, Simonsen EB, Magnusson SP, Aagaard H, Dyhre-Poulsen P. Differences in the movement pattern of a forward lunge in two types of anterior cruciate ligament deficient patients: copers and non-copers. *Clin Biomech (Bristol, Avon)*. 2002;17(8):586-593.
3. Almekinders LC, Pandarinath R, Rahusen FT. Knee stability following anterior cruciate ligament rupture and surgery: the contribution of irreducible tibial subluxation. *J Bone Joint Surg Am*. 2004;86(5):983-987.
4. Anderst WJ, Les C, Tashman S. In vivo serial joint space measurements during dynamic loading in a canine model of osteoarthritis. *Osteoarthritis Cartilage*. 2005;13(9):808-816.
5. Anderst WJ, Tashman S. The association between velocity of the center of closest proximity on subchondral bones and osteoarthritis progression. *J Orthop Res*. 2009;27(1):71-77.

6. Andriacchi TP, Briant PL, Bevill SL, Koo S. Rotational changes at the knee after ACL injury cause cartilage thinning. *Clin Orthop Relat Res*. 2006;442:39-44.
7. Andriacchi TP, Koo S, Scanlan SF. Gait mechanics influence healthy cartilage morphology and osteoarthritis of the knee. *J Bone Joint Surg Am*. 2009;91(suppl 1):95-101.
8. Andriacchi TP, Mundermann A. The role of ambulatory mechanics in the initiation and progression of knee osteoarthritis. *Curr Opin Rheumatol*. 2006;18(5):514-518.
9. Andriacchi TP, Mundermann A, Smith RL, Alexander EJ, Dyrby CO, Koo S. A framework for the in vivo pathomechanics of osteoarthritis at the knee. *Ann Biomed Eng*. 2004;32(3):447-457.
10. Arendt E, Dick R. Knee injury patterns among men and women in collegiate basketball and soccer: NCAA data and review of literature. *Am J Sports Med*. 1995;23(6):694-701.
11. Beard DJ, Murray DW, Gill HS, et al. Reconstruction does not reduce tibial translation in the cruciate-deficient knee an in vivo study. *J Bone Joint Surg Br*. 2001;83(8):1098-1103.
12. Besier TF, Lloyd DG, Cochrane JI, Ackland TR. External loading of the knee joint during running and cutting maneuvers. *Med Sci Sports Exerc*. 2001;33(7):1168-1175.
13. Beynnon BD, Johnson RJ, Abate JA, Fleming BC, Nichols CE. Treatment of anterior cruciate ligament injuries, part I. *Am J Sports Med*. 2005;33(10):1579-1602.
14. Brown TN, Palmieri-Smith RM, McLean SG. Sex and limb differences in hip and knee kinematics and kinetics during anticipated and unanticipated jump landings: implications for anterior cruciate ligament injury. *Br J Sports Med*. 2009;43(13):1049-1056.
15. Bush-Joseph CA, Hurwitz DE, Patel RR, et al. Dynamic function after anterior cruciate ligament reconstruction with autologous patellar tendon. *Am J Sports Med*. 2001;29(1):36-41.
16. Butler DL, Noyes FR, Grood ES. Ligamentous restraints to anterior-posterior drawer in the human knee: a biomechanical study. *J Bone Joint Surg Am*. 1980;62(2):259-270.
17. Butler RJ, Minick KI, Ferber R, Underwood F. Gait mechanics after ACL reconstruction: implications for the early onset of knee osteoarthritis. *Br J Sports Med*. 2009;43(5):366-370.
18. Chaudhari AM, Briant PL, Bevill SL, Koo S, Andriacchi TP. Knee kinematics, cartilage morphology, and osteoarthritis after ACL injury. *Med Sci Sports Exerc*. 2008;40(2):215-222.
19. Dargel J, Feiser J, Gotter M, Pennig D, Koebke J. Side differences in the anatomy of human knee joints. *Knee Surg Sports Traumatol Arthrosc*. 2009;17(11):1368-1376.
20. Georgoulis AD, Papadonikolakis A, Papageorgiou CD, Mitsou A, Stergiou N. Three-dimensional tibiofemoral kinematics of the anterior cruciate ligament-deficient and reconstructed knee during walking. *Am J Sports Med*. 2003;31(1):75-79.
21. Gillquist J, Messner K. Anterior cruciate ligament reconstruction and the long-term incidence of gonarthrosis. *Sports Med*. 1999;27(3):143-156.
22. Gokeler A, Hof AL, Arnold MP, Dijkstra PU, Postema K, Otten E. Abnormal landing strategies after ACL reconstruction [published online ahead of print February 2, 2009]. *Scand J Med Sci Sports*.
23. Ingersoll CD, Grindstaff TL, Pietrosimone BG, Hart JM. Neuromuscular consequences of anterior cruciate ligament injury. *Clin Sports Med*. 2008;27(3):383-404.
24. Kvist J. Rehabilitation following anterior cruciate ligament injury: current recommendations for sports participation. *Sports Med*. 2004;34(4):269-280.
25. Lewek M, Rudolph K, Axe M, Snyder-Mackler L. The effect of insufficient quadriceps strength on gait after anterior cruciate ligament reconstruction. *Clin Biomech (Bristol, Avon)*. 2002;17(1):56-63.
26. Li G, Defrate LE, Rubash HE, Gill TJ. In vivo kinematics of the ACL during weight-bearing knee flexion. *J Orthop Res*. 2005;23(2):340-344.
27. Li G, Moses JM, Papannagari R, Pathare NP, DeFrate LE, Gill TJ. Anterior cruciate ligament deficiency alters the in vivo motion of the tibiofemoral cartilage contact points in both the anteroposterior and mediolateral directions. *J Bone Joint Surg Am*. 2006;88(8):1826-1834.
28. Li G, Papannagari R, DeFrate LE, Yoo JD, Park SE, Gill TJ. The effects of ACL deficiency on mediolateral translation and varus-valgus rotation. *Acta Orthop*. 2007;78(3):355-360.
29. Logan MC, Williams A, Lavelle J, Gedroyc W, Freeman M. Tibiofemoral kinematics following successful anterior cruciate ligament reconstruction using dynamic multiple resonance imaging. *Am J Sports Med*. 2004;32(4):984-992.
30. Lohmander LS, Englund PM, Dahl LL, Roos EM. The long-term consequence of anterior cruciate ligament and meniscus injuries: osteoarthritis. *Am J Sports Med*. 2007;35(10):1756-1769.
31. McLean SG, Felin RE, Suedekum N, Calabrese G, Passerallo A, Joy S. Impact of fatigue on gender-based high-risk landing strategies. *Med Sci Sports Exerc*. 2007;39(3):502-514.
32. Munro CF, Miller DI, Fuglevand AJ. Ground reaction forces in running: a reexamination. *J Biomech*. 1987;20(2):147-155.
33. Myer GD, Paterno MV, Ford KR, Hewett TE. Neuromuscular training techniques to target deficits before return to sport after anterior cruciate ligament reconstruction. *J Strength Cond Res*. 2008;22(3):987-1014.
34. Palmieri-Smith RM, Thomas AC. A neuromuscular mechanism of posttraumatic osteoarthritis associated with ACL injury. *Exerc Sport Sci Rev*. 2009;37(3):147-153.
35. Papannagari R, Gill TJ, Defrate LE, Moses JM, Petruska AJ, Li G. In vivo kinematics of the knee after anterior cruciate ligament reconstruction: a clinical and functional evaluation. *Am J Sports Med*. 2006;34(12):2006-2012.
36. Petersen W, Zantop T. Anatomy of the anterior cruciate ligament with regard to its two bundles. *Clin Orthop Relat Res*. 2007;454:35-47.
37. Pombo MW, Shen W, Fu FH. Anatomic double-bundle anterior cruciate ligament reconstruction: where are we today? *Arthroscopy*. 2008;24(10):1168-1177.
38. Riley PO, Paolini G, Della Croce U, Paylo KW, Kerrigan DC. A kinematic and kinetic comparison of overground and treadmill walking in healthy subjects. *Gait Posture*. 2007;26(1):17-24.
39. Risberg MA, Moksnes H, Storevold A, Holm I, Snyder-Mackler L. Rehabilitation after anterior cruciate ligament injury influences joint loading during walking but not hopping. *Br J Sports Med*. 2009;43(6):423-428.
40. Ristanis S, Stergiou N, Patras K, Tsepis E, Moraiti C, Georgoulis AD. Follow-up evaluation 2 years after ACL reconstruction with bone-patellar tendon-bone graft shows that excessive tibial rotation persists. *Clin J Sport Med*. 2006;16(2):111-116.
41. Roos EM. Joint injury causes knee osteoarthritis in young adults. *Curr Opin Rheumatol*. 2005;17(2):195-200.
42. Rudolph KS, Axe MJ, Snyder-Mackler L. Dynamic stability after ACL injury: who can hop? *Knee Surg Sports Traumatol Arthrosc*. 2000;8(5):262-269.
43. Selvik G. Roentgen stereophotogrammetry: a method for the study of the kinematics of the skeletal system. *Acta Orthop Scand Suppl*. 1989;232:1-51.
44. Stergiou N, Ristanis S, Moraiti C, Georgoulis AD. Tibial rotation in anterior cruciate ligament (ACL)-deficient and ACL-reconstructed knees: a theoretical proposition for the development of osteoarthritis. *Sports Med*. 2007;37(7):601-613.
45. Swirtun LR, Eriksson K, Renstrom P. Who chooses anterior cruciate ligament reconstruction and why? A 2-year prospective study. *Scand J Med Sci Sports*. 2006;16(6):441-446.
46. Tashman S, Anderst W. In-vivo measurement of dynamic joint motion using high speed biplane radiography and CT: application to canine ACL deficiency. *J Biomech Eng*. 2003;125(2):238-245.
47. Tashman S, Anderst W, Kolowich P, Havstad S, Arnoczky S. Kinematics of the ACL-deficient canine knee during gait: serial changes over two years. *J Orthop Res*. 2004;22(5):931-941.
48. Tashman S, Collon D, Anderson K, Kolowich P, Anderst W. Abnormal rotational knee motion during running after anterior cruciate ligament reconstruction. *Am J Sports Med*. 2004;32(4):975-983.
49. Tashman S, Kolowich P, Collon D, Anderson K, Anderst W. Dynamic function of the ACL-reconstructed knee during running. *Clin Orthop Relat Res*. 2007;454:66-73.

50. Teichtahl AJ, Wluka AE, Morris ME, Davis SR, Cicuttini FM. The associations between the dominant and nondominant peak external knee adductor moments during gait in healthy subjects: evidence for symmetry. *Arch Phys Med Rehabil*. 2009;90(2):320-324.
51. Urbach D, Awiszus F. Impaired ability of voluntary quadriceps activation bilaterally interferes with function testing after knee injuries: a twitch interpolation study. *Int J Sports Med*. 2002;23(4):231-236.
52. Vairo GL, Myers JB, Sell TC, Fu FH, Hamer CD, Lephart SM. Neuromuscular and biomechanical landing performance subsequent to ipsilateral semitendinosus and gracilis autograft anterior cruciate ligament reconstruction. *Knee Surg Sports Traumatol Arthrosc*. 2008;16(1):2-14.
53. van Uden CJ, Bloo JK, Kooloos JG, van Kampen A, de Witte J, Wagenaar RC. Coordination and stability of one-legged hopping patterns in patients with anterior cruciate ligament reconstruction: preliminary results. *Clin Biomech (Bristol, Avon)*. 2003;18(1):84-87.
54. Webster KE, Gonzalez-Adrio R, Feller JA. Dynamic joint loading following hamstring and patellar tendon anterior cruciate ligament reconstruction. *Knee Surg Sports Traumatol Arthrosc*. 2004;12(1):15-21.
55. Yagi M, Kuroda R, Nagamune K, Yoshiya S, Kurosaka M. Double-bundle ACL reconstruction can improve rotational stability. *Clin Orthop Relat Res*. 2007;454:100-107.
56. Zantop T, Kubo S, Petersen W, Musahl V, Fu FH. Current techniques in anatomic anterior cruciate ligament reconstruction. *Arthroscopy*. 2007;23(9):938-947.

APPENDIX B

Derivation of the Transversely Isotropic Eight-Chain Network of Freely Jointed Chains

The strain energy function for the transversely isotropic eight-chain network derived from is (Section 6.3.1.4):

$$U_{TI} = U_0 + \frac{nk\Theta}{4}\left(N\sum_{i=1}^{4}\left[\frac{\rho^{(i)}}{N}\beta_\rho^{(i)} + ln\frac{\beta_\rho^{(i)}}{sinh\,\beta_\rho^{(i)}}\right] - \frac{\beta_P}{\sqrt{N}}ln\left[\lambda_{\boldsymbol{a}}^{a^2}\lambda_{\boldsymbol{b}}^{2b^2}\right]\right) + \cdots \quad \text{(B.1)}$$

$$\ldots + \frac{B}{\alpha^2}\{cosh[\alpha(J-1)] - 1\}$$

and

$$\rho = \frac{1}{2}\sqrt{a^2{\lambda_1}^2 + 2b^2{\lambda_2}^2} \quad \text{(B.2)}$$

$$P = \sqrt{N} = \frac{1}{2}\sqrt{a^2 + 2b^2} \quad \text{(B.3)}$$

$$\beta_\rho = \mathcal{L}^{-1}(\rho/N) \quad \text{(B.4)}$$

$$\beta_P = \mathcal{L}^{-1}(P/N) \quad \text{(B.5)}$$

where U_0 is a constant, n is the chain density, k is Boltzmann's constant (1.38065 x 10^{-23} J·K^{-1}), Θ is the absolute temperature, N is the number of rigid chain links per statistical chain, $\mathcal{L}^{-1}$ is the inverse Langevin function, P is the undeformed chain length, $\rho^{(i)}$ is the deformed length of the i^{th} chain, $\lambda_{\mathbf{a-c}}$ are the stretches along the principal material axes, J is the ratio of the deformed volume to the original volume, B controls the bulk compressibility near $J = 1$, and α is a constant that governs the curvature of the hydrostatic pressure versus volume curve for large volume changes.

For the case of unconfined compression:

$$\mathbf{F} = \begin{bmatrix} \lambda_1 & 0 & 0 \\ 0 & \lambda_2 & 0 \\ 0 & 0 & \lambda_3 \end{bmatrix} \quad \text{(B.6)}$$

For a transversely isotropic material, the principal stretches are related by the following expressions:

$$\lambda_1 = \lambda,\ \lambda_2 = \lambda_3 = J/\lambda \tag{B.7}$$

The principal stresses can be derived from Eq. (B.1) via the following equation:

$$T_i = \lambda_i \frac{\mathrm{d}U}{\mathrm{d}\lambda_i} + \mathrm{p}_o \tag{B.8}$$

Applying Eq. (B.8) to Eq. (B.1) and substituting Eqs. (B.6-7) yields the principal stresses:

$$T_1 = \frac{nk\theta a^2}{4J}\left[\frac{{\lambda_1}^2\beta_\rho}{\rho} - \frac{\beta_P}{\sqrt{N}}\right] + B\sinh(J-1) + \mathrm{p}_o \tag{B.9}$$

$$T_2 = T_3 = \frac{nk\theta b^2}{4J}\left[\frac{{\lambda_2}^2\beta_\rho}{\rho} - \frac{\beta_P}{\sqrt{N}}\right] + B\sinh(J-1) + \mathrm{p}_o \tag{B.10}$$

and λ_2 can be related to λ_1 through J:

$$J = \lambda_1{\lambda_2}^2 \rightarrow \lambda_2 = \sqrt{J/\lambda_1} \tag{B.11}$$

In the case of unconfined compression,

$$T_2 = T_3 = 0 \tag{B.12}$$

Thus, setting Eq. (B.10) = 0 and rearranging yields:

$$JB\sinh(J-1) + \mathrm{p}_o = -\frac{nk\theta b^2}{4}\left[\frac{{\lambda_2}^2\beta_\rho}{\rho} - \frac{\beta_P}{\sqrt{N}}\right] \tag{B.13}$$

Substituting Eq. (B.13) into Eq. (B.9):

$$T_1 = \left(\frac{nk\theta a^2}{4J}\left[\frac{{\lambda_1}^2\beta_\rho}{\rho} - \frac{\beta_P}{\sqrt{N}}\right] - \frac{nk\theta b^2}{4J}\left[\frac{{\lambda_2}^2\beta_\rho}{\rho} - \frac{\beta_P}{\sqrt{N}}\right]\right) \tag{B.14}$$

The true stress, T_{11}, can be converted to nominal stress, $T_{0_{11}}$ via:

$$\mathbf{T_0} = J\mathbf{T}\mathbf{F}^{-\boldsymbol{T}} \rightarrow T_{0_1} = T_1\frac{J}{\lambda_1} \tag{B.15}$$

which yields:

$$T_{0_1} = \left(\frac{nk\theta a^2}{4J}\left[\frac{{\lambda_1}^2\beta_\rho}{\rho} - \frac{\beta_P}{\sqrt{N}}\right] - \frac{nk\theta b^2}{4J}\left[\frac{{\lambda_2}^2\beta_\rho}{\rho} - \frac{\beta_P}{\sqrt{N}}\right]\right)\frac{J}{\lambda_1} \tag{B.16}$$

Rearranging terms and simplifying Eq. (B.16) gives the nominal stress in the axial direction [Eq. (6.21)]:

$$T_{0_1 TI} = \frac{nk\theta}{4\lambda_1}\left(a^2\left[\frac{{\lambda_1}^2\beta_\rho}{\rho} - \frac{\beta_P}{\sqrt{N}}\right] - b^2\left[\frac{{\lambda_2}^2\beta_\rho}{\rho} - \frac{\beta_P}{\sqrt{N}}\right]\right) \tag{B.17}$$

REFERENCES

Adatia, A., K. D. Rainsford, et al. (2012). "Osteoarthritis of the Knee and Hip. Part I: Aetiology and Pathogenesis as a Basis for Pharmacotherapy." J Pharm Pharmacol **64**(5): 617-25.

Almekinders, L. C., R. Pandarinath, et al. (2004). "Knee Stability Following Anterior Cruciate Ligament Rupture and Surgery. The Contribution of Irreducible Tibial Subluxation." J Bone Joint Surg Am **86-A**(5): 983-7.

Anderst, W. J., C. Les, et al. (2005). "In Vivo Serial Joint Space Measurements During Dynamic Loading in a Canine Model of Osteoarthritis." Osteoarthr Cartilage **13**(9): 808-16.

Anderst, W. J. and S. Tashman (2009). "The Association between Velocity of the Center of Closest Proximity on Subchondral Bones and Osteoarthritis Progression." J Orthop Res **27**(1): 71-7.

Andriacchi, T. P., P. L. Briant, et al. (2006). "Rotational Changes at the Knee after Acl Injury Cause Cartilage Thinning." Clin Orthop Relat Res **464**(442): 39-44.

Andriacchi, T. P., S. Koo, et al. (2009). "Gait Mechanics Influence Healthy Cartilage Morphology and Osteoarthritis of the Knee." J Bone Joint Surg Am **91**(2 Suppl 1): 95-101.

Andriacchi, T. P. and A. Mundermann (2006). "The Role of Ambulatory Mechanics in the Initiation and Progression of Knee Osteoarthritis." Curr Opin Rheumatol **18**(5): 514-18.

Andriacchi, T. P., A. Mundermann, et al. (2004). "A Framework for the in Vivo Pathomechanics of Osteoarthritis at the Knee." Ann Biomed Eng **32**(3): 447-57.

Armstrong, C. G., W. M. Lai, et al. (1984). "An Analysis of the Unconfined Compression of Articular Cartilage." J Biomech Eng **106**(2): 165-73.

Armstrong, C. G. and V. C. Mow (1982). "Variations in the Intrinsic Mechanical Properties of Human Articular Cartilage with Age, Degeneration, and Water Content." J Bone Joint Surg Am **64**(1): 88-94.

Arruda, E. M. (2011) "Statistical Mechanics Models of Equilibrium Behavior." Personal communication.

Arruda, E. M. and M. C. Boyce (1993). "A 3-Dimensional Constitutive Model for the Large Stretch Behavior of Rubber Elastic-Materials." J Mech Phys Solids **41**(2): 389-412.

Askew, M. J. and V. C. Mow (1978). "Biomechanical Function of the Collagen Fibril Ultrastructure of Articular Cartilage." J Biomech Eng **100**(3): 105-15.

Astephen, J. L., K. J. Deluzio, et al. (2008). "Gait and Neuromuscular Pattern Changes Are Associated with Differences in Knee Osteoarthritis Severity Levels." J Biomech **41**(4): 868-76.

Ateshian, G. A., B. J. Ellis, et al. (2007). "Equivalence between Short-Time Biphasic and Incompressible Elastic Material Responses." J Biomech Eng **129**(3): 405-12.

Ateshian, G. A., W. M. Lai, et al. (1994). "An Asymptotic Solution for the Contact of Two Biphasic Cartilage Layers." J Biomech **27**(11): 1347-60.

Ateshian, G. A., V. Rajan, et al. (2009). "Modeling the Matrix of Articular Cartilage Using a Continuous Fiber Angular Distribution Predicts Many Observed Phenomena." J Biomech Eng **131**(6): 061003.

Ateshian, G. A., W. H. Warden, et al. (1997). "Finite Deformation Biphasic Material Properties of Bovine Articular Cartilage from Confined Compression Experiments." J Biomech **30**(11-12): 1157-64.

Athanasiou, K. A., M. P. Rosenwasser, et al. (1991). "Interspecies Comparisons of in Situ Intrinsic Mechanical Properties of Distal Femoral Cartilage." J Orthop Res **9**(3): 330-40.

Bachrach, N. M., V. C. Mow, et al. (1998). "Incompressibility of the Solid Matrix of Articular Cartilage under High Hydrostatic Pressures." J Biomech **31**(5): 445-51.

Bader, D. L. and G. E. Kempson (1994). "The Short-Term Compressive Properties of Adult Human Articular Cartilage." Biomed Mater Eng **4**(3): 245-56.

Bader, D. L., G. E. Kempson, et al. (1992). "The Effects of Selective Matrix Degradation on the Short-Term Compressive Properties of Adult Human Articular Cartilage." Biochim Biophys Acta **1116**(2): 147-54.

Bae, J. Y., K. S. Park, et al. (2012). "Biomechanical Analysis of the Effects of Medial Meniscectomy on Degenerative Osteoarthritis." Med Biol Eng Comput **50**(1): 53-60.

Bae, W. C., M. M. Payanal, et al. (2010). "Topographic Patterns of Cartilage Lesions in Knee Osteoarthritis." Cartilage **1**(1): 10-19.

Baker-LePain, J. C. and N. E. Lane (2012). "Role of Bone Architecture and Anatomy in Osteoarthritis." Bone **51**(2): 197-203.

Baldwin, M. A., J. E. Langenderfer, et al. (2010). "Development of Subject-Specific and Statistical Shape Models of the Knee Using an Efficient Segmentation and Mesh-Morphing Approach." Comput Methods Programs Biomed **97**(3): 232-40.

Ballyns, J. J. and L. J. Bonassar (2011). "Dynamic Compressive Loading of Image-Guided Tissue Engineered Meniscal Constructs." J Biomech **44**(3): 509-16.

Barker, M. K. and B. B. Seedhom (2001). "The Relationship of the Compressive Modulus of Articular Cartilage with Its Deformation Response to Cyclic Loading: Does Cartilage Optimize Its Modulus So as to Minimize the Strains Arising in It Due to the Prevalent Loading Regime?" Rheumatology **40**(3): 274-84.

Barrance, P. J., G. N. Williams, et al. (2006). "Altered Knee Kinematics in Acl-Deficient Non-Copers: A Comparison Using Dynamic Mri." J Orthop Res **24**(2): 132-40.

Belo, J. N., M. Y. Berger, et al. (2007). "Prognostic Factors of Progression of Osteoarthritis of the Knee: A Systematic Review of Observational Studies." Arthritis Rheum **57**(1): 13-26.

Besier, T. F., G. E. Gold, et al. (2005). "A Modeling Framework to Estimate Patellofemoral Joint Cartilage Stress in Vivo." Med Sci Sports Exerc **37**(11): 1924-30.

Besier, T. F., G. E. Gold, et al. (2008). "The Influence of Femoral Internal and External Rotation on Cartilage Stresses within the Patellofemoral Joint." J Orthop Res **26**(12): 1627-35.

Bevill, S. L., P. L. Briant, et al. (2008). "Central and Peripheral Region Tibial Plateau Chondrocytes Respond Differently to in Vitro Dynamic Compression." Osteoarthr Cartilage **17**(8): 980-7.

Bierma-Zeinstra, S. M. and B. W. Koes (2007). "Risk Factors and Prognostic Factors of Hip and Knee Osteoarthritis." Nat Clin Pract Rheumatol **3**(2): 78-85.

Bingham, J. T., R. Papannagari, et al. (2008). "In Vivo Cartilage Contact Deformation in the Healthy Human Tibiofemoral Joint." Rheumatology **47**(11): 1622-27.

Bischoff, J. E., E. M. Arruda, et al. (2000). "Finite Element Modeling of Human Skin Using an Isotropic, Nonlinear Elastic Constitutive Model." J Biomech **33**(6): 645-52.

Bischoff, J. E., E. M. Arruda, et al. (2002). "A Microstructurally Based Orthotropic Hyperelastic Constitutive Law." J Appl Mech-T ASME **69**(5): 570-79.

Bischoff, J. E., E. M. Arruda, et al. (2004). "A Rheological Network Model for the Continuum Anisotropic and Viscoelastic Behavior of Soft Tissue." Biomech Model Mechanobiol **3**(1): 56-65.

Bitton, R. (2009). "The Economic Burden of Osteoarthritis." Am J Manag Care **15**(8 Suppl): S230-5.

Blagojevic, M., C. Jinks, et al. (2010). "Risk Factors for Onset of Osteoarthritis of the Knee in Older Adults: A Systematic Review and Meta-Analysis." Osteoarthr Cartilage **18**(1): 24-33.

Blankevoort, L. and R. Huiskes (1996). "Validation of a Three-Dimensional Model of the Knee." J Biomech **29**(7): 955-61.

Boschetti, F., F. Gervaso, et al. (2006). "Poroelastic Numerical Modelling of Natural and Engineered Cartilage Based on in Vitro Tests." Biorheology **43**(3-4): 235-47.

Boyan, B. D., L. Tosi, et al. (2012). "Sex Differences in Osteoarthritis of the Knee." J Am Acad Orthop Surg **20**(10): 668-9.

Boyce, M. C. and E. M. Arruda (2000). "Constitutive Models of Rubber Elasticity: A Review." Rubber Chem Technol **73**(3): 504-23.

Boyce, M. C., E. M. Arruda, et al. (1994). "The Large-Strain Compression, Tension, and Simple Shear of Polycarbonate." Polym Eng Sci **34**(9): 716-25.

Brandt, K. D. and M. Palmoski (1976). "Organization of Ground Substance Proteoglycans in Normal and Osteoarthritic Knee Cartilage." Arthritis Rheum **19**(2): 209-15.

Brouwer, G. M., A. W. van Tol, et al. (2007). "Association between Valgus and Varus Alignment and the Development and Progression of Radiographic Osteoarthritis of the Knee." Arthritis Rheum **56**(4): 1204-11.
Brown, C. P., T. C. Nguyen, et al. (2009). "Assessment of Common Hyperelastic Constitutive Equations for Describing Normal and Osteoarthritic Articular Cartilage." Proc Inst Mech Eng H **223**(H6): 643-52.
Brown, T. D. and R. J. Singerman (1986). "Experimental Determination of the Linear Biphasic Constitutive Coefficients of Human Fetal Proximal Femoral Chondroepiphysis." J Biomech **19**(8): 597-605.
Buckley, M. R., A. J. Bergou, et al. (2010). "High-Resolution Spatial Mapping of Shear Properties in Cartilage." J Biomech **43**(4): 796-800.
Buckley, M. R., J. P. Gleghorn, et al. (2008). "Mapping the Depth Dependence of Shear Properties in Articular Cartilage." J Biomech **41**(11): 2430-7.
Buckwalter, J. A., H. J. Mankin, et al. (2005). "Articular Cartilage and Osteoarthritis." Instr Course Lect **54**: 465-80.
Carpenter, R. D., S. Majumdar, et al. (2009). "Magnetic Resonance Imaging of 3-Dimensional in Vivo Tibiofemoral Kinematics in Anterior Cruciate Ligament-Reconstructed Knees." Arthroscopy **25**(7): 760-6.
Carter, D. R., G. S. Beaupre, et al. (2004). "The Mechanobiology of Articular Cartilage Development and Degeneration." Clin Orthop Relat Res **462**(427 Suppl): S69-77.
Carter, D. R. and M. Wong (2003). "Modelling Cartilage Mechanobiology." Philos Trans R Soc Lond B Biol Sci **358**(1437): 1461-71.
Chahine, N. O., C. C. Wang, et al. (2004). "Anisotropic Strain-Dependent Material Properties of Bovine Articular Cartilage in the Transitional Range from Tension to Compression." J Biomech **37**(8): 1251-61.
Chan, D. D., C. P. Neu, et al. (2009). "Articular Cartilage Deformation Determined in an Intact Tibiofemoral Joint by Displacement-Encoded Imaging." Magn Reson Med **61**(4): 989-93.
Chaudhari, A. M., P. L. Briant, et al. (2008). "Knee Kinematics, Cartilage Morphology, and Osteoarthritis after Acl Injury." Med Sci Sports Exerc **40**(2): 215-22.
Chegini, S. and S. J. Ferguson (2010). "Time and Depth Dependent Poisson's Ratio of Cartilage Explained by an Inhomogeneous Orthotropic Fiber Embedded Biphasic Model." J Biomech **43**(9): 1660-6.
Chen, A. C., W. C. Bae, et al. (2001). "Depth- and Strain-Dependent Mechanical and Electromechanical Properties of Full-Thickness Bovine Articular Cartilage in Confined Compression." J Biomech **34**(1): 1-12.
Chouliaras, V., S. Ristanis, et al. (2009). "Anterior Cruciate Ligament Reconstruction with a Quadrupled Hamstrings Tendon Autograft Does Not Restore Tibial Rotation to Normative Levels During Landing from a Jump and Subsequent Pivoting." J Sports Med Phys Fitness **49**(1): 64-70.
Cimmino, M. A. and M. Parodi (2005). "Risk Factors for Osteoarthritis." Semin Arthritis Rheum **34**(6 Suppl 2): 29-34.

Clark, J. M. (1991). "Variation of Collagen Fiber Alignment in a Joint Surface: A Scanning Electron Microscope Study of the Tibial Plateau in Dog, Rabbit, and Man." J Orthop Res **9**(2): 246-57.

Cohen, A. (1991). "A Pade Approximant to the Inverse Langevin Function." Rheologica Acta **30**(3): 270-73.

Cohen, B., W. M. Lai, et al. (1992). Unconfined Compression of Transversely-Isotropic Biphasic Tissues. Winter Annual Meeting of the American Society of Mechanical Engineers, November 8, 1992 - November 13, 1992, Anaheim, CA, USA, Publ by ASME.

Cohen, B., W. M. Lai, et al. (1998a). "A Transversely Isotropic Biphasic Model for Unconfined Compression of Growth Plate and Chondroepiphysis." J Biomech Eng **120**(4): 491-6.

Cohen, J. (1988). Statistical Power Analysis for the Behavioral Sciences. Hillsdale, N.J., L. Erlbaum Associates.

Cohen, N. P., R. J. Foster, et al. (1998b). "Composition and Dynamics of Articular Cartilage: Structure, Function, and Maintaining Healthy State." J Orthop Sports Phys Ther **28**(4): 203-15.

Cohen, Z. A., D. M. McCarthy, et al. (1999). "Knee Cartilage Topography, Thickness, and Contact Areas from Mri: In-Vitro Calibration and in-Vivo Measurements." Osteoarthr Cartilage **7**(1): 95.

Cohen, Z. A., V. C. Mow, et al. (2003). "Templates of the Cartilage Layers of the Patellofemoral Joint and Their Use in the Assessment of Osteoarthritic Cartilage Damage." Osteoarthr Cartilage **11**(8): 569-79.

Coleman, T. F. and Y. Li (1996). "An Interior, Trust Region Approach for Nonlinear Minimization Subject to Bounds." SIAM J Optimiz **6**: 418-45.

Creaby, M. W., Y. Wang, et al. (2010). "Dynamic Knee Loading Is Related to Cartilage Defects and Tibial Plateau Bone Area in Medial Knee Osteoarthritis." Osteoarthr Cartilage **18**(11): 1380-5.

Davis, A. M. (2012). "Osteoarthritis Year in Review: Rehabilitation and Outcomes." Osteoarthr Cartilage **20**(3): 201-6.

DeFrate, L. E., H. Sun, et al. (2004). "In Vivo Tibiofemoral Contact Analysis Using 3d Mri-Based Knee Models." J Biomech **37**(10): 1499-504.

Deneweth, J. M., M. J. Bey, et al. (2010). "Tibiofemoral Joint Kinematics of the Acl-Reconstructed Knee During a Single-Leg Hop Landing." Am J Sports Med **38**(9): 1820-28.

Deneweth, J. M., K. E. Newman, et al. (2013). "Heterogeneity of Tibial Plateau Cartilage in Response to a Physiological Compressive Strain Rate." J Orthop Res **31**(3): 370-5.

Dieppe, P. A. and L. S. Lohmander (2005). "Pathogenesis and Management of Pain in Osteoarthritis." Lancet **365**(9463): 965-73.

DiSilvestro, M. R. and J. K. Suh (2001). "A Cross-Validation of the Biphasic Poroviscoelastic Model of Articular Cartilage in Unconfined Compression, Indentation, and Confined Compression." J Biomech **34**(4): 519-25.

DiSilvestro, M. R. and J. K. Suh (2002). "Biphasic Poroviscoelastic Characteristics of Proteoglycan-Depleted Articular Cartilage: Simulation of Degeneration." Ann Biomed Eng **30**(6): 792-800.

DiSilvestro, M. R., Q. Zhu, et al. (2001). "Biphasic Poroviscoelastic Simulation of the Unconfined Compression of Articular Cartilage: Ii--Effect of Variable Strain Rates." J Biomech Eng **123**(2): 198-200.

Donahue, T. L., M. L. Hull, et al. (2002). "A Finite Element Model of the Human Knee Joint for the Study of Tibio-Femoral Contact." J Biomech Eng **124**(3): 273-80.

Eckstein, F., M. Reiser, et al. (2001). "In Vivo Morphometry and Functional Analysis of Human Articular Cartilage with Quantitative Magnetic Resonance Imaging--from Image to Data, from Data to Theory." Anat Embryol (Berl) **203**(3): 147-73.

Eckstein, F., W. Wirth, et al. (2008). "Patterns of Femorotibial Cartilage Loss in Knees with Neutral, Varus, and Valgus Alignment." Arthritis Rheum **59**(11): 1563-70.

Eckstein, F., W. Wirth, et al. (2010). "Magnitude and Regional Distribution of Cartilage Loss Associated with Grades of Joint Space Narrowing in Radiographic Osteoarthritis--Data from the Osteoarthritis Initiative (Oai)." Osteoarthr Cartilage **18**(6): 760-8.

Edelsten, L., J. E. Jeffrey, et al. (2010). "Viscoelastic Deformation of Articular Cartilage During Impact Loading." Soft Matter **6**(20): 5206-12.

Eisenberg, S. R. and A. J. Grodzinsky (1985). "Swelling of Articular Cartilage and Other Connective Tissues: Electromechanochemical Forces." J Orthop Res **3**(2): 148-59.

Eisenberg, S. R. and A. J. Grodzinsky (1987). "The Kinetics of Chemically Induced Nonequilibrium Swelling of Articular Cartilage and Corneal Stroma." J Biomech Eng **109**(1): 79-89.

Elliott, D. M., D. A. Narmoneva, et al. (2002). "Direct Measurement of the Poisson's Ratio of Human Patella Cartilage in Tension." J Biomech Eng **124**(2): 223-8.

Erne, O. K., J. B. Reid, et al. (2005). "Depth-Dependent Strain of Patellofemoral Articular Cartilage in Unconfined Compression." J Biomech **38**(4): 667-72.

Eyre, D. (2002). "Collagen of Articular Cartilage." Arthritis Res **4**(1): 30-5.

Eyre, D. R. (1991). "The Collagens of Articular Cartilage." Semin Arthritis Rheum **21**(3 Suppl 2): 2-11.

Eyre, D. R., M. A. Weis, et al. (2006). "Articular Cartilage Collagen: An Irreplaceable Framework?" Eur Cells Mater **12**: 57-63.

Federico, S. and W. Herzog (2008). "On the Anisotropy and Inhomogeneity of Permeability in Articular Cartilage." Biomech Model Mechanobiol **7**(5): 367-78.

Feller, J. A., A. A. Amis, et al. (2007). "Surgical Biomechanics of the Patellofemoral Joint." Arthroscopy **23**(5): 542-53.

Felson, D. T. (1996). "Does Excess Weight Cause Osteoarthritis and, If So, Why?" Ann Rheum Dis **55**(9): 668-70.

Felson, D. T. (2004). "Risk Factors for Osteoarthritis: Understanding Joint Vulnerability." Clin Orthop Relat Res(427 Suppl): S16-21.

Felson, D. T., R. C. Lawrence, et al. (2000). "Osteoarthritis: New Insights. Part 1: The Disease and Its Risk Factors." Ann Intern Med **133**(8): 635-46.

Felson, D. T., J. Niu, et al. (2007). "Correlation of the Development of Knee Pain with Enlarging Bone Marrow Lesions on Magnetic Resonance Imaging." Arthritis Rheum **56**(9): 2986-92.
Flandry, F. and G. Hommel (2011). "Normal Anatomy and Biomechanics of the Knee." Sports Med Arthrosc **19**(2): 82-92.
Fleming, B. C., M. J. Hulstyn, et al. (2005). "Ligament Injury, Reconstruction and Osteoarthritis." Curr Opin Orthop **16**(5): 354-62.
Foroughi, N., R. Smith, et al. (2009). "The Association of External Knee Adduction Moment with Biomechanical Variables in Osteoarthritis: A Systematic Review." Knee **16**(5): 303-9.
Fortin, M., J. Soulhat, et al. (2000). "Unconfined Compression of Articular Cartilage: Nonlinear Behavior and Comparison with a Fibril-Reinforced Biphasic Model." J Biomech Eng **122**(2): 189-95.
Froimson, M. I., A. Ratcliffe, et al. (1997). "Differences in Patellofemoral Joint Cartilage Material Properties and Their Significance to the Etiology of Cartilage Surface Fibrillation." Osteoarthr Cartilage **5**(6): 377-86.
Gannon, A. R., T. Nagel, et al. (2012). "The Role of the Superficial Region in Determining the Dynamic Properties of Articular Cartilage." Osteoarthr Cartilage **20**(11): 1417-25.
Garg, A. and P. S. Walker (1990). "Prediction of Total Knee Motion Using a Three-Dimensional Computer-Graphics Model." J Biomech **23**(1): 45-58.
Giuliani, J. R., K. G. Kilcoyne, et al. (2009). "Anterior Cruciate Ligament Anatomy: A Review of the Anteromedial and Posterolateral Bundles." J Knee Surg **22**(2): 148-54.
Gomoll, A. H. (2011). "High Tibial Osteotomy for the Treatment of Unicompartmental Knee Osteoarthritis: A Review of the Literature, Indications, and Technique." Phys Sportsmed **39**(3): 45-54.
Gomoll, A. H., G. Filardo, et al. (2012). "Surgical Treatment for Early Osteoarthritis. Part I: Cartilage Repair Procedures." Knee Surg Sports Traumatol Arthrosc **20**(3): 450-66.
Goodfellow, J., D. S. Hungerford, et al. (1976). "Patello-Femoral Joint Mechanics and Pathology. 1. Functional Anatomy of the Patello-Femoral Joint." J Bone Joint Surg Br **58**(3): 287-90.
Goudakos, I. G., C. Konig, et al. (2009). "Stair Climbing Results in More Challenging Patellofemoral Contact Mechanics and Kinematics Than Walking at Early Knee Flexion under Physiological-Like Quadriceps Loading." J Biomech **42**(15): 2590-96.
Gray, H. (1918). Anatomy of the Human Body, Lea & Febiger.
Gu, W. Y., W. M. Lai, et al. (1997). "A Triphasic Analysis of Negative Osmotic Flows through Charged Hydrated Soft Tissues." J Biomech **30**(1): 71-8.
Gulati, A., R. Chau, et al. (2009). "Localization of the Full-Thickness Cartilage Lesions in Medial and Lateral Unicompartmental Knee Osteoarthritis." J Orthop Res **27**(10): 1339-46.
Han, S. K., S. Federico, et al. (2005). "An Articular Cartilage Contact Model Based on Real Surface Geometry." J Biomech **38**(1): 179-84.

Hasler, E. M., W. Herzog, et al. (1999). "Articular Cartilage Biomechanics: Theoretical Models, Material Properties, and Biosynthetic Response." Crit Rev Biomed Eng **27**(6): 415-88.
Haughom, B., W. Schairer, et al. (2012). "Abnormal Tibiofemoral Kinematics Following Acl Reconstruction Are Associated with Early Cartilage Matrix Degeneration Measured by Mri T1rho." Knee **19**(4): 482-7.
Haut Donahue, T. L., M. L. Hull, et al. (2004). "The Sensitivity of Tibiofemoral Contact Pressure to the Size and Shape of the Lateral and Medial Menisci." J Orthop Res **22**(4): 807-14.
Hawker, G. A., S. Mian, et al. (2011). "Osteoarthritis Year 2010 in Review: Non-Pharmacologic Therapy." Osteoarthr Cartilage **19**(4): 366-74.
Hayes, W. C., L. M. Keer, et al. (1972). "A Mathematical Analysis for Indentation Tests of Articular Cartilage." J Biomech **5**(5): 541-51.
Hayes, W. C. and L. F. Mockros (1971). "Viscoelastic Properties of Human Articular Cartilage." J Appl Physiol **31**(4): 562-8.
Heiden, T. L., D. G. Lloyd, et al. (2009). "Knee Joint Kinematics, Kinetics and Muscle Co-Contraction in Knee Osteoarthritis Patient Gait." Clin Biomech **24**(10): 833-41.
Hellio Le Graverand, M. P., R. J. Buck, et al. (2009). "Subregional Femorotibial Cartilage Morphology in Women--Comparison between Healthy Controls and Participants with Different Grades of Radiographic Knee Osteoarthritis." Osteoarthr Cartilage **17**(9): 1177-85.
Hendren, L. and P. Beeson (2009). "A Review of the Differences between Normal and Osteoarthritis Articular Cartilage in Human Knee and Ankle Joints." Foot (Edinb) **19**(3): 171-6.
Herzog, W., S. Diet, et al. (1998). "Material and Functional Properties of Articular Cartilage and Patellofemoral Contact Mechanics in an Experimental Model of Osteoarthritis." J Biomech **31**(12): 1137-45.
Holmes, M. H. and V. C. Mow (1990). "The Nonlinear Characteristics of Soft Gels and Hydrated Connective Tissues in Ultrafiltration." J Biomech **23**(11): 1145-56.
Hootman, J. M. and C. G. Helmick (2006). "Projections of Us Prevalence of Arthritis and Associated Activity Limitations." Arthritis Rheum **54**(1): 226-9.
Hori, R. Y. and L. F. Mockros (1976). "Indentation Tests of Human Articular Cartilage." J Biomech **9**(4): 259-68.
Hoshino, Y. and S. Tashman (2012). "Internal Tibial Rotation During in Vivo, Dynamic Activity Induces Greater Sliding of Tibio-Femoral Joint Contact on the Medial Compartment." Knee Surg Sports Traumatol Arthrosc **20**(7): 1268-75.
Huang, C. Y., V. C. Mow, et al. (2001). "The Role of Flow-Independent Viscoelasticity in the Biphasic Tensile and Compressive Responses of Articular Cartilage." J Biomech Eng **123**(5): 410-7.
Hubbard, M. (1993). "Computer Simulation in Sport and Industry." J Biomech **26 Suppl 1**: 53-61.
Hubley-Kozey, C. L., N. A. Hill, et al. (2009). "Co-Activation Differences in Lower Limb Muscles between Asymptomatic Controls and Those with Varying

Degrees of Knee Osteoarthritis During Walking." Clin Biomech **24**(5): 407-14.
Hunter, D. J., Y. Zhang, et al. (2006). "Increase in Bone Marrow Lesions Associated with Cartilage Loss: A Longitudinal Magnetic Resonance Imaging Study of Knee Osteoarthritis." Arthritis Rheum **54**(5): 1529-35.
Hunter, D. J., Y. Zhang, et al. (2005). "Structural Factors Associated with Malalignment in Knee Osteoarthritis: The Boston Osteoarthritis Knee Study." J Rheumatol **32**(11): 2192-9.
Javidan, P., G. J. Adamson, et al. (2013). "The Effect of Medial Opening Wedge Proximal Tibial Osteotomy on Patellofemoral Contact." Am J Sports Med **41**(1): 80-6.
Jeffery, A. K., G. W. Blunn, et al. (1991). "Three-Dimensional Collagen Architecture in Bovine Articular Cartilage." J Bone Joint Surg Br **73**(5): 795-801.
Jurvelin, J. S., J. P. Arokoski, et al. (2000). "Topographical Variation of the Elastic Properties of Articular Cartilage in the Canine Knee." J Biomech **33**(6): 669-75.
Jurvelin, J. S., M. D. Buschmann, et al. (2003). "Mechanical Anisotropy of the Human Knee Articular Cartilage in Compression." Proc Inst Mech Eng H **217**(3): 215-9.
Keenan, K. E., S. Pal, et al. (2012). "A Viscoelastic Constitutive Model Can Accurately Represent Entire Creep Indentation Tests of Human Patella Cartilage." J Appl Biomech.
Kempson, G. E., M. A. Freeman, et al. (1968). "Tensile Properties of Articular Cartilage." Nature **220**(5172): 1127-8.
Kenawey, M., E. Liodakis, et al. (2011). "Effect of the Lower Limb Rotational Alignment on Tibiofemoral Contact Pressure." Knee Surg Sports Traumatol Arthrosc **19**(11): 1851-59.
Kiviranta, P., J. Rieppo, et al. (2006). "Collagen Network Primarily Controls Poisson's Ratio of Bovine Articular Cartilage in Compression." J Orthop Res **24**(4): 690-9.
Koo, S. and T. P. Andriacchi (2007). "A Comparison of the Influence of Global Functional Loads Vs. Local Contact Anatomy on Articular Cartilage Thickness at the Knee." J Biomech **40**(13): 2961-66.
Koo, S. and T. P. Andriacchi (2008). "The Knee Joint Center of Rotation Is Predominantly on the Lateral Side During Normal Walking." J Biomech **41**(6): 1269-73.
Koo, S., J. H. Rylander, et al. (2011). "Knee Joint Kinematics During Walking Influences the Spatial Cartilage Thickness Distribution in the Knee." J Biomech **44**(7): 1405-09.
Korhonen, R. K. and W. Herzog (2008). "Depth-Dependent Analysis of the Role of Collagen Fibrils, Fixed Charges and Fluid in the Pericellular Matrix of Articular Cartilage on Chondrocyte Mechanics." J Biomech **41**(2): 480-5.
Korhonen, R. K., M. S. Laasanen, et al. (2003). "Fibril Reinforced Poroelastic Model Predicts Specifically Mechanical Behavior of Normal, Proteoglycan

Depleted and Collagen Degraded Articular Cartilage." J Biomech **36**(9): 1373-9.
Korhonen, R. K., M. S. Laasanen, et al. (2002). "Comparison of the Equilibrium Response of Articular Cartilage in Unconfined Compression, Confined Compression and Indentation." J Biomech **35**(7): 903-9.
Kovach, I. S. (1996). "A Molecular Theory of Cartilage Viscoelasticity." Biophys Chem **59**(1-2): 61-73.
Kozanek, M., A. Hosseini, et al. (2009). "Tibiofemoral Kinematics and Condylar Motion During the Stance Phase of Gait." J Biomech **42**(12): 1877-84.
Krishnan, R., S. Park, et al. (2003). "Inhomogeneous Cartilage Properties Enhance Superficial Interstitial Fluid Support and Frictional Properties, but Do Not Provide a Homogeneous State of Stress." J Biomech Eng **125**(5): 569-77.
Kühl, E., K. Garikipati, et al. (2005). "Remodeling of Biological Tissue: Mechanically Induced Reorientation of a Transversely Isotropic Chain Network." J Mech Phys Solids **53**(7): 1552-73.
Kühn, W. and F. Grun (1942). "Relations between Elastic Constants and the Strain Birefringence of High-Elastic Substances." Kolloid-Zeitschrift **101**(3): 248-71.
Kwan, M. K., W. M. Lai, et al. (1990). "A Finite Deformation Theory for Cartilage and Other Soft Hydrated Connective Tissues--I. Equilibrium Results." J Biomech **23**(2): 145-55.
Laasanen, M. S., S. Saarakkala, et al. (2003). "Ultrasound Indentation of Bovine Knee Articular Cartilage in Situ." J Biomech **36**(9): 1259-67.
Lai, W. M., J. S. Hou, et al. (1991). "A Triphasic Theory for the Swelling and Deformation Behaviors of Articular Cartilage." J Biomech Eng **113**(3): 245-58.
Lai, W. M., V. C. Mow, et al. (1981). "Effects of Nonlinear Strain-Dependent Permeability and Rate of Compression on the Stress Behavior of Articular Cartilage." J Biomech Eng **103**(2): 61-6.
Lai, W. M., V. C. Mow, et al. (1993). "Constitutive Modeling of Articular Cartilage and Biomacromolecular Solutions." J Biomech Eng **115**(4B): 474-80.
Langelier, E. and M. D. Buschmann (2003). "Increasing Strain and Strain Rate Strengthen Transient Stiffness but Weaken the Response to Subsequent Compression for Articular Cartilage in Unconfined Compression." J Biomech **36**(6): 853-9.
Lanir, Y. (1987a). "Biorheology and Fluid Flux in Swelling Tissues, Ii. Analysis of Unconfined Compressive Response of Transversely Isotropic Cartilage Disc." Biorheology **24**(2): 189-205.
Lanir, Y. (1987b). "Biorheology and Fluid Flux in Swelling Tissues. I. Bicomponent Theory for Small Deformations, Including Concentration Effects." Biorheology **24**(2): 173-87.
LaPrade, R. F., A. H. Engebretsen, et al. (2007a). "The Anatomy of the Medial Part of the Knee." J Bone Joint Surg Am **89**(9): 2000-10.

LaPrade, R. F., P. M. Morgan, et al. (2007b). "The Anatomy of the Posterior Aspect of the Knee. An Anatomic Study." J Bone Joint Surg Am **89**(4): 758-64.
Laufer, S. (2003). "Role of Eicosanoids in Structural Degradation in Osteoarthritis." Curr Opin Rheumatol **15**(5): 623-7.
Lawrence, R. C., D. T. Felson, et al. (2008). "Estimates of the Prevalence of Arthritis and Other Rheumatic Conditions in the United States. Part Ii." Arthritis Rheum **58**(1): 26-35.
Leigh, J. P., W. Seavey, et al. (2001). "Estimating the Costs of Job Related Arthritis." J Rheumatol **28**(7): 1647-54.
Leveille, S. G., Y. Zhang, et al. (2005). "Sex Differences in Musculoskeletal Pain in Older Adults." Pain **116**(3): 332-8.
Lewis, R. J., A. K. MacFarland, et al. (1998). "Material Properties and Biosynthetic Activity of Articular Cartilage from the Bovine Carpo-Metacarpal Joint." Osteoarthr Cartilage **6**(6): 383-92.
Li, G., S. E. Park, et al. (2005a). "The Cartilage Thickness Distribution in the Tibiofemoral Joint and Its Correlation with Cartilage-to-Cartilage Contact." Clin Biomech **20**(7): 736-44.
Li, L. P. and K. B. Gu (2011). "Reconsideration on the Use of Elastic Models to Predict the Instantaneous Load Response of the Knee Joint." Proc Inst Mech Eng H **225**(9): 888-96.
Li, L. P. and W. Herzog (2004a). "The Role of Viscoelasticity of Collagen Fibers in Articular Cartilage: Theory and Numerical Formulation." Biorheology **41**(3-4): 181-94.
Li, L. P. and W. Herzog (2004b). "Strain-Rate Dependence of Cartilage Stiffness in Unconfined Compression: The Role of Fibril Reinforcement Versus Tissue Volume Change in Fluid Pressurization." J Biomech **37**(3): 375-82.
Li, L. P., W. Herzog, et al. (2005b). "The Role of Viscoelasticity of Collagen Fibers in Articular Cartilage: Axial Tension Versus Compression." Med Eng Phys **27**(1): 51-7.
Li, L. P., A. Shirazi-Adl, et al. (2002). "Alterations in Mechanical Behaviour of Articular Cartilage Due to Changes in Depth Varying Material Properties--a Nonhomogeneous Poroelastic Model Study." Comput Methods Biomech Biomed Engin **5**(1): 45-52.
Li, L. P., J. Soulhat, et al. (1999). "Nonlinear Analysis of Cartilage in Unconfined Ramp Compression Using a Fibril Reinforced Poroelastic Model." Clin Biomech **14**(9): 673-82.
Liu, F., M. Kozanek, et al. (2010). "In Vivo Tibiofemoral Cartilage Deformation During the Stance Phase of Gait." J Biomech **43**(4): 658-65.
Liu, J., J. K. Udupa, et al. (2008). "Rigid Model-Based 3d Segmentation of the Bones of Joints in Mr and Ct Images for Motion Analysis." Med Phys **35**(8): 3637-49.
Logan, M. C., A. Williams, et al. (2004). "Tibiofemoral Kinematics Following Successful Anterior Cruciate Ligament Reconstruction Using Dynamic Multiple Resonance Imaging." Am J Sports Med **32**(4): 984-92.

Lotjonen, P., P. Julkunen, et al. (2009). "Strain-Dependent Modulation of Ultrasound Speed in Articular Cartilage under Dynamic Compression." Ultrasound Med Biol **35**(7): 1177-84.
Lu, X. L. and V. C. Mow (2008). "Biomechanics of Articular Cartilage and Determination of Material Properties." Med Sci Sports Exerc **40**(2): 193-9.
Ma, J., H. Narayanan, et al. (2010). Experimental and Computational Investigation of Viscoelasticity of Native and Engineered Ligament and Tendon. Iutam Symposium on Cellular, Molecular and Tissue Mechanics, Proceedings. New York, Springer. **16:** 3-17.
Ma, J., M. J. Smietana, et al. (2012). "Three-Dimensional Engineered Bone-Ligament-Bone Constructs for Anterior Cruciate Ligament Replacement." Tissue Eng Part A **18**(1-2): 103-16.
MacKintosh, F. C., J. Kas, et al. (1995). "Elasticity of Semiflexible Biopolymer Networks." Phys Rev Lett **75**(24): 4425-28.
Mak, A. F. (1986). "The Apparent Viscoelastic Behavior of Articular Cartilage--the Contributions from the Intrinsic Matrix Viscoelasticity and Interstitial Fluid Flows." J Biomech Eng **108**(2): 123-30.
Mak, A. F., W. M. Lai, et al. (1987). "Biphasic Indentation of Articular Cartilage--I. Theoretical Analysis." J Biomech **20**(7): 703-14.
Maly, M. R. (2008). "Abnormal and Cumulative Loading in Knee Osteoarthritis." Curr Opin Rheumatol **20**(5): 547-52.
Mann, R. A. and J. Hagy (1980). "Biomechanics of Walking, Running, and Sprinting." Am J Sports Med **8**(5): 345-50.
Mansour, J. M. and V. C. Mow (1976). "The Permeability of Articular Cartilage under Compressive Strain and at High Pressures." J Bone Joint Surg Am **58**(4): 509-16.
Maroudas, A., P. Bullough, et al. (1968). "The Permeability of Articular Cartilage." J Bone Joint Surg Br **50**(1): 166-77.
Maroudas, A. I. (1976). "Balance between Swelling Pressure and Collagen Tension in Normal and Degenerate Cartilage." Nature **260**(5554): 808-9.
McKinley, T. O., M. J. Rudert, et al. (2004a). "Incongruity Versus Instability in the Etiology of Posttraumatic Arthritis." Clin Orthop Relat Res(423): 44-51.
McKinley, T. O., M. J. Rudert, et al. (2004b). "Pathomechanic Determinants of Posttraumatic Arthritis." Clin Orthop Relat Res(427 Suppl): S78-88.
McWilliams, D. F., B. F. Leeb, et al. (2011). "Occupational Risk Factors for Osteoarthritis of the Knee: A Meta-Analysis." Osteoarthr Cartilage **19**(7): 829-39.
Meachim, G. (1972). "Light Microscopy of Indian Ink Preparations of Fibrillated Cartilage." Ann Rheum Dis **31**(6): 457-64.
Mizrahi, J., A. Maroudas, et al. (1986). "The "Instantaneous" Deformation of Cartilage: Effects of Collagen Fiber Orientation and Osmotic Stress." Biorheology **23**(4): 311-30.
Moerman, K. M., C. A. Holt, et al. (2009). "Digital Image Correlation and Finite Element Modelling as a Method to Determine Mechanical Properties of Human Soft Tissue in Vivo." J Biomech **42**(8): 1150-3.

Moger, C. J., K. P. Arkill, et al. (2009). "Cartilage Collagen Matrix Reorientation and Displacement in Response to Surface Loading." J Biomech Eng **131**(3): 031008.
Moisio, K., A. Chang, et al. (2011). "Varus-Valgus Alignment: Reduced Risk of Subsequent Cartilage Loss in the Less Loaded Compartment." Arthritis Rheum **63**(4): 1002-9.
Mow, V. C. (1977). "Biphasic Rheological Properties of Cartilage [Proceedings]." Bull Hosp Joint Dis **38**(2): 121-4.
Mow, V. C., G. A. Ateshian, et al. (1993). "Biomechanics of Diarthrodial Joints: A Review of Twenty Years of Progress." J Biomech Eng **115**(4B): 460-7.
Mow, V. C., M. C. Gibbs, et al. (1989). "Biphasic Indentation of Articular Cartilage--Ii. A Numerical Algorithm and an Experimental Study." J Biomech **22**(8-9): 853-61.
Mow, V. C. and X. E. Guo (2002). "Mechano-Electrochemical Properties of Articular Cartilage: Their Inhomogeneities and Anisotropies." Annu Rev Biomed Eng **4**: 175-209.
Mow, V. C., M. H. Holmes, et al. (1984). "Fluid Transport and Mechanical Properties of Articular Cartilage: A Review." J Biomech **17**(5): 377-94.
Mow, V. C., S. C. Kuei, et al. (1980). "Biphasic Creep and Stress Relaxation of Articular Cartilage in Compression? Theory and Experiments." J Biomech Eng **102**(1): 73-84.
Mow, V. C. and C. C. Wang (1999). "Some Bioengineering Considerations for Tissue Engineering of Articular Cartilage." Clin Orthop Relat Res(367 Suppl): S204-23.
Muir, H., P. Bullough, et al. (1970). "The Distribution of Collagen in Human Articular Cartilage with Some of Its Physiological Implications." J Bone Joint Surg Br **52**(3): 554-63.
Murphy, L. and C. G. Helmick (2012). "The Impact of Osteoarthritis in the United States: A Population-Health Perspective." Am J Nurs **112**(3 Suppl 1): S13-9.
Muthuri, S. G., M. Hui, et al. (2011a). "What If We Prevent Obesity? Risk Reduction in Knee Osteoarthritis Estimated through a Meta-Analysis of Observational Studies." Arthritis Care Res (Hoboken) **63**(7): 982-90.
Muthuri, S. G., D. F. McWilliams, et al. (2011b). "History of Knee Injuries and Knee Osteoarthritis: A Meta-Analysis of Observational Studies." Osteoarthritis Cartilage **19**(11): 1286-93.
Myers, E. R., W. M. Lai, et al. (1984). "A Continuum Theory and an Experiment for the Ion-Induced Swelling Behavior of Articular Cartilage." J Biomech Eng **106**(2): 151-8.
Noyori, K., T. Takagi, et al. (1998). "Characterization of the Macromolecular Components of the Articular Cartilage Surface." Rheumatol Int **18**(2): 71-7.
O'Connor, M. I. (2007). "Sex Differences in Osteoarthritis of the Hip and Knee." J Am Acad Orthop Surg **15 Suppl 1**: S22-5.
Oiestad, B. E., I. Holm, et al. (2010). "Knee Function and Prevalence of Knee Osteoarthritis after Anterior Cruciate Ligament Reconstruction: A

Prospective Study with 10 to 15 Years of Follow-Up." Am J Sports Med **38**(11): 2201-10.
Oloyede, A., R. Flachsmann, et al. (1992). "The Dramatic Influence of Loading Velocity on the Compressive Response of Articular Cartilage." Connect Tissue Res **27**(4): 211-24.
Palmer, J. S. and M. C. Boyce (2008). "Constitutive Modeling of the Stress-Strain Behavior of F-Actin Filament Networks." Acta Biomaterialia **4**(3): 597-612.
Park, S. and G. A. Ateshian (2006). "Dynamic Response of Immature Bovine Articular Cartilage in Tension and Compression, and Nonlinear Viscoelastic Modeling of the Tensile Response." J Biomech Eng **128**(4): 623-30.
Parsons, J. R. and J. Black (1977). "The Viscoelastic Shear Behavior of Normal Rabbit Articular Cartilage." J Biomech **10**(1): 21-9.
Pena, E., B. Calvo, et al. (2007). "Effect of the Size and Location of Osteochondral Defects in Degenerative Arthritis. A Finite Element Simulation." Comput Biol Med **37**(3): 376-87.
Pena, E., B. Calvo, et al. (2006). "Why Lateral Meniscectomy Is More Dangerous Than Medial Meniscectomy. A Finite Element Study." J Orthop Res **24**(5): 1001-10.
Poole, A. R., T. Kojima, et al. (2001). "Composition and Structure of Articular Cartilage: A Template for Tissue Repair." Clin Orthop Relat Res(391 Suppl): S26-33.
Poole, C. A. (1997). "Articular Cartilage Chondrons: Form, Function and Failure." J Anat **191 (Pt 1)**: 1-13.
Powers, C. M., F. G. Shellock, et al. (1998). "Quantification of Patellar Tracking Using Kinematic Mri." J Magn Reson Imaging **8**(3): 724-32.
Prodromos, C. C., F. H. Fu, et al. (2008). "Controversies in Soft-Tissue Anterior Cruciate Ligament Reconstruction: Grafts, Bundles, Tunnels, Fixation, and Harvest." J Am Acad Orthop Surg **16**(7): 376-84.
Quinn, T. M., E. B. Hunziker, et al. (2005). "Variation of Cell and Matrix Morphologies in Articular Cartilage among Locations in the Adult Human Knee." Osteoarthr Cartilage **13**(8): 672-78.
Rees, D. (2006). Basic Engineering Plasticity: An Introduction with Engineering and Manufacturing Applications, Butterworth-Heinemann.
Reynaud, B. and T. M. Quinn (2006). "Anisotropic Hydraulic Permeability in Compressed Articular Cartilage." J Biomech **39**(1): 131-7.
Ristanis, S., G. Giakas, et al. (2003). "The Effects of Anterior Cruciate Ligament Reconstruction on Tibial Rotation During Pivoting after Descending Stairs." Knee Surg Sports Traumatol Arthrosc **11**(6): 360-5.
Ristanis, S., N. Stergiou, et al. (2005). "Excessive Tibial Rotation During High-Demand Activities Is Not Restored by Anterior Cruciate Ligament Reconstruction." Arthroscopy **21**(11): 1323-9.
Ronken, S., M. P. Arnold, et al. (2012). "A Comparison of Healthy Human and Swine Articular Cartilage Dynamic Indentation Mechanics." Biomech Model Mechanobiol **11**(5): 631-9.

Rossi, R., D. E. Bonasia, et al. (2011). "The Role of High Tibial Osteotomy in the Varus Knee." J Am Acad Orthop Surg **19**(10): 590-9.
Roughley, P. J. (2006). "The Structure and Function of Cartilage Proteoglycans." Eur Cells Mater **12**: 92-101.
Salmon, L. J., V. J. Russell, et al. (2006). "Long-Term Outcome of Endoscopic Anterior Cruciate Ligament Reconstruction with Patellar Tendon Autograft: Minimum 13-Year Review." Am J Sports Med **34**(5): 721-32.
Sanchez, A. R., 2nd, M. T. Sugalski, et al. (2006). "Anatomy and Biomechanics of the Lateral Side of the Knee." Sports Med Arthrosc **14**(1): 2-11.
Sandell, L. J. (2012). "Etiology of Osteoarthritis: Genetics and Synovial Joint Development." Nat Rev Rheumatol **8**(2): 77-89.
Schinagl, R. M., D. Gurskis, et al. (1997). "Depth-Dependent Confined Compression Modulus of Full-Thickness Bovine Articular Cartilage." J Orthop Res **15**(4): 499-506.
Seed, S. M., K. C. Dunican, et al. (2009). "Osteoarthritis: A Review of Treatment Options." Geriatrics **64**(10): 20-9.
Seedhom, B., T. Takeda, et al. (1979). "Mechanical Factors and Patellofemoral Osteoarthrosis." Ann Rheum Dis **38**(4): 307-16.
Seifzadeh, A., D. C. Oguamanam, et al. (2012). "Determination of Nonlinear Fibre-Reinforced Biphasic Poroviscoelastic Constitutive Parameters of Articular Cartilage Using Stress Relaxation Indentation Testing and an Optimizing Finite Element Analysis." Comput Methods Programs Biomed **107**(2): 315-26.
Setton, L. A., D. M. Elliott, et al. (1999). "Altered Mechanics of Cartilage with Osteoarthritis: Human Osteoarthritis and an Experimental Model of Joint Degeneration." Osteoarthr Cartilage **7**(1): 2-14.
Setton, L. A., V. C. Mow, et al. (1995). "Mechanical Behavior of Articular Cartilage in Shear Is Altered by Transection of the Anterior Cruciate Ligament." J Orthop Res **13**(4): 473-82.
Setton, L. A., H. Tohyama, et al. (1998). "Swelling and Curling Behaviors of Articular Cartilage." J Biomech Eng **120**(3): 355-61.
Setton, L. A., W. Zhu, et al. (1993). "The Biphasic Poroviscoelastic Behavior of Articular Cartilage: Role of the Surface Zone in Governing the Compressive Behavior." J Biomech **26**(4-5): 581-92.
Sharma, L. (2001a). "Local Factors in Osteoarthritis." Curr Opin Rheumatol **13**(5): 441-6.
Sharma, L., J. Song, et al. (2001b). "The Role of Knee Alignment in Disease Progression and Functional Decline in Knee Osteoarthritis." JAMA **286**(2): 188-95.
Shelburne, K. B., M. R. Torry, et al. (2005). "Muscle, Ligament, and Joint-Contact Forces at the Knee During Walking." Med Sci Sports Exerc **37**(11): 1948-56.
Shepherd, D. E. and B. B. Seedhom (1999a). "The 'Instantaneous' Compressive Modulus of Human Articular Cartilage in Joints of the Lower Limb." Rheumatology **38**(2): 124-32.

Shepherd, D. E. and B. B. Seedhom (1999b). "Thickness of Human Articular Cartilage in Joints of the Lower Limb." Ann Rheum Dis **58**(1): 27-34.
Shirazi, R. and A. Shirazi-Adl (2009). "Analysis of Partial Meniscectomy and Acl Reconstruction in Knee Joint Biomechanics under a Combined Loading." Clin Biomech (Bristol, Avon) **24**(9): 755-61.
Shirazi, R., A. Shirazi-Adl, et al. (2008). "Role of Cartilage Collagen Fibrils Networks in Knee Joint Biomechanics under Compression." J Biomech **41**(16): 3340-8.
Smith, C. K., M. L. Hull, et al. (2006). "Lengthening of a Single-Loop Tibialis Tendon Graft Construct after Cyclic Loading: A Study Using Roentgen Stereophotogrammetric Analysis." J Biomech Eng **128**(3): 437-42.
Sokoloff, L. (1966). "Elasticity of Aging Cartilage." Fed Proc **25**(3): 1089-95.
Soltz, M. A. and G. A. Ateshian (2000). "A Conewise Linear Elasticity Mixture Model for the Analysis of Tension-Compression Nonlinearity in Articular Cartilage." J Biomech Eng **122**(6): 576-86.
Soulhat, J., M. D. Buschmann, et al. (1999). "A Fibril-Network-Reinforced Biphasic Model of Cartilage in Unconfined Compression." J Biomech Eng **121**(3): 340-7.
Spilker, R. L., J. K. Suh, et al. (1992). "A Finite Element Analysis of the Indentation Stress-Relaxation Response of Linear Biphasic Articular Cartilage." J Biomech Eng **114**(2): 191-201.
Srikanth, V. K., J. L. Fryer, et al. (2005). "A Meta-Analysis of Sex Differences Prevalence, Incidence and Severity of Osteoarthritis." Osteoarthr Cartilage **13**(9): 769-81.
Stergiou, N., S. Ristanis, et al. (2007). "Tibial Rotation in Anterior Cruciate Ligament (Acl)-Deficient and Acl-Reconstructed Knees: A Theoretical Proposition for the Development of Osteoarthritis." Sports Med **37**(7): 601-13.
Suh, J. K. and S. Bai (1998). "Finite Element Formulation of Biphasic Poroviscoelastic Model for Articular Cartilage." J Biomech Eng **120**(2): 195-201.
Sun, D. D., X. E. Guo, et al. (2004). "The Influence of the Fixed Negative Charges on Mechanical and Electrical Behaviors of Articular Cartilage under Unconfined Compression." J Biomech Eng **126**(1): 6-16.
Suri, S. and D. A. Walsh (2012). "Osteochondral Alterations in Osteoarthritis." Bone **51**(2): 204-11.
Swann, A. C. and B. B. Seedhom (1993). "The Stiffness of Normal Articular Cartilage and the Predominant Acting Stress Levels: Implications for the Aetiology of Osteoarthrosis." Br J Rheumatol **32**(1): 16-25.
Symmons, D., C. Mathers, et al. (2003). Global Burden of Osteoarthritis in the Year 2000. , World Health Organization.
Szarko, M., K. Muldrew, et al. (2010). "Freeze-Thaw Treatment Effects on the Dynamic Mechanical Properties of Articular Cartilage." BMC Musculoskelet Disord **11**: 231.

Sztrolovics, R., J. Grover, et al. (2002). "The Characterization of Versican and Its Message in Human Articular Cartilage and Intervertebral Disc." J Orthop Res **20**(2): 257-66.
Tashman, S., W. Anderst, et al. (2004a). "Kinematics of the Acl-Deficient Canine Knee During Gait: Serial Changes over Two Years." J Orthop Res **22**(5): 931-41.
Tashman, S., D. Collon, et al. (2004b). "Abnormal Rotational Knee Motion During Running after Anterior Cruciate Ligament Reconstruction." Am J Sports Med **32**(4): 975-83.
Tashman, S., P. Kolowich, et al. (2007). "Dynamic Function of the Acl-Reconstructed Knee During Running." Clin Orthop Relat Res **465**(454): 66-73.
Taylor, Z. A. and K. Miller (2006). "Constitutive Modeling of Cartilaginous Tissues: A Review." J Appl Biomech **22**(3): 212-29.
Thambyah, A., A. Nather, et al. (2006). "Mechanical Properties of Articular Cartilage Covered by the Meniscus." Osteoarthr Cartilage **14**(6): 580-8.
Thompson, W. O., F. L. Thaete, et al. (1991). "Tibial Meniscal Dynamics Using Three-Dimensional Reconstruction of Magnetic Resonance Images." Am J Sports Med **19**(3): 210-5; discussion 15-6.
Toivanen, A. T., M. Heliovaara, et al. (2010). "Obesity, Physically Demanding Work and Traumatic Knee Injury Are Major Risk Factors for Knee Osteoarthritis--a Population-Based Study with a Follow-up of 22 Years." Rheumatology (Oxford) **49**(2): 308-14.
Treloar, L. R. G. (1946). "The Elasticity of a Network of Long-Chain Molecules. I." Trans Faraday Soc **42**(1-2): 83-94.
Treppo, S., H. Koepp, et al. (2000). "Comparison of Biomechanical and Biochemical Properties of Cartilage from Human Knee and Ankle Pairs." J Orthop Res **18**(5): 739-48.
van der Kraan, P. M. (2012). "Osteoarthritis Year 2012 in Review: Biology." Osteoarthritis Cartilage **20**(12): 1447-50.
van Eijden, T. M., E. Kouwenhoven, et al. (1986). "A Mathematical Model of the Patellofemoral Joint." J Biomech **19**(3): 219-29.
Van Thiel, G. S., R. M. Frank, et al. (2011). "Biomechanical Evaluation of a High Tibial Osteotomy with a Meniscal Transplant." J Knee Surg **24**(1): 45-53.
Verteramo, A. and B. B. Seedhom (2004). "Zonal and Directional Variations in Tensile Properties of Bovine Articular Cartilage with Special Reference to Strain Rate Variation." Biorheology **41**(3-4): 203-13.
Wan, L. Q., X. E. Guo, et al. (2010). "A Triphasic Orthotropic Laminate Model for Cartilage Curling Behavior: Fixed Charge Density Versus Mechanical Properties Inhomogeneity." J Biomech Eng **132**(2): 024504.
Wang, C. C., N. O. Chahine, et al. (2003). "Optical Determination of Anisotropic Material Properties of Bovine Articular Cartilage in Compression." J Biomech **36**(3): 339-53.
Wang, C. C., C. T. Hung, et al. (2001). "An Analysis of the Effects of Depth-Dependent Aggregate Modulus on Articular Cartilage Stress-Relaxation Behavior in Compression." J Biomech **34**(1): 75-84.

Wang, M. C. and E. Guth (1952). "Statistical Theory of Networks of Non-Gaussian Flexible Chains." J Chem Phys **20**(7): 1144-57.
Wilson, W., J. M. Huyghe, et al. (2006). "A Composition-Based Cartilage Model for the Assessment of Compositional Changes During Cartilage Damage and Adaptation." Osteoarthr Cartilage **14**(6): 554-60.
Wilson, W., J. M. Huyghe, et al. (2007). "Depth-Dependent Compressive Equilibrium Properties of Articular Cartilage Explained by Its Composition." Biomech Model Mechanobiol **6**(1-2): 43-53.
Wilson, W., C. C. van Donkelaar, et al. (2005a). "A Fibril-Reinforced Poroviscoelastic Swelling Model for Articular Cartilage." J Biomech **38**(6): 1195-204.
Wilson, W., C. C. van Donkelaar, et al. (2004). "Stresses in the Local Collagen Network of Articular Cartilage: A Poroviscoelastic Fibril-Reinforced Finite Element Study." J Biomech **37**(3): 357-66.
Wilson, W., C. C. van Donkelaar, et al. (2005b). "The Role of Computational Models in the Search for the Mechanical Behavior and Damage Mechanisms of Articular Cartilage." Med Eng Phys **27**(10): 810-26.
Wilson, W., B. van Rietbergen, et al. (2003). "Pathways of Load-Induced Cartilage Damage Causing Cartilage Degeneration in the Knee after Meniscectomy." J Biomech **36**(6): 845-51.
Wirth, W., M. P. Hellio Le Graverand, et al. (2009). "Regional Analysis of Femorotibial Cartilage Loss in a Subsample from the Osteoarthritis Initiative Progression Subcohort." Osteoarthr Cartilage **17**(3): 291-7.
Wong, B. L. and R. L. Sah (2010). "Mechanical Asymmetry During Articulation of Tibial and Femoral Cartilages: Local and Overall Compressive and Shear Deformation and Properties." J Biomech **43**(9): 1689-95.
Wong, M., M. Ponticiello, et al. (2000). "Volumetric Changes of Articular Cartilage During Stress Relaxation in Unconfined Compression." J Biomech **33**(9): 1049-54.
Woo, S. L., W. H. Akeson, et al. (1976). "Measurements of Nonhomogeneous, Directional Mechanical Properties of Articular Cartilage in Tension." J Biomech **9**(12): 785-91.
Woo, S. L., P. Lubock, et al. (1979). "Large Deformation Nonhomogeneous and Directional Properties of Articular Cartilage in Uniaxial Tension." J Biomech **12**(6): 437-46.
Woo, S. L., B. R. Simon, et al. (1980). "Quasi-Linear Viscoelastic Properties of Normal Articular Cartilage." J Biomech Eng **102**(2): 85-90.
Wu, J. Z., W. Herzog, et al. (1998). "Articular Joint Mechanics with Biphasic Cartilage Layers under Dynamic Loading." J Biomech Eng **120**(1): 77-84.
Youn, I., J. B. Choi, et al. (2006). "Zonal Variations in the Three-Dimensional Morphology of the Chondron Measured in Situ Using Confocal Microscopy." Osteoarthr Cartilage **14**(9): 889-97.
Young, A. A., R. C. Appleyard, et al. (2007). "Dynamic Biomechanics Correlate with Histopathology in Human Tibial Cartilage: A Preliminary Study." Clin Orthop Relat Res **462**(9): 212-20.

Zhang, Y., M. Nevitt, et al. (2011). "Fluctuation of Knee Pain and Changes in Bone Marrow Lesions, Effusions, and Synovitis on Magnetic Resonance Imaging." Arthritis Rheum **63**(3): 691-9.